University of Central Florida

STARS

2023

Transportation Electrification in Interdependent Power and Transportation Systems - Analysis, Planning, and Operation

Sina Baghali
University of Central Florida

TRANSPORTATION ELECTRIFICATION IN INTERDEPENDENT POWER AND
TRANSPORTATION SYSTEMS – ANALYSIS, PLANNING, AND OPERATION

by

SINA BAGHALI
B.S., University of Tabriz, 2016
M.S., K. N. Toosi University of Technology, 2019

A dissertation submitted in partial fulfilment of the requirements
for the degree of Doctor of Philosophy
in the Department of Civil, Environmental, and Construction Engineering
in the College of Engineering and Computer Science
at the University of Central Florida
Orlando, Florida

Summer Term
2023

Major Professor: Zhaomiao Guo

ABSTRACT

Electric vehicles (EVs) are one of the eminent alternatives to decarbonize the transportation sector. However, large-scale EV adoption brings new challenges and opportunities to both transportation and power systems (TPSs). The challenges include the lack of understanding of EV driving behaviors and the associated charging demand (CD) distribution, the complex interaction of the decentralized decision-makers from TPSs, and the insufficient infrastructure from TPSs to accommodate the growing CD of EVs. On the other hand, the opportunities include benefiting the power systems by leveraging vehicle-to-grid (V2G) technologies and improving transportation mobility by incorporating strategic infrastructure planning.

The goal of this dissertation is to address the challenges and leverage opportunities associated with large-scale EV adoption from planning and operational perspectives in TPSs. We have the following objectives:

1. Better understanding the impacts of driving patterns on the spatio-temporal distribution of EV CD.

2. Investigate the value of EVs on the coupled TPSs.

3. Plan the supporting power and transportation infrastructure for the growing CD of EVs.

More specifically, we first utilized machine learning approaches to model and forecast CD of EVs based on their driving behavior. Secondly, we propose a multi-agent model that captures the decentralized interactions between key stakeholders in TPSs to investigate the value of EVs in distribution system support. Thirdly, we modeled infrastructure planning for EV adoption from two perspectives: 1) We study the multi-stage DG and CS planning problem considering decentralized investors in a multi-agent optimization framework to understand the system evolvement. 2)

We study the centralized CS planning problem in a bi-level programming framework to optimize transportation mobility by strategically placing CSs. To overcome the computational difficulties, we have proposed effective computational algorithms based on exact convex reformulation and value-decomposition algorithms. Our numerical examples demonstrate that the proposed models can identify the equilibrium investment patterns of DGs and CSs, as well as determine the optimal locations of CSs from a centralized entity's perspective. Additionally, our operational framework shows how EVs can provide system support for load pickup with endogenously determined incentives and energy prices. These modeling and computational strategies can provide foundations for future investigation, planning, and market design with large-scale EVs in coupled TPSs.

ACKNOWLEDGMENTS

There is a large number of people that I would like to thank individually for making my Ph.D. graduation happens.

First of all, I am very grateful to my advisor, Dr. Zhaomiao Guo, for all his support. I learned from him how to approach fundamental real-world problems and how to address them systematically. I will forever be thankful to him for his never-ending support and helpful career advice. Besides I would like to express my deepest appreciation to my previous advisor, Dr. Junjian Qi for his consistent support, invaluable guidance, and encouragement in my professional life during the Ph.D.

I am also thankful to my dissertation committee members, professors Naveen Eluru, Samiul Hasan, and Wei Sun for providing me with invaluable feedback on my research.

Likewise, I am deeply grateful to my parents, Hossein and Hafezeh, who put their own dreams on hold to ensure that I could fulfill mine. Additionally, I want to express my appreciation to my sisters, Sarah and Sima, who played a significant role in helping me reach the place I am now.

I would like to especially thank my better half Saman, for her endless love and support. She gave me the courage and confidence to take the final steps of my Ph.D. journey.

TABLE OF CONTENTS

LIST OF FIGURES

LIST OF TABLES

CHAPTER 1: INTRODUCTION

Background and Motivation

Increasing global warming, air pollution, and other severe consequences of excessive fossil fuel consummation have been a wake-up call for policymakers to take practical measures and reduce carbon emissions. The International Energy Agency (IEA) has examined various emission scenarios across different sectors in their recent report [1], investigating the net zero emission (NZE) policy. In Fig. 1.1, the report's CO_2 emission projections are presented under three possible scenarios: 1) NZE scenario, where all nations implement NZE policies, 2) Announced pledged scenario (APS), where only the 50 nations that have committed to NZE policies do so, and 3) Stated policies scenario (STEPS), where nations adhere to their current NZE policies.
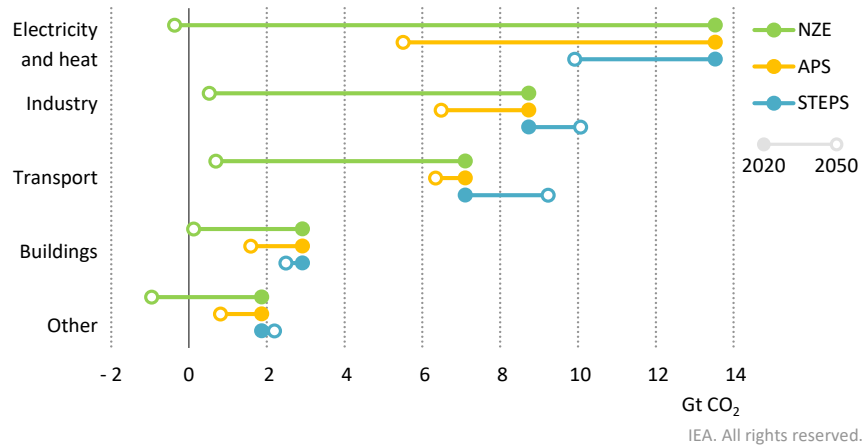
Figure 1.1: CO_2 emission outlook by sector and scenario [1]

Fig. 1.1 shows that the electricity and industrial sectors are responsible for the highest CO_2 emissions, with the transportation sector closely behind. It is also evident that if the current policies outlined in STEPS are maintained, CO_2 emissions from the transportation sector will continue to

rise, necessitating strict policy implementation in line with the NZE scenario to meet the 2050 targets.

There has been a growing effort from both the power and transportation systems (TPSs) to become more eco-friendly by promoting intermittent renewable energy sources and electric vehicles (EVs). These developments open ways for new technologies providing more efficient energy sources and greener transportation alternatives. As a result, transportation electrification using EVs has been widely pursued as part of NZE policies. As shown in Fig. 1.2, the number of EVs globally has surged from 2 million in 2016 to 16.5 million in 2021 over the past five years [2]
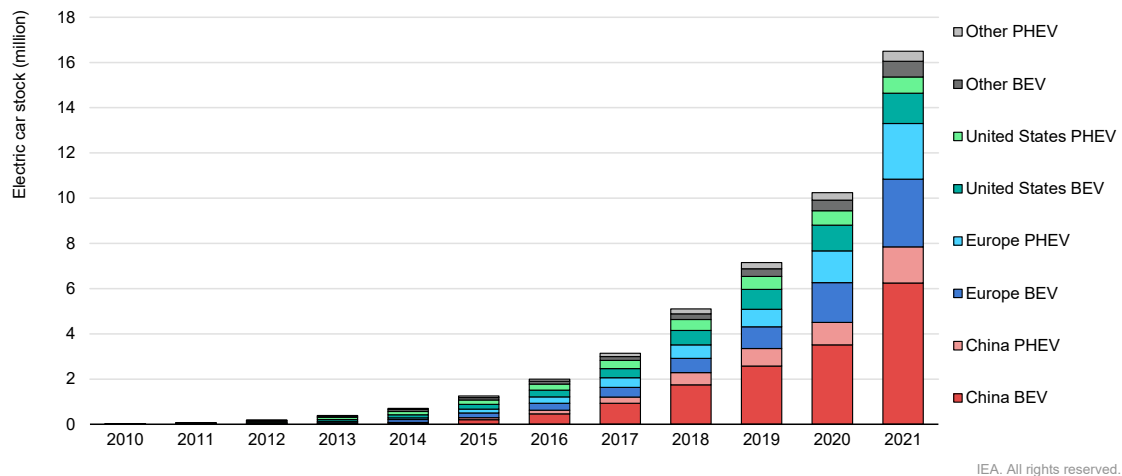
Figure 1.2: Global market share of EVs by type and region 2010–2021 [2].

The rising popularity of EVs has led to a corresponding increase in the need for charging infrastructure and electricity demand, as demonstrated by the upward trend in the number of charging stations (CSs) across the US (refer to Fig. 1.3). In 2021, there were approximately 50,000 EV CSs in the US [3]. With the Biden administration's passage of the $2 trillion infrastructure bill, this number is projected to reach at least 500,000 by 2030 [4].

The transportation sector's progress in adopting EVs has placed a significant burden on the power
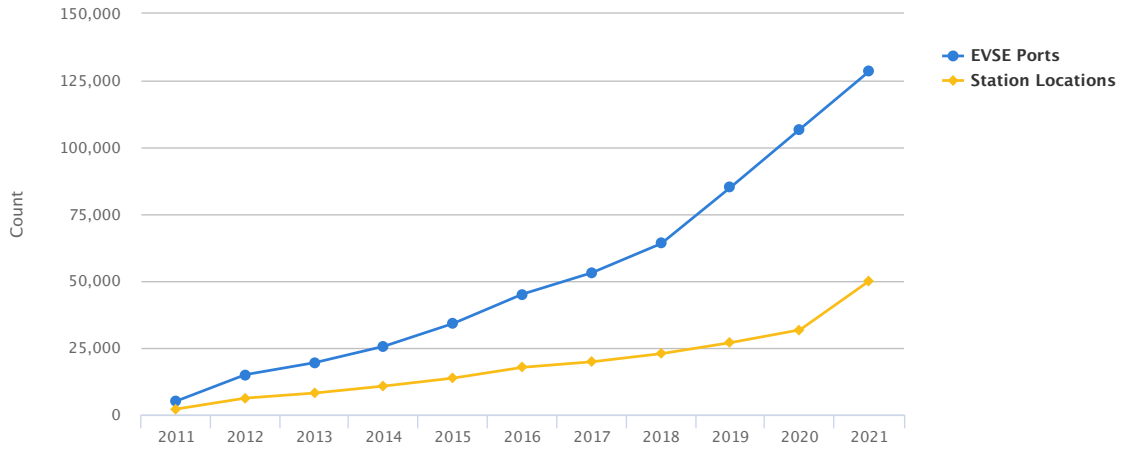
Figure 1.3: Public and private EV charging infrastructure in the US 2011–2021 [3].

system, which must handle the increased charging demand (CD). The International Energy Agency (IEA) predicts that by 2030, EVs will consume roughly 4% of the world's total electricity demand under the APS scenario, amounting to 1,100 TWh, and could rise to 1,500 TWh if the NZE target is achieved by 2030 [2] (refer to Fig. 1.4). Therefore, the EV adoption pathway requires careful consideration and planning from TPSs.
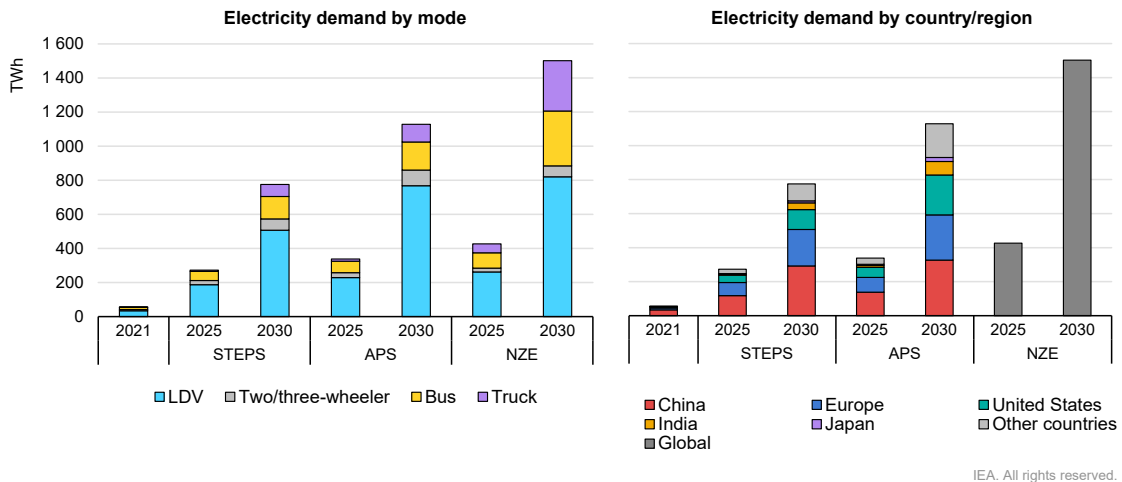
Figure 1.4: Electricity demand outlook of EVs by scenario, mode, and region [2].

As part of the energy sector, the power distribution system (DS) requires dependable methods to estimate and model the dynamic CD of EVs. This is necessary to accommodate energy generation and consider operational factors. However, the dynamic nature of CD is heavily dependent on drivers' choices and their trip requirements, which are linked with the transportation network (TN), thereby coupling distribution and transportation systems (DTSs). Moreover, the advent of vehicle-to-grid (V2G) technologies enables EVs to provide energy back to the system, which can be beneficial for the system but needs careful consideration and scheduling. While EVs can provide auxiliary services to the system with V2G [5], a large number of EVs can also cause significant electricity demand on DSs [2] and place more stress on the systems [6]. Therefore, systematic approaches that consider DTSs are necessary to better understand the CD of EVs and promote V2G participation. In realistic settings, such an approach must also consider the decentralized nature of decision-makers involved in DTSs and their individual objectives. Additionally, modeling interdependent systems results in a high-dimensional, nonlinear, and non-convex model that is exceedingly challenging to solve [7].

In summary, this dissertation studies the following challenges and opportunities of EV adoption in the DTSs:

- The CD dependability on EV drivers' travel behavior.

- The complex interaction of decentralized decision-makers involved in coupled DTSs.

- The energy and charging infrastructure planning to accommodate the large-scale EV adoption.

- The benefit of EVs providing system support with V2G technologies and the transportation mobility improvement with strategic planning of CS locations.

Goals and Contributions

This dissertation aims to explore and propose ways to tackle/exploit the mentioned challenges/opportunities that arise with the large-scale adoption of EV adoption. The following objectives have been identified:

- Gain a deeper understanding of how driving patterns influence the charging demand (CD) of electric vehicles (EVs) by leveraging emerging data.

- Examine the benefits and value that EVs bring to integrated power and transportation systems.

- Develop plans for the necessary infrastructure, including power DSs and charging stations (CSs), to accommodate the increasing charging demand for EVs.

To provide solutions for the mentioned objectives, we have contributed to the field of modeling EVs in interconnected DTS in the following areas:

- We utilized data analytic methods to model and forecast daily CD patterns of EVs using GPS data. Furthermore, we analyzed the travel behavior of EVs in comparison to conventional ICEVs commuting in the same urban network. We examined the spatiotemporal CD of EVs based on their recorded SOC and developed machine-learning techniques to forecast the CD of EVs based on trip parameters such as trip distances and their start and end times.

- We have created a market-based modeling framework to explore the possible benefits of EVs in providing energy support to the system during times of stressed operation. This model accounts for the decentralized decision-making of EV drivers in coupled DTSs and is a unique,

computationally feasible modeling framework that considers the concerns of various stakeholders and the operating properties of both transportation and power networks. Moreover, the proposed model calculates the incentives of EV grid services and the corresponding distribution of EV traffic flow endogenously. Such a model enables comprehensive analyses of the interdependence between transportation and power networks and the spatial-temporal value of EVs for DS load balancing.

- We have approached the planning perspective by formulating the problem of expanding the capacity of CS and DGs as a multi-stage multi-agent optimization problem. This model provides a practical framework to better understand the interaction between private investors and the increasing number of EVs. It incorporates both long-term planning and short-term operational decision-making and explicitly captures the feedback effects of CS availability and EV adoption, while also endogenously determining locational electricity prices. The original high-dimensional non-convex problem is further reformulated as a convex problem for an efficient solution.

- To model the decision-making of centralized entities and policymakers in CS planning, we have proposed a bi-level programming framework that includes both the decentralized decision-making of lower-level stakeholders and the CS investment location decision-making of centralized entities at the upper level. To efficiently solve the highly complex bi-level problem and understand the impact and interaction of centralized CS investment decisions on coupled systems, we have developed a solution approach using value decomposition algorithms that is highly scalable.

Outline

The remaining chapters of the dissertation are organized as follows.

6

CHAPTER 2 offers a comprehensive literature review on EV adoption, CD analysis, and systems analysis with EVs.

CHAPTER 3 details the proposed machine learning approach for modeling and forecasting the CD of EVs.

CHAPTER 4 focuses on the proposed market-based modeling framework, which considers the decentralized decision-making of EV drivers over coupled DTSs in the context of incentivizing EVs for DS load pickup.

CHAPTER 5 builds upon the proposed market-based modeling framework by introducing a stochastic model that considers uncertainties from both transportation and power systems. The chapter evaluates the impact of stochasticity on the performance of the proposed framework in uncertain emergency situations.

CHAPTER 6 presents the proposed multi-stage multi-agent model for the CS and distributed generator (DG) expansion planning problem.

CHAPTER 7 introduces a bi-level programming framework for modeling the decision-making of centralized investors, which incorporates the proposed market framework at the lower level and proposes a solution algorithm to solve the complex bi-level problem.

CHAPTER 2: LITERATURE REVIEW

This chapter aims to present an overview of the relevant studies conducted on the modeling of electric vehicles and charging infrastructure. The literature review is comprehensively divided into three distinct categories, including data analytic methodologies, infrastructure planning strategies, and vehicle-to-grid (V2G) modeling for system support.

Data analytic approaches for CD modeling of EVs

The modeling and prediction of the charging demand (CD) of electric vehicles (EVs) has garnered significant attention from the research community, leading to the development of an extensive body of literature. This literature can be examined from two primary perspectives: 1) the input data utilized, and 2) the applied modeling methodologies. Survey data is a widely used source for multiple studies on EV driving and charging behavior modeling [8–10]. However, the collection of survey data may be expensive, and it can only provide a perception of travel behavior. Mobile phone and social network data with location tags may not be suitable for analyzing EV behavior accurately because the mode of transportation cannot be precisely estimated. GPS data, among mobility data sources, is the most appropriate for modeling and estimating the actual behavior of EVs [11]. High-resolution location tracking enables the recording of driving distances for each trip, calculation of resulting CD, and estimation of locations where charging stations are most needed. Additionally, the high sample frequency of GPS data can enable accurate modeling of the temporal behaviors of EVs. In earlier studies [12, 13], the GPS data of conventional internal combustion engine vehicles (ICEVs) were used to infer EV charging behaviors based on their travel patterns. Current studies also use GPS data from ICEVs to explore the feasibility and potential of electrifying the existing transportation fleet [14, 15]. These data sources, however, cannot fully

account for EV behavior since they are either small-scale data of limited ICEVs or GPS data of specific vehicle types, such as taxi fleets [12, 14, 15].

Upon selecting a suitable data source, researchers utilize different methodologies to model and estimate the charging and travel behavior of electric vehicles (EVs). One of the most popular methods used in many studies is stochastic modeling, which investigates the stochastic behavior of charging demand (CD) [9, 16–21]. Monte-Carlo Simulation (MCS) is the basis of stochastic modeling, where a considerable number of scenarios are generated for travel parameters and trip chains are developed to calculate EV charging behavior [17–19, 22, 23]. However, MCS needs to generate a large number of scenarios to be accurate, which can make the problem computationally expensive. Additionally, the correlation of travel parameters is neglected in this method since scenarios are generated independently for each parameter. Ashtari et al. [16] proposed a stochastic method that incorporates the correlation of parameters in their distributions. However, this method only considers the correlation of two parameters. Another stochastic method, the Markov-chain model, is implemented for modeling EV charging behavior [21]. This method requires fewer scenarios than MCS. However, it is necessary to group the status of EV travel into different steps to form an accurate Markov transition matrix, which still has computational challenges. Moreover, aggregating the traveling status of EVs into discrete steps introduces inaccuracies into the model.

In recent years, researchers have started to utilize machine learning algorithms such as k-nearest neighbours (KNN) [9] and artificial neural networks [8, 24, 25] for CD estimation. However, some studies such as [24, 25] incorporate probabilistic models to generate synthetic trips to overcome the limited size of their input data. In [8], a large survey dataset is used for estimating the travel parameters and CD. However, the authors assume unrealistic scenarios such as smart charging of EV users where a centralized entity determines the optimal charging time and shifts the charging time to hours with a low charging price. Furthermore, they assume that vehicles will only charge after their last trip of the day, neglecting the possibility of charging during work hours and other

9

public charging options.

Charging station and energy generation planning for EV adoption

The CS planning problem has received attention from both power and transportation disciplines. Research from a power system perspective has focused on CS capacity planning for minimizing costs and the impact of Evs on the DSs [26–30], and improving services to the customers (drivers) by reducing their wait time at CSs [31, 32]. Authors in [33], developed a game theoretical method to allocate both CSs and DGs in DS network to fulfill the growing system demand and CD. [34] formulates a stochastic model for optimal siting and sizing of DGs and CSs considering both economical and environmental factors. However, both of the mentioned studies have a power system centric approach and do not consider the EV growth and travel and charging behavior in the TN. Research from a TS perspective has investigated the siting and sizing of CSs in TNs as a facility location and allocation problem to better serve the charging demand and fulfill travel needs [35–38]. Majority of literature in this direction have modeled the individual decision making of the drivers and investors in the TN without considering the operational characteristic of the DS [39–42].

However, both transportation and power systems have become increasingly coupled with a high level of EV penetration in current research [43–45]. For example, [43] developed a modeling framework to determine an optimal allocation of a given number of public CSs to maximize social welfare in the coupled transportation and power network; [44] proposed a model for the expansion planning of urban transportation and charging networks ensuring the best investment strategies for both TS and DS; [45] studied the wireless charging location for electric bus transportation where the power system was modeled at the higher level and the TS at the lower level. However, this school of literature typically assumes a central-planner perspective, which may not represent the

interaction of decentralized decision-makers.

Authors in [46], have considered the decentralized decision making of competitors from both DS and TS in the CS planning problem. The shortcoming of this work is that they have not considered the generation expansion and multi-stage modeling of the problem which is essential for understanding the evolution of the system given a specific long-term EV penetration target. Authors in [47] modeled the evolution of a charging infrastructure in the TN with a multi-period study. In each period, more EV traffic flow would be added to the network by considering additional origin and destination (OD) pairs. In [48], the long-term CS expansion problem is studied by considering finite stages of OD demands throughout the planning horizon. The scope of these two studies is from the TN perspective without considering the charging requirements of CSs from the power system perspective. On the other hand, [45] takes into account the power system modeling along with the TN in a multi-stage framework. In this study, the authors have focused on CS siting and sizing problems for electric buses, and the power system is modeled assuming the CD of CSs can be fulfilled without considering generation expansions. Additionally, focusing on the electric buses, this model has not considered the individual decision and preferences of private EV drivers.

EV system support in emergency conditions

In recent literature, the researchers have proposed direct coordinated methods and indirect market frameworks to alleviate the charging impacts and promote EV participation in grid services in stressed conditions [49]. Direct methods include reconfiguration techniques with EVs to support system performance [50], controlling devices/techniques to manage the power flow on the lines and feeders [51], and managing charging demand during EVs' dwelling time at charging stations (CSs) [52, 53]. In direct coordinated frameworks, a centralized entity, e.g., distribution system operator (DSO) or charging station aggregator (CSA), manages the charging demand during the charging

11

sessions. For example, [52, 53] aim to shift the charging demand overtime to minimize the cost of charging or maximize the profit of the centralized entity based on exogenous daily energy prices. Other researchers proposed coordination methods to provide better DS operation [54, 55]. For example, [54] proposes a charging strategy for CSs to manage congestion in DS, and [55] uses EVs to provide ancillary services. The results of the mentioned methods show limited V2G participation because EVs attend CSs mostly for charging their vehicles [54], and they don't have the personal incentives to participate in the V2G program. Although these studies aim to provide decision support to manage EV charging, the main drawback is that they typically assume a centralized perspective, which neglects the individual needs of customers [49] and consider energy prices as exogenous parameters.

In indirect market-based frameworks, decentralized approaches are proposed to mitigate some limitations of the direct coordinated charging frameworks. In [56], incentive-based demand response is proposed to mitigate overloads on distribution feeders and minimize the cost of customers with flexible loads like EVs. However, the incentives are selected from pre-defined sets without the guarantee of their optimality [57]. Authors in [58, 59] proposed multi-agent equilibrium-based frameworks for load control to maintain the reliable operation of DS and consider customers' requirements. However, they haven't considered EVs in their modelings. Multiple researchers proposed new market schemes based on the conventional market framework to alleviate system stress with EVs [6, 49, 57, 60, 61]. For example, [60] proposes a hierarchical control technique to manage EVs in congestion management. The DSO is at the highest level in this hierarchy with indirect control over fleet operator (FO) based on the electricity market, and the FO has the lower-level control over EVs based on the charging price. Similar hierarchy control is proposed in [6] where a capacity market operator is introduced to manage the interaction of DSO and FO without considering transportation network and other important variables in EVs decision makings such as travel time. Furthermore, dynamic tariffs and subsidies are considered to control and promote

the participation of EVs in stressed/congested DSs in [49, 57, 62]. The electricity prices are determined in the day-ahead electricity markets, and the dynamic tariffs/subsidiaries are provided to customers with flexible loads in real-time when the system experiences stress/congestion [49, 57]. In [61], sub-markets are formed in parts of the systems that are experiencing congestion to promote EV aggregators to contribute to congestion management. The mentioned approaches based on the electricity market require intense data transmission and specific agreements between the different entities, e.g., DSO and EV aggregators, to manage the market. Modeling such interactions have complex implementations and require iterative bidding strategies to solve the electricity market problem. In addition, although EVs are primarily used for mobility purposes, all of these studies largely ignore EV travel behaviors and travel demand over transportation networks. This drawback may undermine the applicability of these studies to investigate complex feedback effects between transportation and power systems.

In terms of EV modeling, power system literature can be divided into two categories. The first category considers the transportation network as a black box and uses statistical methods or machine learning techniques to model the temporal charging demand function, which is further treated as an input for power system modeling. For example, authors in [63] used probability distribution functions of daily travel mileage and arrival times of vehicles to model the temporal behavior of charging demand; authors in [8] have explored machine learning techniques for predicting charging demand load. The disadvantages of these approaches include their heavy reliance on the empirical model and historical data such that the performance of predictive models is not guaranteed with evolving transportation and power systems. The second category tries to use traffic assignment models to describe the distribution of the vehicles, which can provide more insights on EV travel behavior [64]. For example, [65] uses dynamic traffic assignment based on cell transmission models to consider the traveling requirements of mobile energy sources through transportation system; [46] proposed a coupled transportation and distribution system modeling based on traffic

13

wave theory. However, the travel and charging decision making of EV drivers are not modeled in these works. Authors in [66] establish a power and transportation equilibrium model to incorporate drivers' decision makings, but this work uses a heuristic-iterative solution approach, and load pick-up is not considered. We developed the individual decision making of EVs further in [67] based on the classic combined distribution and assignment (CDA) model, but [67] focuses on transmission systems and does not consider incentivizing EVs' participation in DS support.

CHAPTER 3: INVESTIGATING THE SPATIOTEMPORAL CHARGING DEMAND AND TRAVEL BEHAVIOR OF ELECTRIC VEHICLES USING GPS DATA: A MACHINE LEARNING APPROACH[1]

Introduction

The first step in analyzing a new phenomenon is to observe its behavior and its impacts on the surroundings. EVs being the new addition to the transportation system require careful consideration since not only they would impact the transportation system but also their CD will impact the power systems. Now that market penetration of EVs is increasing, their addition may change the travel behavior of drivers and pose a significant electricity demand on the power system. Additionally, the CD of EVs depends on the travel behavior of EVs, which is inherently uncertain, causing the forecasting of the daily CD to be a challenging task. Data analysis gives us a powerful tool to analyze EVs and their adoption of the system. Here, we use the recorded GPS data of EVs and conventional gasoline-powered vehicles from the same city to investigate the potential shift in the travel behavior of drivers from conventional ICEVs to EVs and forecast the spatiotemporal patterns of daily CD based on the drivers trip parameters. Unlike other studies that considered GPS data of ICEVs as EVs, we have examined the data of actual EVs and provided extensive comparison on the traveling behavior of EVs and ICEVs commuting in the same urban network. Data analytic measures are calculated to make the comparisons and machine learning approaches are implemented to forecast the daily CD. We have analyzed the CD of EVs based on their recorded SOC without making assumptions on EVs' initial SOC and energy consumption based on the traveling

---

[1]This chapter is developed based on the article published in [68]:
S. Baghali, Z. Guo, and S. Hassan, "Investigating the Spatiotemporal Charging Demand and Travel Behavior of Electric Vehicles Using GPS Data: A Machine Learning Approach", in *2022 IEEE Power & Energy Society General Meeting (PESGEM)*. IEEE, 2022. Link.

distances, which is a prevalent assumption made in different studies due to the lack of information in the data sets. Lastly, different from studies that have focused on temporal behavior of the CD, we have developed forecasting models to extract and estimate both the spatial and temporal behavior of CD. Our analysis reveals that the travel behavior of EVs and conventional vehicles are similar. Also, the forecasting results indicate that the developed models can generate accurate spatiotemporal patterns of the daily CD.

Data Description

We will use vehicle energy dataset (VED) [2], which is a publicly available data set containing GPS trajectories of a limited number of personal cars including both ICEVs and EVs in Ann Arbor, Michigan, the USA from Nov 2017 to Nov 2018 [69]. This is a unique data set providing high-resolution data of EVs' energy consumption and their SOC. The VED contains trajectories of 383 vehicles, including 264 ICEVs, 92 hybrid EVs (HEVS), and 27 plug-in HEV (PHEVs/EVs). The VED consists of dynamic and static data sets; Static data contains vehicle parameters (e.g., vehicle ID, vehicle type, vehicle class, etc.), and dynamic data contains high-resolution daily trip trajectories and other trip parameters (e.g., day number, trip number, latitude, location latitude, and longitude, etc.). We will derive the vehicle IDs of EVs from static data and use them to extract the dynamic data of EVs based on vehicle ID. The collected dynamic data has different features of the trips. Among them, we will use day number, vehicle ID, trip number, timestamps (ms), latitude, longitude, and SOC of batteries. Table 3.1 shows a sample of the input data with the selected features for an EV as an example.

We can calculate the trip duration and end time by considering the last timestamp recorded for each trip. Trip distance is another important parameter that can be extracted with the recorded latitudes

---

[2]Data: https://github.com/gsoh/VED

TABLE 3.1 INPUT DATA EXAMPLE

Day No.	Vehicle ID	Trip No.	Time stamp (ms)	Latitude (deg)	Longitude (deg)	SOC (%)
5.5602	371	1288	0	42.2776	-83.7537	94.344
5.5602	371	1288	600	42.2776	-83.7537	94.344
5.5602	371	1288	700	42.2776	-83.7537	94.344
5.5602	371	1288	1700	42.2776	-83.7537	94.344

and longitudes at each timestamp by calculating the distance between each consecutively recorded timestamp and aggregating over the records of each trip using the Haversian formula [70]. The other key feature of the input data is the recorded SOC of batteries in each timestamp. Therefore, we don't need to make assumptions about the initial SOC of EVs and calculate the consumed energy based on trip distance. With the recorded SOC values, we can determine the consumed energy in trips and calculate the CD.

After applying all the data prepossessing procedures discussed above, we can derive the parameters of each trip, i.e., trip start time, end time, origin and destination (OD) locations, and consumed energy.

Travel behavior comparison

The processed input data contains the records of 4,109 trips made by EVs during one year. This data can be used to extract the distribution of trip parameters, e.g., trip distance, trip start and end time, number of daily trips, etc., and presents an opportunity to compare the behavior of EVs and conventional ICEVs. Therefore, we repeated the same initial data processing on the dynamic trip data of ICEVs, and the result was the records of 18,936 trips made by ICEVs. We will use both of these data sets to compare the travel behavior between ICEVs and EVs.

Fig. 3.1 shows the distribution of daily trip distances for both EVs (Fig. 3.1a) and ICEVs (Fig.3.1b). The short distance trips (0~20 Km) are more prevalent in both types of vehicles, and the main difference is the maximum trip distance. ICEVs have a higher maximum trip distance (110 Km), where the maximum trip distance recorded for EVs is 35 Km. One can infer that ICEVs are preferred for long-distance trips. However, since the frequency of such trips is low, no general trends can be derived.
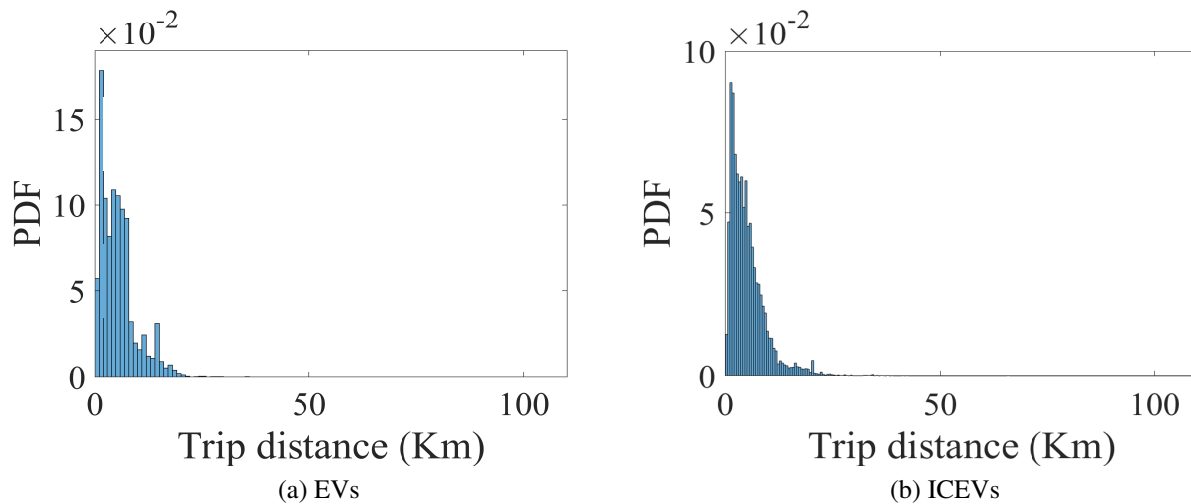
(a) EVs   (b) ICEVs

Figure 3.1: Distribution of daily trips' distances (a) EVs (b) ICEVs

The trips' start and end time distributions are shown in Fig. 3.2 and 3.3 for both types of vehicles. There are no major differences between the trip start time distributions for EVs and ICEVs (see Fig. 3.2). Minor difference can be seen in the trip end time of EVs compared to ICEVs. EVs tend to finish their trips less during $t = 23 \sim 1$ (see Fig. 3.3a), whereas more trip end time has been recorded for ICEVs during that time (see Fig. 3.3b). Also, trip end time during $t = 10 \sim 15$ has been more prevalent among EVs compared to ICEVs. This might be because of the charging needs of EVs after the trips or user preference of the drivers.
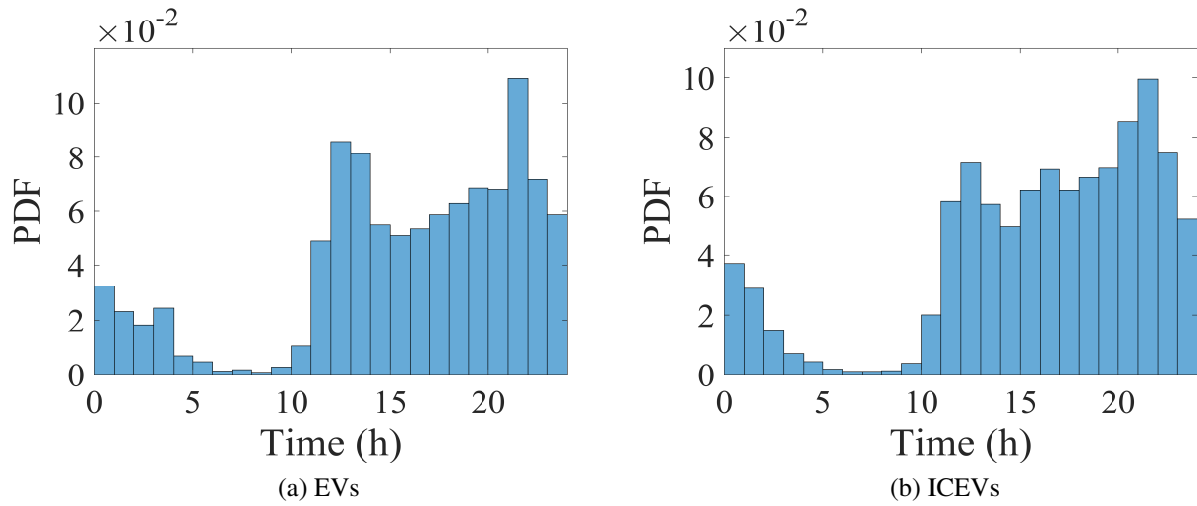
(a) EVs

(b) ICEVs

Figure 3.2: Distribution of daily trips' start time (a) EVs (b) ICEVs
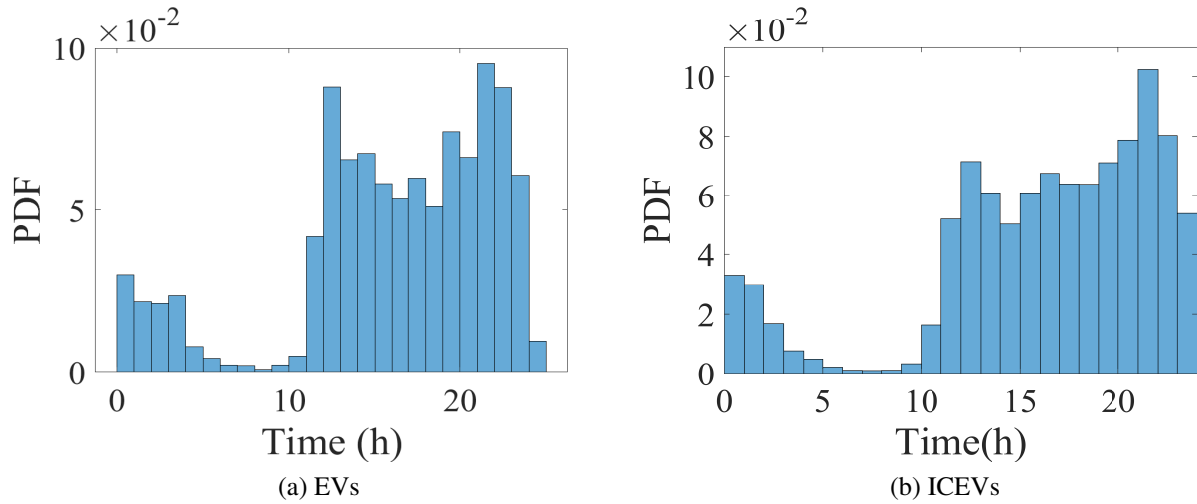
(a) EVs

(b) ICEVs

Figure 3.3: Distribution of daily trips' end time (a) EVs (b) ICEVs

In summary, EVs and ICEVs have similar patterns on trip start/end time and distance per trip. But ICEVs owners may be more likely to have more daily trips and ICEVs are preferred for trips with long distances. Also, EVs tend to end their trip more during the afternoons and less close to the

midnight.

Charging Demand Modeling

In this section, we will derive the daily spatiotemporal CD behavior based on the input data. In order to detect the charging events, we will compare the SOC of the EVs at the end of each trip ($\text{SOC}_k^{\text{arr}}$) and compare it to the start SOC of the next trip ($\text{SOC}_{k+1}^{\text{dep}}$) with k representing the trip index of the EV in the same day. If $\text{SOC}_{k+1}^{\text{dep}} > \text{SOC}_k^{\text{arr}}$, trip k would be a charging event starting at the end time of the same trip k. The CD can be calculated as the multiplication of the difference between SOCs for the two consecutive trips or the required SOC (SOC^{req}) and the battery capacity of each EV (Cap_v):

$$\text{SOC}^{\text{req}} = \text{SOC}_{k+1}^{\text{dep}} - \text{SOC}_k^{\text{arr}} \tag{3.1}$$

$$\text{CD}_k = \begin{cases} \text{SOC}^{\text{req}} \times \text{Cap}_v & \text{if } \text{SOC}^{\text{req}} > 0 \\ 0 & \text{Otherwise} \end{cases} \tag{3.2}$$

The temporal behavior of CD also depends on the charging duration (ΔT), i.e., the amount of time required to receive the demanded energy (CD_k). This duration is directly proportional to the required CD and inversely proportional to the charging rate (α) and charging efficiency (η), which depend on the battery characteristics and the installed charger. This relation is presented in (3.3). We assumed that the demand (CD_k) will be imposed on the system at the end time of trip k lasting for a duration of ΔT_k.

$$\Delta T_k = \frac{\text{CD}_k}{\alpha \cdot \eta} \tag{3.3}$$

Additionally, the location of the charging event will be the destination of trip k, providing the spatial characteristics of the CD. Going through all the trips of EVs, we derived the charging

location for each EV (see Fig. 3.4a) – locations are color-coded for different EVs. We observe more charging instances located in the central part of the city compared to the other regions. The study region can be divided into finite number of zones $\{z_i\}_{1 \leq i \leq n}$ covering different parts of the region, with n being the total number of zones, to categorize the spatial distribution of charging events. The system operator (SO) can divide the region based on its requirements and judgments to any number of zones with various shapes; To ensure each zone has enough number of charging records, here we have considered to have $n = 9$ charging zones as shown in Fig.3.4b, which will be used to estimate the spatial location of the CD.

(a)   (b)
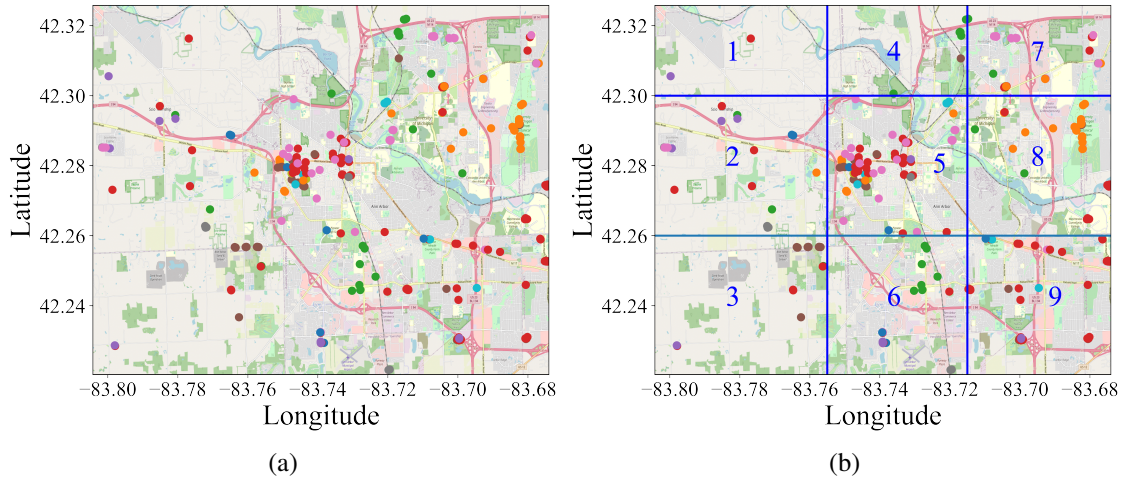
Figure 3.4: (a) Spatial distribution of charging events for different EVs and (b) considered charging zones of the city

From the power system prospective, the SO can use the calculated CD and the expected charging location for operational purposes, e.g., day-ahead generation dispatch, real time energy management, etc. Additionally, the system planner can use the predicted spatial-temporal CD for the future expansion of charging infrastructure and estimate the required charging station capacities at different locations.

Methodologies

In this section, we will develop forecasting models to estimate the spatiotemporal pattern of daily CD. In addition, we will prepare the input data and define our input features and targets.

Prepare Model Input Features

At the start of each trip, the known parameters are a) trip start time, b) origin location, and c) start SOC (SOC^{dep}). Our objective is to predict whether the EV will charge at the destination location; if yes, which zone and when this charging event will happen, and how much energy it will charge.

Predicting the choice of charging at the end of a trip and the charging zone can be modeled as a classification problem. We will label each charging event trip of the input data based on the number of the zone of the event $L = i$ ($1 \leq i \leq n$), defined in Section 3, and define a dummy zone $L = n + 1$ for the trips where no charging happens at the end of the trip. Table 3.2 shows how this labeling works on the example input data with $n = 9$. Trips 2 and 4 are not considered as charging event trips because $\text{SOC}^{\text{req}} < 0$ and trip 4 is the last trip of the day with no information of the next trip's SOC^{dep} in the next day (day 6). Therefore, the labels for these two trips are 10. Trips 1 and 3 are charging event trips with $\text{SOC}^{\text{req}} > 0$. The labels for these two trips are determined based on their destination locations, and they are in zones 9 and 8, respectively.

The temporal behavior of this CD depends on the end time and charging duration and can be determined based on the procedure presented in Section 3 using (3.2) and (3.3).

In summary, the input features of our problem are vehicle ID and current trip's start time, origin location, and SOC^{dep} and we will use them to train the forecasting models.

TABLE 3.2 PROCESSED DATA EXAMPLE FOR THE FORECASTING MODELS

Vehicle ID	Trip No.	T^{str} (h)	T^{end} (h)	Origin location		Label	SOC^{dep} %	SOC^{req} %
				Latitude	Longitude			
371	1	13.44	13.75	42.277	-83.75	9	40.92	41.96
371	2	18.47	18.56	42.253	-83.674	10	45.69	0
371	3	18.96	19.06	42.256	-83.696	8	33.13	46.99
371	4	15.45	15.57	42.302	-83.704	10	64.67	0

Forecasting Models

The forecasting targets in our modeling are the label of the trip, trip end time, and SOC^{Req}. Table 3.3 shows the input features and the targets based on Table 3.2 as an example. Note that we calculate the CD only for trips with charging events, so we need to add charging labels as an input feature for forecasting the CD.

TABLE 3.3 INPUT FEATURES AND TARGETS OF THE EXAMPLE DATA

Input features						Targets	
Vehicle ID	T^{str} (h)	SOC^{dep} %	Origin location		Label	T^{end} (h)	SOC^{req} %
			Latitude	Longitude			
371	13.44	40.92	42.277	-83.75	9	13.75	41.96
371	18.47	45.69	42.253	-83.674	10	18.56	0
371	18.96	33.13	42.256	-83.696	8	19.06	46.99
371	15.45	64.67	42.302	-83.704	10	15.57	0

Five forecasting methods, namely K-nearest neighbor (KNN), decision tree (DT), random forest (RF), artificial neural networks (ANNs), and deep artificial neural networks (DANNs) were considered to predict each target. The considered methods have been widely used in machine learning applications and the detailed comparison on these methods are presented in [71]. We will train the models and determine their hyper parameters separately for each target with the defined input features. These parameters include the number of neighbors for the KNN method, tree depth for DT and RF methods, number of neurons for ANN, and number of neurons on each hidden layer

23

for the DANN method. We investigated the performance of the models for a range of parameters by observing the accuracy of the classification for trip label prediction and the forecasting error for the trip end time and required SOC. The selected parameters and performance evaluation of the forecasting models are discussed in Section 3.

Results

Parameter Settings

Before feeding the input data to the forecasting models, we extract the trips made in days with charging event occurrence (1,062 trips) and split them into training sets and test sets – 25 % test set and 75% training sets. Scickit-learn library was used to train the KNN, DT, and RF models, and TensorFlow library were used to train the ANN based models. All the implementations were done on the Python software.

We trained the forecasting methods for a range of modeling parameters using the training sets and observed the performance of the methods on test set to select the best modeling parameters. Table 3.4 summarizes the selected parameters for different forecasting methods. For the DANN method, the number of hidden layers more than the mentioned layers in Table 3.4 resulted in less accuracy. Therefore, we limited the number of layers to 2 for CS zone (label) and trip end time prediction, and 3 layers for SOC^{req} prediction.

According to [72], the battery capacities of EVs studied in the VED data set is in the range of $20\sim25$ KWh. Therefore, we consider the battery characteristics of Fiat500E, which is reported as one of the popular EVs in Alternative Fuels Data Center [73] and has a battery capacity of 24 KWh. We assume a charging rate of $\alpha = 6.6$ KW (i.e., level 2 charging) and the charging efficiency to be $\eta = 0.9$ [73] for CD demand calculations mentioned in (3.3).

Table 3.4 Forecasting model parameters

Target	KNN	DT	RF	ANN	DANN	
	neighbors	tree depth	tree depth	neurons	Layers	Neurons
Label	11	8	6	400	2	500,100
T^{end}	4	8	18	500	2	400,100
$\mathrm{SOC}^{\mathrm{req}}$	10	4	5	400	3	900,500,100

Charging Demand Forecasting

After determining the parameters for each forecasting model, we compared their performance for predicting each target on the test data set (see Table 3.5). The RF method provided the highest accuracy for charging zone label prediction and the least RMSE value for the trip end time and the DT method had the least RMSE value for predicting the required SOC. Even though ANN-based models have provided superior performance in other machine learning studies [8, 74], simpler models (KNN, DT, and RF) provided better results for our dataset. The low accuracy of label prediction stems from the small number of charging event trips (446 trips) compared to all of the trips made in days with charging events (1,062 trips) and a large number of classes/zones (10 classes).

Table 3.5 Performance of forecasting models on the test set: classifying accuracy for label prediction and RMSE value for T^{end} and $\mathrm{SOC}^{\mathrm{req}}$

Target	KNN	DT	RF	ANN	DANN
Label (%)	63.91	63.53	73.97	65.73	65.78
T^{end} (h)	0.39	0.17	0.15	0.19	0.19
$\mathrm{SOC}^{\mathrm{req}}$ (%)	17.05	15.55	15.79	21.73	17.57

We selected the best forecasting models for each target and predicted the spatiotemporal pattern of daily CD (see Figure 3.5). We considered two cases for forecasting the $\mathrm{SOC}^{\mathrm{req}}$ 1) using the

25

predicted labels as the input feature of the trained DT model and 2) using the actual labels of the trips. Charging start times were based on the predicted trip end times, and the resulting daily CDs were calculated using the procedure delineated in Section 3.

Comparing the estimated demands from case 1 and the test data (see Fig. 3.5a and 3.5c) shows that the developed classifier failed to detect the charging events in zone 1. This discrepancy is because of the less recorded charging events in this zone (see Fig. 3.4b). On the contrary, most of the charging events are predicted to occur at zone 5, which has more charging records in the input data, causing a significant spike in CD of this zone at $t = 11 \sim 12$. Moreover, the estimated CD for case 1 follows the temporal pattern of the CD during $t = 0 \sim 6$ but performs poorly in the afternoon (see Fig. 3.5a) because more charging events are predicted to be at zone 5 and most of the charging events in this zone happen in $t = 11 \sim 16$.

Passing the actual zones from the test data for forecasting the SOC^{req} (case 2) improved the temporal pattern in the afternoon and the nighttime (see Fig. 3.5b). The accurate charging zones have reduced the charging events in zone 5 and we no longer observe the high peak CD during $t = 11 \sim 12$ (compare Fig.3.5a and 3.5b). This increase in accuracy points out the importance of charging zone prediction in determining CD's temporal and spatial behavior.

For comparing the temporal pattern of CD, we have derived the total daily CD (see Fig. 3.5d). The estimated CD after midnight until the morning ($t = 0 \sim 6$) follows the same pattern in both cases and resembles the actual CD derived from test data. However, in the afternoon, the prediction inaccuracy in charging zones resulted in inaccurate temporal estimates for case 1, especially after $t = 17$.

The SO and system planners can use the estimated spatio-temporal CD in different applications: 1) The predicted zonal CD in Fig. 3.5b can be used for day ahead generation dispatch and other operational planning purposes. For example, it is estimated that the CD at zone 8 would be high

26
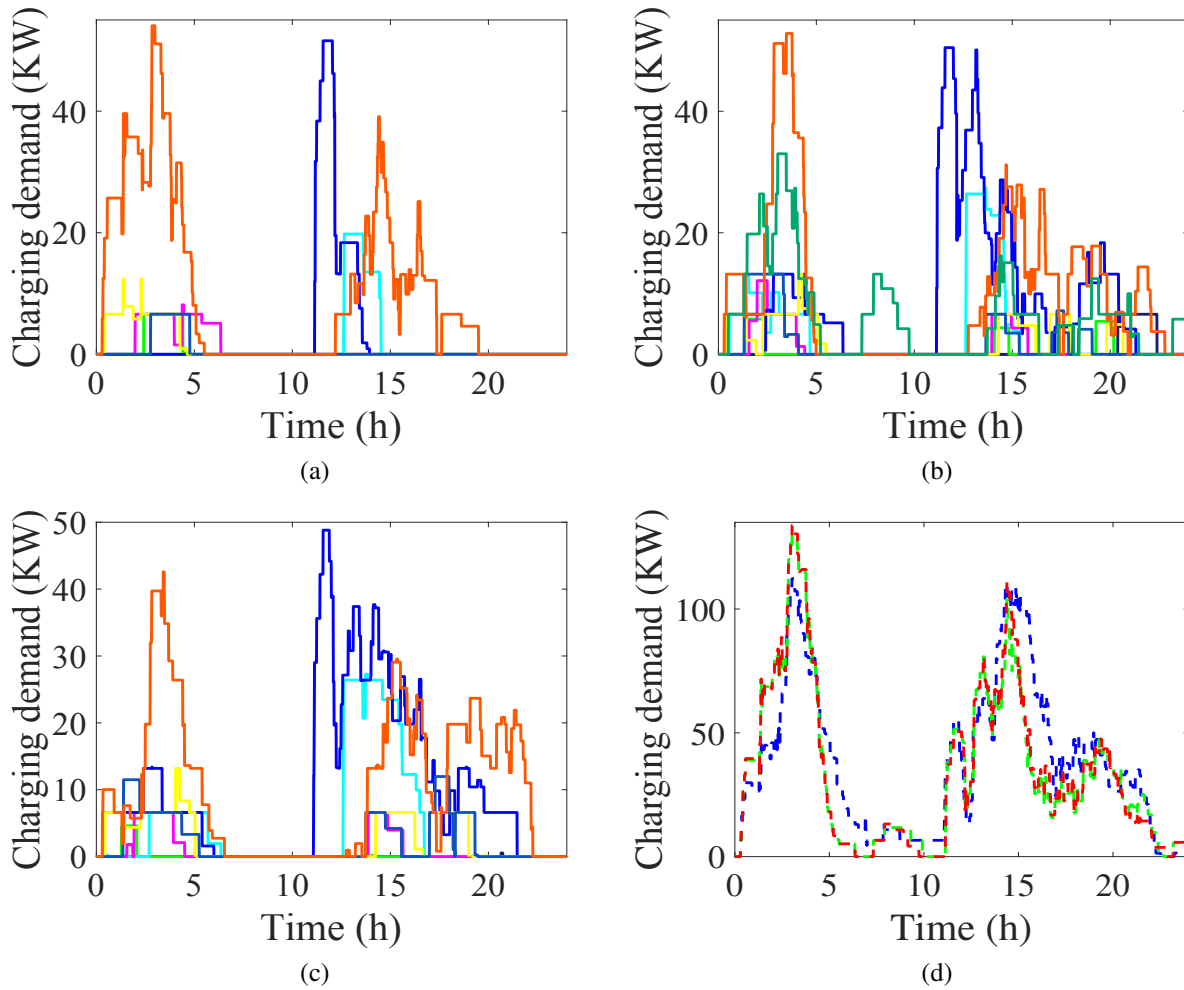
Figure 3.5: Zonal CD for (a) case 1 (b) case 2 (c) test data, and (d) total CD; ── zone 1, ── zone 2, ── zone 3, ── zone 4, ── zone 5, ── zone 6, ── zone 7, ── zone 8, ── zone 9; -·- Test data, -·- Estimated case 1, -·- Estimated case 2.

during the morning. Therefore, the SO would consider allotting sufficient energy generation in the day ahead planning of that zone. 2) The system planner can use the expected zonal CD for inferring user preferences and expanding the CS infrastructures. For example, the daily CD pattern shows higher CD at zones 5 and 8 compared to the other zones (see Fig. 3.5b), which can be good candidates for CS expansion.

Summary and Future Extensions

Estimating EVs' daily CD's spatial and temporal pattern is a vital factor in modeling uncertainties in power systems. CD pattern is closely related to the travel behavior of EVs. In this study, we use the VED, a high-resolution GPS data set of both EVs and conventional vehicles, to investigate the potential differences in the travel behavior of EVs and conventional vehicles and analyzed the real spatiotemporal pattern of CD. Our analyses showed that the travel behavior of EVs is similar to ICEVs in terms of trip start and end time, and trip distance. But EVs tend to have fewer daily trips compared to ICEVs.

After processing the GPS trajectories of EVs, we developed forecasting models to predict the spatiotemporal pattern of CD based on the known information at the starting point of the trips. The spatial pattern of CD was modeled as a classification problem, where the charging event locations were grouped in different zones. The CD and its temporal pattern were estimated using a decision tree and random forest regressors with high accuracy.

The small scale of the input data limited the performance of the forecasting model, and we will examine the models on larger data sets as more data sets are becoming available for EVs. Future extension should also investigate the potential reasons of different predicting accuracy to better understand the applicability of machine learning algorithms. Another extension of this work is to develop a forecasting model to predict the daily CD based on the historical travel data rather than based on information at the starting point of each trip.

CHAPTER 4: ELECTRIC VEHICLES FOR DISTRIBUTION SYSTEM LOAD PICKUP UNDER STRESSED CONDITIONS: A NETWORK EQUILIBRIUM APPROACH[1]

Introduction

Power distribution systems (DSs) have an ever-increasing electricity demand that requires long-term planning and proactive management. The growing demand would cause line congestion and low voltage, which may trigger contingencies such as line outages. As DSs are operated with radial topology, outage of a line means the loss of all loads at downstream nodes. When the DS is under stressed conditions, which means the system is heavily loaded, the bus voltage may appear to be over low, and distribution lines may be congested. A remedy to circumvent severe contingencies and blackouts is to shed some load, ensuring the security of the whole network.

The growing market penetration of electric vehicles (EVs) can provide auxiliary services to the system with vehicle-to-grid (V2G) technologies; on the other hand, they can impose large electricity demand on DSs causing more stress on the systems. Additionally, the driving patterns of EV drivers and their dependency on the transportation network make charging demands highly unpredictable. Therefore, systematic approaches considering both distribution and transportation systems are required to better understand the charging demand of EVs and promote V2G participation to reduce system stress.

Here, we will investigate the potential effects of EVs on reducing the load shedding in heavily

---

[1]This paper is developed based on the paper published in [75]:
S. Baghali, Z. Guo, W. Wei, and M. Shahidehpour, "Electric Vehicles for Distribution System Load Pickup Under Stressed Conditions: A Network Equilibrium Approach", in *IEEE Transactions on Power Systems*, IEEE, 2022. Link.

loaded distribution systems (DSs). Given proper incentives, a considerable number of EVs could provide vital support to holding the load and improving operating flexibility. A market-based modeling framework that incorporates the decentralized decision-making of EV drivers over coupled transportation and distribution networks is missing in the context of incentivizing EVs for DSs load pickup. We propose a network equilibrium model that integrates market clearing in DSs and traffic flow balance in transportation systems. This model captures the decentralized interactions between key stakeholders in transportation and distribution networks as well as the spatial distribution of EV traffic in response to endogenously determined incentive signals. To mitigate the computational challenges brought by the non-convex network equilibrium model, we develop an equivalent convex reformulation with guaranteed global convergence. Numerical studies are conducted to demonstrate the effectiveness of the proposed model and computational performance. The proposed method could provide a fundamental tool for analyzing interdependent transportation and distribution networks coupled by charging facilities and EVs.

More specifically, the contribution of the proposed model is twofold.

- First, unlike studies that haven't considered transportation system requirements for EV participation in power system support, we propose a network equilibrium model that captures the complex interactions between key stakeholders in both distribution and transportation systems. Also, the proposed model endogenously determines the incentives of EV grid service and the corresponding EV traffic flow distribution. Such a model allows for rigorous analyses on transportation-power interdependence and the spatial-temporal value of EVs on DS load pickup.

- Second, we propose an exact convex reformulation of the network equilibrium model with a guaranteed global convergence property. This model does not rely on the iterative bidding strategies of market-based approaches. The convex reformulation in this paper can be

30

solved by a commercial nonlinear solver to the global optimum without convergence issue. In addition, we provide a reformulation strategy to handle network equilibrium models incorporating spatio-temporal clearing conditions on EV traffic flow in transportation systems as well as the clearing conditions on energy exchange between the stakeholders in DSs to quantify EV incentives.

The following list provides the definition of all the notations and indices used for the problem modeling in this chapter.

Sets and Indices

- $\mathcal{A}$: Set of transportation links, indexed by a

- $\mathcal{E}$: Set of EV groups indexed by e
  - $\mathcal{E}^{\tau}$: set of group e EVs arriving at CSs at time τ

- $\mathcal{I}$: Set of distribution system nodes, indexed by i or j
  - $\mathcal{I}^{\text{CS}}$: set of CS nodes
  - $\mathcal{I}^{\text{DG}}$: set of distributed generation nodes
  - $\mathcal{I}^{L}$: set of load nodes

- $\mathcal{L}$: Set of distribution lines indexed by l

- $\mathcal{N}$: Set of transportation nodes indexed by n or m
  - $\mathcal{R}$: set of vehicle departure nodes, indexed by r
  - $\mathcal{S}$: set of charging locations, indexed by s

- $\mathcal{T}$: Set of time periods, indexed by t or τ
  - $\mathcal{T}^{\text{arr}}$: Set of EVs' arrival time period at CSs

Parameters

- β_k/ϵ: Coefficients/error term in drivers' utility function

- ΔT: Time duration in one period (e.g., 1 hour)

- ζ^e: Battery capacity degradation rate of group e EVs

- $\lambda_{l,t}$: Binary indicator of the status of line l at time t

- $\omega_{i,t}$: Weights of load-pickup priority at node i and time t

- A: Transportation node-link incidence matrix

- $C_i(\cdot)$: ost of energy production of DG i

- Cap^e: Total nominal battery capacity of group e EVs

- $\mathrm{Cap}^{\mathrm{end},e}$: Normalized battery capacity at the end of life for group e EVs

- $C^{\mathrm{rep},e}$: Replacement cost of the battery for group e EVs

- $C^{\mathrm{res},e}$: Residual battery value of group e EVs

- $d^{\mathrm{shelf},e}$: Shelf degradation of group e EVs

- E_{rs}: OD incidence vector of OD pair rs

- $\mathrm{FN}_l/\mathrm{TN}_l$: Start/end nodes of line l

- K: A large value for relaxing constraints

- $\mathrm{LF}_{l,i}/\mathrm{LT}_{l,i}$: Incidence matrices with element l, i: equals to 1 if line l starts/connects from/to node i and zero otherwise

- $\bar{P}_{i,t}^d/\bar{Q}_{i,t}^d$: Maximum expected active/reactive load demand at node i and time t

- $\bar{P}_{r,e}^{\mathrm{ch}}/\bar{P}_{r,e}^{\mathrm{dch}}$: Maximum charge/discharge rate of group e EVs departing from r

- Q_r^e: Departing flow at location r of group e EVs

- $\bar{q}_{rs}^\tau$: Conventional vehicles travel demand from node r to node s at time τ

- r_l/x_l: Resistance/reactance of line l

- S^{base}: The nominal apparent power of the DS

- S_l^{max}: Maximum apparent power of line l

- $\text{SOC}_{r,e}^{\text{arr}}/\text{SOC}_{r,e}^{\text{dep}}$: Arrival/minimum required departure SOC of group e EVs departing from node r

- $\underline{\text{SOC}}^e/\overline{\text{SOC}}^e$: Minimum/maximum SOC permissible for group e EVs

- $tt_a(\cdot)$: Link travel time function of link a

- $T_{r,e}^{\text{arr}}/T_{r,e}^{\text{dep}}$: Arrival/departure time of group e EVs to/from CSs traveling from r

- $U_{rs}^e(.)$: Utility function for group e EVs on route rs

- $V_i^{\text{min}}/V_i^{\text{max}}$: Minimum/maximum voltage at node i

Variables

- α_{rs}^e: Incentives for group e EVs choosing CS s from r

- η_{rs}^τ: The dual variable for vehicle flow conservation

- μ/ν: Dual variables of the market clearing constraints in the reformulated problem

- $\rho_{i,t}$: Electricity price at node i and time t

- $C_{i,r,t}^{\text{deg},e}$: Degradation cost of group e EVs traveling from r to CS i during t

- $\mathrm{cap}_{i,r,t}^{\mathrm{loss},e}$: Reduced battery capacity of group e EVs departing from r at CS i during t due to degradation

- $d_{i,r,t}^{e}$: Actual battery degradation of group e EVs at CS $i(s)$ departing from r during t

- $d_{i,r,t}^{\mathrm{cycle},e}$: Battery cycle degradation of group e EVs departing from r at CS i during t

- $p_{i,r,t}^{e}$: Aggregated energy charged/discharged of group e EVs at CS $i(s)$, traveling from r at time t

- $p_{i,t}^{d}/q_{i,t}^{d}$: Active/reactive load demand at node i and time t

- $p_{i,t}^{s}/q_{i,t}^{s}$: Active/reactive power supply at node i and time t

- $p_{i,t}^{\mathrm{CS}}$: Aggregated energy discharged at CS $i(s)$ at time t (negative means energy charged)

- $p_{i,t}^{\mathrm{DG}}$: Active power generation of DG at node i and time t

- $pf_{l,t}/qf_{l,t}$: Active/reactive power flow on line l at time t

- $q_{ri}^{\prime e}/q_{rs}^{e}$: EVs from group e departing from r demanded at/traveling to CS $i(s)$

- $\mathrm{soc}_{i,r,t}^{e}$: SOC of group e EVs departing from r at CS $i(s)$ and time t

- tt_{rs}: Travel time between locations r and s

- v_{a}^{τ}: Total traffic flow on link a at time step τ

- $v_{i,t}$: Squared voltage magnitude at node i and time t

- $\bar{x}_{rs}/x_{rs}$: Link traffic flow of conventional/electric vehicles from r to s

- $z_{i,r,t}^{e}$: Intermediate variable to represent $p_{i,r,t}^{e}$

Modeling Overview

Stressed conditions may potentially lead to more severe power outages without proper considerations. One of the top priorities of DSOs is to ensure the reliability of DSs so that stressed conditions require effective response to alleviate load shedding. As for CSAs and DGs, they can gain extra revenue due to supplying power effectively over time and space during these stressed conditions. Similarly, for EV drivers, they can strategically choose charging locations to potentially earn extra income for providing V2G services to mitigate the "stressed" conditions.

We aim to capture the interactions between four types of stakeholders in transportation and DSs, i.e., flexible DGs (e.g., diesel generators and gas turbines), DSO, CSA, and EV drivers, for modeling the load pickup in DSs that are operating under stressed conditions. To model coupled distribution and transportation systems, parameters from both systems are needed. However, we note that the parameters we used in our models, such as network parameters, travel demand, and charging behavior, are typical parameters used in distribution and transportation system modeling.

Fig. 4.1 summaries the overall modeling framework, including the stakeholders' objectives, main decision variables, and their interactions. DSO purchases energy from DGs and CSA to maximize load pickup and minimize its costs; DGs aim to maximize their profits by selling the generated energy to the DS. On the other hand, the CSA maximizes its profit by managing EV charging and energy exchange with the DSO. Note that CSA can either purchase energy from the system (if it is required to charge the EVs) or provide energy to DSO whenever EVs want to participate in system support by discharging their stored energy similar to energy storage systems [76]. The EVs' charging flexibility will determine the incentives they receive. A market clearing is enforced on the energy exchange in the system which requires the supplied energy by CSA and DGs to be equal to the energy demanded by DSs (including load pickup and charging demand). The other main interaction is between the EV owners and CSA. EVs travel through transportation networks and
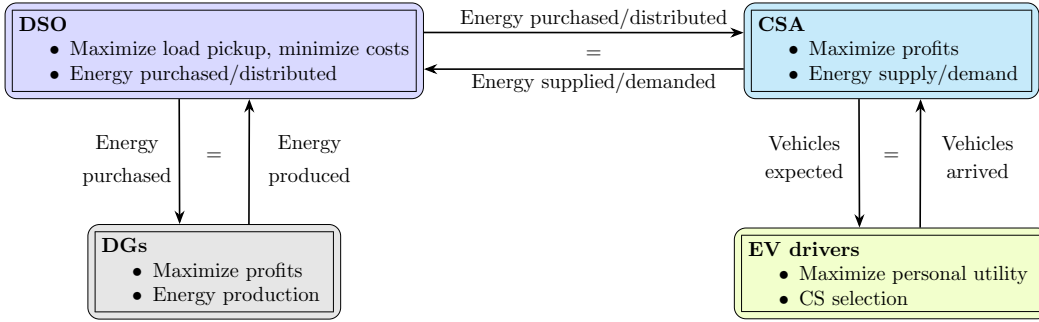
Figure 4.1: Stakeholders' modeling framework with their objectives and main decision variables

select a CS to maximize their individual utilities. A market clearing condition is considered on this interaction which balances the number of EVs selecting a CS with the number of EVs expected by CSA. This modeling framework mainly focuses on applications such as system analyses or policy-making instead of real-time operational decision-making. The proposed models could be adopted by government agencies for urban planning and regulations on EVs' participation in grid services. They can also be used by utility companies to understand the spatial-temporal capacity of EVs in DS support and the required spatial-temporal incentives considering individual EV's behavior. The following section will present the mathematical modeling of each stakeholder and their interactions.

Mathematical Modeling

In this section, we present the mathematical formulations of the proposed network equilibrium models in a coupled distribution and transportation system presented in Fig. 4.1. We first outline the decentralized decision making of each stakeholder in the network framework. Second, we formulate the clearing conditions to model their interactions and interpret their correspondence to energy price and charging incentives.

DG Owners Modeling

Each DG i ($\in \mathcal{I}^{DG}$) determines its generation quantity $p_{i,t}^{DG}$ for each time step t ($\in \mathcal{T}$) to optimize its profits. Because individual DG generation capacity is limited and below the threshold of the DSO dispatch, we assume DG owners are perfectly competitive and do not have the market power to influence the locational electricity prices $\rho_{i,t}$. Therefore, the decision making of all DG owners can be aggregated into a single optimization problem, as formulated in model (4.1).

$$\max_{\boldsymbol{p}^{DG} \geq \boldsymbol{0}} \sum_{i \in \mathcal{I}^{DG}} \sum_{t \in \mathcal{T}} \left(\rho_{i,t} p_{i,t}^{DG} - C_i(p_{i,t}^{DG}) \right) \tag{4.1a}$$

$$\text{s.t. } \underline{P}_{i,t}^{DG} \leq p_{i,t}^{DG} \leq \bar{P}_{i,t}^{DG}, \ \forall i \in \mathcal{I}^{DG}, t \in \mathcal{T}. \tag{4.1b}$$

Objective (4.1a) maximizes the profits of DG owners calculated as the total revenue $\sum \rho_{i,t} p_{i,t}^{DG}$ subtracting the total production costs $\sum_{i \in \mathcal{I}^{DG}} \sum_{t \in \mathcal{T}} C_i(p_{i,t}^{DG})$. We assume $C_i(\cdot)$ to be a convex function with respect to $p_{i,t}^{DG}$ [77], with different cost parameters for different DGs. This implies a non-decreasing marginal cost. Constraint (4.1b) determines the upper and lower bounds of power generation at DG node i for time t. For the cases when DGs can be disconnected from the systems, $\underline{P}_{i,t}^{DG} = 0$.

DSO Modeling

One of the key responsibilities of a DSO is to maintain services in stressed conditions. Given different characteristics of the loads (e.g., hospital, emergency responses) and limited resources available, the DSO may need to prioritize the load pickup procedures. We assume that the DSO intends to maximize the importance of loads being served within the system while minimizing the

cost of energy purchased, which can be formulated in the model (4.2).

$$\max_{\substack{\boldsymbol{p^d}, \boldsymbol{v} \geq 0, \\ \boldsymbol{p^s}, \boldsymbol{pf}, \boldsymbol{qf}}} \quad \sum_{i \in \mathcal{I}^L} \sum_{t \in \mathcal{T}} \omega_{i,t} p_{i,t}^d - \sum_{i \in \mathcal{I}^{\mathrm{DG}} \cup \mathcal{I}^{\mathrm{CS}}} \sum_{t \in \mathcal{T}} \rho_{i,t} p_{i,t}^s \tag{4.2a}$$

$$\text{s.t.} \quad \sum_{l \in \mathcal{L}} pf_{l,t} \cdot \mathrm{LT}_{l,i} - \sum_{l \in \mathcal{L}} pf_{l,t} \cdot \mathrm{LF}_{l,i} = p_{i,t}^d - p_{i,t}^s, \ \forall i \in \mathcal{I}, t \in \mathcal{T} \tag{4.2b}$$

$$\sum_{l \in \mathcal{L}} qf_{l,t} \cdot \mathrm{LT}_{l,i} - \sum_{l \in \mathcal{L}} qf_{l,t} \cdot \mathrm{LF}_{l,i} = q_{i,t}^d - q_{i,t}^s, \ \forall i \in \mathcal{I}, t \in \mathcal{T} \tag{4.2c}$$

$$0 \leq p_{i,t}^d \leq \bar{P}_{i,t}^d, \ \forall i \in \mathcal{I}^l, t \in \mathcal{T} \tag{4.2d}$$

$$q_{i,t}^d = (\bar{Q}_{i,t}^d / \bar{P}_{i,t}^d) \cdot p_{i,t}^d, \ \forall i \in \mathcal{I}^l, t \in \mathcal{T} \tag{4.2e}$$

$$pf_{l,t}^2 + qf_{l,t}^2 \leq \lambda_{l,t} \cdot (S_l^{\max})^2, \ \forall l \in \mathcal{L}, t \in \mathcal{T} \tag{4.2f}$$

$$v_{\mathrm{FN}_l,t} - v_{\mathrm{TN}_l,t} \leq (1 - \lambda_{l,t}) \cdot K + 2 \cdot (r_l \cdot pf_{l,t} + x_l \cdot qf_{l,t}), \forall l \in \mathcal{L}, t \in \mathcal{T} \tag{4.2g}$$

$$v_{\mathrm{FN}_l,t} - v_{\mathrm{TN}_l,t} \geq (\lambda_{l,t} - 1) \cdot K + 2 \cdot (r_l \cdot pf_{l,t} + x_l \cdot qf_{l,t}), \forall l \in \mathcal{L}, t \in \mathcal{T} \tag{4.2h}$$

$$(V_i^{\min})^2 \leq v_{i,t} \leq (V_i^{\max})^2, \ \forall i \in \mathcal{I}, t \in \mathcal{T}. \tag{4.2i}$$

Objective (4.2a) maximizes the weighted sum of load demand $\sum_{i \in \mathcal{I}^l} \sum_{t \in \mathcal{T}} \omega_{i,t} p_{i,t}^d$, where the weights $\omega_{i,t}$ determine the priority of the loads; $\sum_{i \in \mathcal{I}^{\mathrm{DG}} \cup \mathcal{I}^{\mathrm{CS}}} \sum_{t \in \mathcal{T}} \rho_{i,t} p_{i,t}^s$ is the cost of energy purchased from DG/CSA, who want to participate in the system support services. Operational constraints are formulated in (4.2b)-(4.2i), which are adapted based on the Dist-Flow equations proposed in [78] and later adopted in [50, 79]. Active and reactive power flow balances are modeled in (4.2b) and (4.2c), respectively. Constraint (4.2d) limits the served load demand to be less than the expected load demand at each node. Constraint (4.2e) maintains the same power factor for the restored loads as the expected loads. Constraint (4.2f) limits power flow not exceeding line capacity considering binary line status $\lambda_{l,t}$, with 0 indicating line outage. Constraints (4.2g) and (4.2h) calculate the voltage at each node. K is a big number to ensure that when line l is discon-

nected at t (i.e., $\lambda_{l,t} = 0$), the voltages of FN_l and TN_l are independent. Constraint (4.2i) defines the acceptable voltage range at each node.

CSA Modeling

There could be different market settings for CS competition, including oligopoly and perfect competition. In this paper, we assume CSs compete in a perfectly competitive market because of two main reasons. First, the charging service is a homogeneous product. Different brands/stations can hardly differentiate their services besides location and charging time. Therefore, for the same location and same charging time, if a station sets a price slightly higher than the other, no customers will likely be attracted to that CS. This phenomenon has been widely observed in gas station competition, where stations at the same intersection will have identical prices. Second, there are usually many CS providers who are not coordinated with each other to strategically set their prices. Therefore, each CS provider may not have the market power to strategically influence the market prices. Perfect competition assumption has been adopted in EV charging literature [39, 80, 81].

Due to the challenges of communicating and controlling EVs/CSs individually for DSO, a CSA is typically needed to coordinate the power transactions between all CSs and DS. The CSA aims to maximize its profits [82] while maintaining the required charging demand of EVs. The decision making of the CSA is formulated in model (4.3).

$$\max_{\boldsymbol{p}^{\mathrm{CS}},\boldsymbol{q}',\boldsymbol{soc}} \quad \sum_{i\in\mathcal{I}^{\mathrm{CS}}}\sum_{t\in\mathcal{T}}\rho_{i,t}p_{i,t}^{\mathrm{CS}} - \sum_{r\in\mathcal{R}}\sum_{i\in\mathcal{I}^{\mathrm{CS}}}\sum_{e\in\mathcal{E}}\alpha_{rs}^{e}q_{ri(s)}^{\prime e} - \sum_{i\in\mathcal{I}^{\mathrm{CS}}}\sum_{r\in\mathcal{R}}\sum_{t\in\mathcal{T}}\sum_{e\in\mathcal{E}}C_{i,r,t}^{\mathrm{deg},e} \tag{4.3a}$$

$$\text{s.t.} \quad \mathrm{soc}_{i,r,t}^{e} = \mathrm{soc}_{i,r,t-1}^{e} - p_{i,r,t}^{e}/\mathrm{Cap}^{e}, \ \forall i\in\mathcal{I}^{\mathrm{CS}}, r\in\mathcal{R}, e\in\mathcal{E}, t\in(T_{r,e}^{\mathrm{arr}},T_{r,e}^{\mathrm{dep}}] \tag{4.3b}$$

$$q_{ri(s)}^{\prime e}\underline{\mathrm{SOC}}^{e} \le \mathrm{soc}_{i,r,t}^{e} \le q_{ri(s)}^{\prime e}\overline{\mathrm{SOC}}^{e}, \ \forall i\in\mathcal{I}^{\mathrm{CS}}, r\in\mathcal{R}, e\in\mathcal{E}, t\in[T_{r,e}^{\mathrm{arr}},T_{r,e}^{\mathrm{dep}}] \tag{4.3c}$$

$$\mathrm{soc}_{i,r,T_{r,e}^{\mathrm{arr}}}^{e} = q_{ri(s)}^{\prime e}\mathrm{SOC}_{r,e}^{\mathrm{arr}}, \ \forall i\in\mathcal{I}^{\mathrm{CS}}, r\in\mathcal{R}, e\in\mathcal{E} \tag{4.3d}$$

$$\mathrm{soc}_{i,r,T_{r,e}^{\mathrm{dep}}}^{e} \ge q_{ri(s)}^{\prime e}\mathrm{SOC}_{r,e}^{\mathrm{dep}}, \ \forall i\in\mathcal{I}^{\mathrm{CS}} r\in\mathcal{R}, e\in\mathcal{E} \tag{4.3e}$$

$$-q_{ri(s)}^{\prime e}\bar{P}_{r,e}^{\mathrm{ch}} \le p_{i,r,t}^{e} \le q_{ri(s)}^{\prime e}\bar{P}_{r,e}^{\mathrm{dch}} \ \forall i\in\mathcal{I}^{\mathrm{CS}}, r\in\mathcal{R}, e\in\mathcal{E}, t\in[T_{r,e}^{\mathrm{arr}},T_{r,e}^{\mathrm{dep}}] \tag{4.3f}$$

$$p_{i,t}^{\mathrm{CS}} = \sum_{r\in\mathcal{R}}\sum_{e\in\mathcal{E}}\frac{p_{i,r,t}^{e}}{S^{\mathrm{base}}}, \ \forall i\in\mathcal{I}^{\mathrm{CS}}, t\in[T_{r,e}^{\mathrm{arr}},T_{r,e}^{\mathrm{dep}}]. \tag{4.3g}$$

Objective (4.3a) maximizes the CSA's profits, which is calculated as revenue made by selling the electricity to the DSO $\sum_{i\in\mathcal{I}^{\mathrm{CS}}}\sum_{t\in\mathcal{T}}\rho_{i,t}p_{i,t}^{\mathrm{CS}}$ subtracting incentives $\sum_{r\in\mathcal{R}}\sum_{i\in\mathcal{I}^{CS}}\sum_{e\in\mathcal{E}}\alpha_{rs}^{e}q_{rs}^{\prime e}$ and battery degradation compensation $\sum_{i\in\mathcal{I}^{CS}}\sum_{e\in\mathcal{E}}\sum_{t\in\mathcal{T}}C_{i,r,t}^{\mathrm{deg},e}$ paid to EV drivers. Note that $p_{i,t}^{\mathrm{CS}}$ can have negative values representing that EVs are charging instead of discharging. In this case, $\sum_{i\in\mathcal{I}^{\mathrm{CS}}}\sum_{t\in\mathcal{T}}\rho_{i,t}p_{i,t}^{\mathrm{CS}}$ would be the cost for CSA to charge EVs. Power prices $\rho_{i,t}$ and EV incentives α_{rs}^{e} are endogenously determined by market in the modeling framework, as discussed in Section 4. We note that when an oligopolistic market setting is of interest, where private-owned CSs strategically adjust prices to compete for clients, one will need to explicitly consider prices as decisions of CS providers instead of using the market equilibrium prices. In addition, if one focuses on the dominant charging provider, if there exists one, a Stackelberg game-theoretical modeling framework is more appropriate. However, if the focus is on the optimal pricing strategies of individual private-owned CSs, they can be usually studied individually. In this case, it may not be necessary to consider the entire transportation and DSs as the way we did in this study. For example, authors in [83] and [84] modeled the interaction of EVs with CS proposing novel algorithms for determining the payment exchanges among them without considering coupled transportation

and power system requirements.

Constraints (4.3b)-(4.3g) specify EVs' SOC transition and requirements that the CSA needs to fulfill. We discretize EVs into different homogeneous groups e based on their travel and charging characteristics, including arriving/departing time $T_{r,e}^{\text{arr}}/T_{r,e}^{\text{dep}}$, and arriving/departing SOC $\text{SOC}_{r,e}^{\text{arr}}/\text{SOC}_{r,e}^{\text{dep}}$, meaning that EVs who have similar available battery SOC, charging demand and travel schedules are grouped together. Incentives α_{rs}^e depend on EV groups and will be endogenously determined by market. For example, an EV with high SOC^{arr}, low charging needs, long dwelling time, and connected to CS during periods when load-pickup services are needed will receive higher incentives. Constraint (4.3b) models the dynamics of the SOC of EVs from r at CS i. Constraint (4.3c) limits the maximum and minimum SOC of each EV group based on the drivers' desired SOC range. Constraints (4.3d) and (4.3e) specify the initial arrival SOC and minimum departure SOC for each EV group at charging location i. Constraint (4.3f) restricts the charging/discharging power of EVs at each time step t to be within a certain range based on battery/charger characteristics. We modeled the number of EVs demanded by CSA at each CS as variable $q_{ri(s)}^{\prime e}$. This variable plays an important role in coupling transportation and DS which is further discussed in Section 4. Constraint (4.3g) determines the total power supply/demand of CS $i \in \mathcal{I}^{\text{CS}}$ at time t by summing the normalized discharging/charging of EVs at each station.

Battery degradation by continuous charging and discharging of the battery is one of the main concerns discouraging drivers from participating in V2G services. Battery degradation consists of shelf and cycle degradation [85]. In this paper, the Ah-throughput counting model [86] is used to model the mentioned degradation types. The degradation cost of EVs $C_{i,r,t}^{\text{deg},e}$ is formulated in model (4.4), which is adapted from [50] to consider EV groups and time index.

$$z_{i,r,t}^e \geq p_{i,r,t}^e \ \forall i \in \mathcal{I}^{\text{CS}}, r \in \mathcal{R}, e \in \mathcal{E}, t \in \mathcal{T} \tag{4.4a}$$

$$z_{i,r,t}^e \geq -p_{i,r,t}^e \ \forall i \in \mathcal{I}^{\text{CS}}, r \in \mathcal{R}, e \in \mathcal{E}, t \in \mathcal{T} \tag{4.4b}$$

$$\text{cap}_{i,r,t}^{\text{loss},e} = \zeta^e \cdot z_{i,r,t}^e \cdot \Delta T, \ \forall i \in \mathcal{I}^{CS}, r \in \mathcal{R}, t \in [T_r^{\text{arr}}, T_{r,e}^{\text{dep}}] \tag{4.4c}$$

$$d_{i,r,t}^{\text{cycle},e} = \frac{\text{cap}_{i,r,t}^{\text{loss},e}}{1 - \text{Cap}^{\text{end},e}}, \ \forall i \in \mathcal{I}^{CS}, r \in \mathcal{R}, e \in \mathcal{E}, t \in [T_{r,e}^{\text{arr}}, T_{r,e}^{\text{dep}}] \tag{4.4d}$$

$$d_{i,r,t}^e = \max\{d_{i,r,t}^{\text{cycle},e}, d^{\text{shelf},e}\},$$
$$\forall i \in \mathcal{I}^{CS}, r \in \mathcal{R}, e \in \mathcal{E}, t \in [T_r^{\text{arr}}, T_{r,e}^{\text{dep}}] \tag{4.4e}$$

$$C_{i,r,t}^{\text{deg},e} = d_{i,r,t}^e (C^{\text{rep},e} - C^{\text{res},e})\text{Cap}^e,$$
$$\forall i \in \mathcal{I}^{CS}, r \in \mathcal{R}, e \in \mathcal{E}, t \in [T_r^{\text{arr}}, T_{r,e}^{\text{dep}}]. \tag{4.4f}$$

EV Drivers Modeling

We have modeled the charging schedule of EVs based on their SOC requirements as part of CSA responsibilities in (4.3). In this section, we will model the routing and charging location choices of decentralized EVs in transportation systems. The utility function U_{rs}^e of a driver in group e selecting station s from r is formulated in (4.5) [50, 67]. Without loss of generality, we assume that EV drivers make charging location choices based on four factors: locational attractiveness $\beta_{0,s}$, travel time $-\beta_1 tt_{rs}$, charging cost/revenue from charging/discharging $\beta_2 \alpha_{rs}^e$, and a random term ϵ. Other exogenous factors can also be included in (4.5) without affecting the modeling and computational strategies proposed in this paper. For example, different strategies of CSs for attracting EVs can be modeled as a part of locational attractiveness ($\beta_{0,s}$) to reflect different levels of convenience which will influence the incentive offered by each CS. We can also model CSs with different characteristics at the same location by adding dummy nodes (s') to the main node

(s), which are connected by links with zero travel time, as illustrated in Fig. 4.2.

$$U_{rs}^e = \beta_{0,s} - \beta_1 tt_{rs} + \beta_2 \alpha_{rs}^e + \epsilon. \tag{4.5}$$
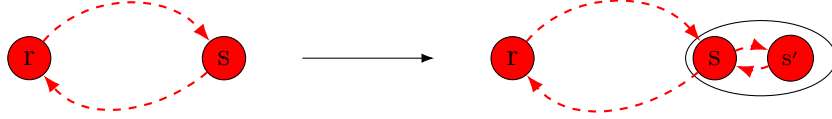
Figure 4.2: Dummy node illustration

From an environmental perspective, incentives should not encourage EVs to take long trips just for charging or grid support. In the proposed utility function (4.5), an EV chooses a charging location and a route to maximize utilities, considering the total travel time and charging cost. Traveling a longer distance may consume more time, especially considering potential traffic congestion. Therefore, our model has considered the fact that EVs prefer to receive/provide service in nearby CSs when holding other factors constant. If the utility coefficient of the travel time is sufficiently large, no EV will seek lower charging prices or higher service incentives by traveling a longer distance. To explicitly restrict EVs from making long-distance travel for charging/discharging services, one can directly limit the candidate CSs to be within a range of the EV origins. As an alternative solution, one can also explicitly maximize the total system welfare, including congestion/environmental impacts, with an upper-level optimization to decide the optimal incentives for the societal benefits. Optimizing system welfare considering environmental impacts is beyond the scope of this study and will be left for the future.

The destination choice of EVs (q_{rs}^e) and path travel time (tt_{rs}) are coupled. On one hand, the CS selection of EV drivers impacts the travel demand distribution that will affect the travel time for all drivers. On the other hand, the CS selection partially depends on travel time tt_{rs} (see (4.5)).

To capture these couplings, we adopt the CDA model [87] to model their destination choices and route choices simultaneously, as formulated in (4.6). Notice that $\forall \tau \in \mathcal{T}^{\mathrm{arr}}$, we will solve CDA_τ for the traffic pattern at time τ.

$$\min_{\boldsymbol{x},\bar{\boldsymbol{x}},\boldsymbol{q} \geq \boldsymbol{0}} \quad \sum_{a \in \mathcal{A}} \int_0^{v_a^\tau} tt_a(u)\mathrm{d}u + \frac{1}{\beta_1} \sum_{r \in \mathcal{R}, s \in \mathcal{S}} \sum_{e \in \mathcal{E}^\tau} q_{rs}^e \left(\ln q_{rs}^e - 1 - \beta_2 \alpha_{rs}^e - \beta_{0,s}\right) \tag{4.6a}$$

$$\text{s.t.} \quad \boldsymbol{v}^\tau = \sum_{r \in \mathcal{R}, s \in \mathcal{S}} \boldsymbol{x}_{rs}^\tau + \sum_{r \in \bar{\mathcal{R}}, s \in \bar{\mathcal{S}}} \bar{\boldsymbol{x}}_{rs}^\tau, \ \forall \tau \in \mathcal{T}^{\mathrm{arr}} \tag{4.6b}$$

$$(\boldsymbol{\eta}_{rs}^\tau) \quad A\boldsymbol{x}_{rs}^\tau = \sum_{e \in \mathcal{E}^\tau} q_{rs}^e E_{rs}, \ \forall r \in \mathcal{R}, s \in \mathcal{S}, \tau \in \mathcal{T}^{\mathrm{arr}} \tag{4.6c}$$

$$A\bar{\boldsymbol{x}}_{rs}^\tau = \bar{q}_{rs}^\tau E_{rs}, \ \forall r \in \bar{\mathcal{R}}, s \in \bar{\mathcal{S}}, \tau \in \mathcal{T}^{\mathrm{arr}} \tag{4.6d}$$

$$\sum_{s \in \mathcal{S}} q_{rs}^e = Q_r^e, \forall r \in \mathcal{R}, e \in \mathcal{E}^\tau. \tag{4.6e}$$

The objective function in (4.6a) consists of two parts: the first part is the summation of the area under all the link travel cost functions $tt_a(\cdot)$ (e.g., Bureau of Public Roads (BPR) function)[2]; the second being the entropy of traffic distribution $q_{rs}^e(\ln q_{rs}^e - 1)$ and utility terms (excluding time) in (4.5) [88]. Objective (4.6a) is constructed to guarantee that the optimal solutions of (4.6) are consistent with the first Wardrop principal [89] and the multinomial logit destination choice assumption. For technical details to prove this claim, one can refer to [87]. Constraint (4.6b) calculates link flows by summing link flows of EVs (x_{rs}^τ) and conventional vehicles ($\bar{x}_{rs}^\tau$) travelling at the same time period τ over all origin and destination pairs. Constraints (4.6c-4.6d) are the vehicle flow conservation at each node for EV travel demand q_{rs}^e and conventional vehicle travel demand $\bar{q}_{rs}^\tau$, respectively. Constraint (4.6e) guarantees the summation of EV traffic flow distribution to each s (q_{rs}^e) equals the total EV travel demand from r, (Q_r^e). The equilibrium travel time for each OD pair

---

[2]This model is general and able to include the situation when transportation links are disrupted using a reduced link capacity or significantly large free-flow travel time in the travel cost functions $tt_a(\cdot)$.

rs can be calculated as $tt_{rs} \doteq \eta^{\tau}_{rs,r} - \eta^{\tau}_{rs,s}$, where $\eta^{\tau}_{rs,i}$ is the dual variable for constraint (4.6c).

Market Clearing Conditions

In a stable market, the power purchased by DSO needs to be balanced with locational power generation. In addition, EV demanded by CSA at each CS needs to be balanced with EV traveling to that station. The hourly market clearing conditions can be stated as (4.7). (4.7a) guarantees that the total energy purchased by DSO is equal to the total energy generated at each node including DGs and CSs. (4.7b) enforces the balance between EV flow of group e demanded and supplied at each location s from r. This equation couples the traffic flow (q^e_{rs}) determined from the CDA problem (4.6) with the number of EVs (q'^e_{rs}) demanded in the CSA modeling (4.3).

$$(\rho_{i,t}) \qquad p^s_{i,t} = p^{DG}_{i,t} + P^{CS}_{i,t}, \ \forall i \in \mathcal{I}^{DG} \cup \mathcal{I}^{CS}, \ \forall t \in \mathcal{T} \qquad (4.7a)$$

$$(\alpha^e_{rs}) \qquad q'^e_{rs} = q^e_{rs}, \ \forall r \in \mathcal{R}, s \in \mathcal{S}, e \in \mathcal{E}. \qquad (4.7b)$$

Locational prices of electricity $\rho_{i,t}$ and EV incentives α^e_{rs} can be interpreted as dual variables for the market clearing conditions, respectively. The clearing conditions help us to model the interdependencies of both transportation and DSs along with the models defined in (4.1)~(4.6). Note that the CSA sells/purchases electricity to/from the DSO based on the electricity price ($\rho_{i,t}$). On the other hand, EVs will receive incentives (α^e_{rs}) from the CSA based on their participation in DS support and their charging requirements. Note that both incentives and energy prices are endogenously determined in the network equilibrium framework. The incentives could be negative if EVs need to charge a significant amount of energy while providing minimum services. In other words, the incentives can be interpreted as the net value of the system support service payments

subtracting charging costs.

Remark 1: In this paper, we use a Walras equilibrium concept [90], where pricing will dynamically be adjusted until supply and demand are balanced. In the proposed method, CSA does not assume how many EVs participate in the market. Instead, CSA will have its desired EV flow (i.e., demand) based on the EV incentives CSA needs to offer. On the other hand, EVs have no obligation to support the system, and they make decisions based on their charging needs and the provided incentives to maximize their utility. The decentralized decision making of individual EVs will determine the total EV supply at each location. EV incentives are endogenously determined by the market clearing conditions (4.7) rather than arbitrarily set by the operator. Therefore, the magnitude of incentives for providing grid services depends on the relationship between EV supply and demand. If the EV supply is less than the demand, EV incentives will increase. Since we assume that EVs make decisions to optimize their utilities, which include incentives and travel time, as long as the economic incentive is sufficiently large, more EVs will participate in system service. On the other hand, CSA aims to maximize their profits. Therefore, the EV demand will decrease if CSA needs to pay higher incentives to the EV drivers. Additionally, if the system operator imposes a higher penalty on load shedding, the locational demand of V2G services will increase, which will lead to a higher incentive. Then more EVs will be attracted to participate in the grid-service market.

Remark 2: The proposed modeling framework can be extended to consider the case where the CSA initiates contracts with DGs to purchase energy at a negotiated price. In our proposed method, the energy exchanges are modeled via power flow constraints and clearing conditions in the power balance. If CSA and DGs are involved in private contracts, we can define new variables for energy exchanges to model specific agreements between CSA and the DGs. In addition, we can add the cost/revenue terms to their objective functions based on the detailed pricing terms in their contract. While the prices/costs for the contracted energy transactions will be given exogenously based on

the contracts, the real-time market prices will still be determined by the current form of the clearing condition in (4.7). Therefore, from a computational perspective, the convex reformulation will still apply.

Remark 3: As mentioned previously, this modeling framework focuses on supporting system analyses and policy-making in a predefined stressed condition instead of real-time decision support facing uncertainties. Therefore, the variables in our models are all under that specific scenario. However, these models can be extended to consider various sources of uncertainties applying stochastic programming techniques for the decision-making of each stakeholders. One can consider the uncertainties as different scenarios using the sample average approximation (SAA) method [91]. The compact form of the model remains the same except for augmenting variables to be scenario-dependent. Therefore, the proposed solution method still applies, despite more variables and constraints in the equilibrium model.

Convex Reformulation

The decision making of each stakeholder and market clearing conditions presented in Sections 4∼4 are interdependent and need to be solved simultaneously to achieve the equilibrium solutions. However, we note that the optimization problems of decision makers have a special structure that the objective functions (i.e., functions (4.1a), (4.2a), (4.3a), and (4.6a)) are convex and separable once ρ and α are fixed. In addition, the constraint sets of each stakeholder are independent and convex. We will leverage these characteristics to develop an equivalent convex reformulation, as illustrated in the remaining of this section.

Given any ρ and α, since models (4.1) ∼ (4.3) and (4.6) are completely separable, we can linearly combine models (4.1) ∼ (4.3) and (4.6), which leads to problem (4.8). In other words, the optimal

solutions of problem (4.8) will be identical with the optimal solutions to models (4.1) $\sim$ (4.3) and (4.6) given any ρ and α. This is more formally stated in Lemma 1. Note that we have scaled each objection functions and grouped the terms with energy price (ρ) and incentives (α) in the objective function (4.8).

Lemma 1 (Combined Problem for Models (4.1) $\sim$ (4.3) and (4.6)). *Given any ρ and α, the optimal solutions of problem (4.8) are identical with the optimal solutions of models (4.1) $\sim$ (4.3) and (4.6), when models (4.1) $\sim$ (4.3) and (4.6) are solved individually with ρ and α.*

Proof. Lemma 1 follows directly from the separable nature of models (4.1) $\sim$ (4.3) and (4.6) given ρ and α. $\qquad\qquad\qquad\qquad\qquad\qquad\qquad\qquad\qquad\qquad\qquad\qquad\qquad\qquad\square$

$$
\begin{aligned}
\max_{\substack{(p^d, p^{DG}, v, x, \bar{x}, q, q') \geq 0, \\ p^s, pf, qf, p^{CS}, soc}} & \sum_{t \in \mathcal{T}} \left[\sum_{i \in \mathcal{I}^L} \omega_{i,t} p_{i,t}^d - \sum_{i \in \mathcal{I}^{DG}} C(p_{i,t}^{DG}) - \sum_{i \in \mathcal{I}^{CS}, r \in \mathcal{R}, e \in \mathcal{E}} C_{i,r,t}^{deg,e} \right] \\
& - \sum_{\tau \in \mathcal{T}^{arr}} \sum_{e \in \mathcal{E}^\tau} \sum_{r \in R, s \in S} \frac{q_{rs}^e}{\beta_2} \left(\ln q_{rs}^e - 1 - \beta_0^s \right) - \frac{\beta_1}{\beta_2} \sum_{\tau \in \mathcal{T}^{arr}, a \in \mathcal{A}} \int_0^{v_a^\tau} tt_a(u) du \\
& + \sum_{t \in \mathcal{T}} \sum_{i \in \mathcal{I}^{CS} \cup \mathcal{I}^{CS}} \rho_{i,t} \left(-p_{i,t}^s + p_{i,t}^{DG} + P_{i,t}^{CS} \right) + \sum_{r \in \mathcal{R}, s \in \mathcal{S}, e \in \mathcal{E}} \alpha_{rs}^e \left(q_{rs}^e - q_{rs}^{'e} \right) \qquad (4.8) \\
& \text{s.t} \quad (6.1b), (4.2b) \sim (4.2i), (4.3b) \sim (4.3g), (4.4), (4.6b) \sim (4.6e).
\end{aligned}
$$

We note that to achieve equilibrium, ρ and α cannot take any arbitrary values. They need to guarantee the market clearing conditions (6.6). To calculate the market clearing prices/incentives ρ^* and α^*, we introduce another convex optimization problem, as shown in (4.9). The only difference between model (4.9) and (4.8) is that the objective function in model (4.9) does not have terms $\sum_{t \in \mathcal{T}} \sum_{i \in \mathcal{I}^{CS} \cup \mathcal{I}^{CS}} \rho_{i,t}(-p_{i,t}^s + p_{i,t}^{DG} + P_{i,t}^{CS})$ and $\sum_{r \in \mathcal{R}, s \in \mathcal{S}, e \in \mathcal{E}} \alpha_{rs}^e(q_{rs}^e - q_{rs}^{'e})$ but add market clearing (4.7)

48

as constraint in model (4.9). We state that the optimal dual multipliers of constraint (6.6) in model (4.9), denoted as $\boldsymbol{\mu}^*$ and $\boldsymbol{\nu}^*$, will be the market clearing prices/incentives of the original problem in Lemma 2.

$$
\max_{\substack{(\boldsymbol{p^d},\boldsymbol{p^{DG}},\boldsymbol{v},\boldsymbol{x},\boldsymbol{\bar{x}},\boldsymbol{q},\boldsymbol{q'})\geq\boldsymbol{0}, \\ \boldsymbol{p^s},\boldsymbol{pf},\boldsymbol{qf},\boldsymbol{p},\boldsymbol{p^{CS}},\boldsymbol{soc}}} \sum_{t\in\mathcal{T}} \left[\sum_{i\in\mathcal{I}} \omega_{i,t} p_{i,t}^d - \sum_{i\in\mathcal{I}^{DG}} C(p_{i,t}^{DG}) - \sum_{i\in\mathcal{I}^{CS},r\in\mathcal{R},e\in\mathcal{E}} C_{i,r,t}^{deg,e} \right]
$$
$$
- \sum_{\tau\in\mathcal{T}^{arr}} \sum_{e\in\mathcal{E}^{\tau}} \sum_{r\in R,s\in S} \frac{q_{rs}^e}{\beta_2} \left(\ln q_{rs}^e - 1 - \beta_0^s\right) - \frac{\beta_1}{\beta_2} \sum_{\tau\in\mathcal{T}^{arr},a\in\mathcal{A}} \int_0^{v_a^{\tau}} tt_a(u)du \qquad (4.9)
$$
$$
\text{s.t} \quad (4.1b),(4.2b)\sim(4.2i),(4.3b)\sim(4.3g),(4.4),(4.6b)\sim(4.6e),(4.7).
$$

Lemma 2 (Market Clearing Prices and Dual Multipliers). *The optimal dual multipliers $\boldsymbol{\mu}^*$ and $\boldsymbol{\nu}^*$ of constraint (4.7) in model (4.9) are market clearing prices/incentives corresponding to market clearing conditions (4.7) in the original problem.*

Proof. (A) We rewrite model (4.9) as maxmin problem (4.10), in which we relax constraint (4.7) using method of Lagrange multipliers. Since $\boldsymbol{\mu}$ and $\boldsymbol{\nu}$ can take any real values when minimizing the objective function, model (4.10) enforces $-p_{i,t}^s + p_{i,t}^{DG} + P_{i,t}^{CS} = 0$ and $q_{rs}^e - q_{rs}^{\prime e} = 0$; otherwise objective function of (4.10) will achieve $-\infty$ by selecting appropriate $\mu_{i,t}$ and ν_{rs}^e and cannot be a maximum. This is why model (4.9) and the maxmin problem (4.10) are equivalent.

$$\max_{\substack{(\boldsymbol{p^d},\boldsymbol{p^{DG}},\boldsymbol{v},\boldsymbol{x},\boldsymbol{\bar{x}},\boldsymbol{q},\boldsymbol{q'})\geq 0,\ \boldsymbol{\mu},\boldsymbol{\nu} \\ \boldsymbol{p^s},\boldsymbol{pf},\boldsymbol{qf},\boldsymbol{p^{CS}},\mathbf{soc}}} \min \sum_{t\in\mathcal{T}} \left[\sum_{i\in\mathcal{I}^L} \omega_{i,t} p_{i,t}^d - \sum_{i\in\mathcal{I}^{DG}} C(p_{i,t}^{DG}) - \sum_{i\in\mathcal{I}^{CS},r\in\mathcal{R},e\in\mathcal{E}} C_{i,r,t}^{deg,e} \right]$$

$$-\sum_{\tau\in\mathcal{T}^{arr}}\sum_{e\in\mathcal{E}^\tau}\sum_{r\in R,s\in S} \frac{q_{rs}^e}{\beta_2}\left(\ln q_{rs}^e - 1 - \beta_0^s\right) - \frac{\beta_1}{\beta_2}\sum_{\tau\in\mathcal{T}^{arr},a\in\mathcal{A}} \int_0^{v_a^\tau} tt_a(u) du$$

$$+\sum_{t\in\mathcal{T}}\sum_{i\in\mathcal{I}^{CS}\cup\mathcal{I}^{CS}} \mu_{i,t}\left(-p_{i,t}^s + p_{i,t}^{DG} + P_{i,t}^{CS}\right) + \sum_{r\in\mathcal{R},s\in\mathcal{S},e\in\mathcal{E}} \nu_{rs}^e\left(q_{rs}^e - q_{rs}^{'e}\right) \qquad (4.10)$$

$$\text{s.t} \quad (4.1b), (4.2b)\sim(4.2i), (4.3b)\sim(4.3g), (4.4), (4.6b)\sim(4.6e).$$

(B) Since model (4.9) is a convex optimization problem and there exists at least one strictly feasible solutions, based on Slater's condition, strong duality holds. Therefore, the optimum of minmax problem (4.11) is identical to the optimum of maxmin problem (4.10). Since model (4.8) and model (4.11) are identical if we let $\boldsymbol{\rho} = \boldsymbol{\mu}^*$ and $\boldsymbol{\alpha} = \boldsymbol{\nu}^*$, the primal solutions of model (4.10) will also maximize (4.8). Based on Lemma 1, the primal solutions will also optimize models (4.1) $\sim$ (4.3) and (4.6), which means they are also the optimal decisions from each stakeholders given $\boldsymbol{\mu}$ and $\boldsymbol{\nu}$.

$$\min_{\boldsymbol{\mu},\boldsymbol{\nu}} \max_{\substack{(\boldsymbol{p^d},\boldsymbol{p^{DG}},\boldsymbol{v},\boldsymbol{x},\boldsymbol{\bar{x}},\boldsymbol{q},\boldsymbol{q'})\geq 0, \\ \boldsymbol{p^s},\boldsymbol{pf},\boldsymbol{qf},\boldsymbol{p^{CS}},\mathbf{soc}}} \sum_{t\in\mathcal{T}} \left[\sum_{i\in\mathcal{I}^L} \omega_{i,t} p_{i,t}^d - \sum_{i\in\mathcal{I}^{DG}} C(p_{i,t}^{DG}) - \sum_{i\in\mathcal{I}^{CS},r\in\mathcal{R},e\in\mathcal{E}} C_{i,r,t}^{deg,e} \right]$$

$$-\sum_{\tau\in\mathcal{T}^{arr}}\sum_{e\in\mathcal{E}^\tau}\sum_{r\in R,s\in S} \frac{q_{rs}^e}{\beta_2}\left(\ln q_{rs}^e - 1 - \beta_0^s\right) - \frac{\beta_1}{\beta_2}\sum_{\tau\in\mathcal{T}^{arr},a\in\mathcal{A}} \int_0^{v_a^\tau} tt_a(u) du$$

$$+\sum_{t\in\mathcal{T}}\sum_{i\in\mathcal{I}^{CS}\cup\mathcal{I}^{CS}} \mu_{i,t}\left(-p_{i,t}^s + p_{i,t}^{DG} + P_{i,t}^{CS}\right) + \sum_{r\in\mathcal{R},s\in\mathcal{S},e\in\mathcal{E}} \nu_{rs}^e\left(q_{rs}^e - q_{rs}^{'e}\right) \qquad (4.11)$$

$$\text{s.t} \quad (4.1b), (4.2b)\sim(4.2i), (4.3b)\sim(4.3g), (4.4), (4.6b)\sim(4.6e).$$

Because of (A) and (B), the optimal dual multipliers $\boldsymbol{\mu}^*$ and $\boldsymbol{\nu}^*$ of constraint (4.7) in model (4.9) are

market clearing prices/incentives corresponding to market clearing conditions (4.7) in the original problem. □

Now, we can have the equivalent convex reformulation of the network equilibrium problems, as stated in Theorem 1.

Theorem 1 (Equivalent Convex Reformulation of Network Equilibrium Problems). *The optimal primal variables of convex model (4.9) and optimal dual variables of constraint (4.7) are the equilibrium solutions of the original equilibrium problem (i.e., models (4.1) $\sim$ (4.3), (4.6), and (4.7).*

Proof. Since the optimal dual multipliers μ^* and ν^* of constraint (6.6) in model (4.9) are market clearing prices/incentives based on Lemma 2, and the optimal prime variables of model (4.9) maximizes optimization problems (4.1) $\sim$ (4.3) and (4.6) when $\rho = \mu^*$ and $\alpha = \nu^*$ based on Lemma 1, solving model (6.7a) will recover optimal solutions and prices/incentives of the original equilibrium problem (i.e., models (4.1) $\sim$ (4.3), (4.6), and (4.7). □

Numerical Simulations

We will implement the models and reformulation techniques on two test systems for evaluating the potential impacts of EVs on DS support and draw system insights. Throughout this section, the term "node" is reserved to refer to the nodes of DS unless clarified. We implemented and solved our model on Pyomo 5.6.7 [92,93] and IPOPT 3.12.13 [94], respectively. All the experiments were run on a 3.6 GHz 9-Core Intel Core i9 with 64 GB of RAM, under UBUNTU 18.04.2.

Four-node Test System

We start with a four-node test system shown in Fig. 4.3. Nodes 2 and 3, representing CSs, are the connecting points between distribution and transportation systems. Nodes 2~4 are load nodes. Loads at node 3 have higher priority ($\omega_3 = 60$) compared to nodes 2 and 4 ($\omega_2 = \omega_4 = 50$). The daily trend of load demand is adopted from the PJM data set [95][3]. Assuming nodes have different user types (e.g., residential or industrial), we assigned 45 % of the total load to node 2, 35 % to node 3, and 20 % to node 4. The reported results in system pu are based on $S^{\text{base}} = 1000$ kVA. All the distribution lines have the same capacity of $S_l^{\max} = 2$ (pu). The capacity of all transportation links is 20 (vehicles/hour).
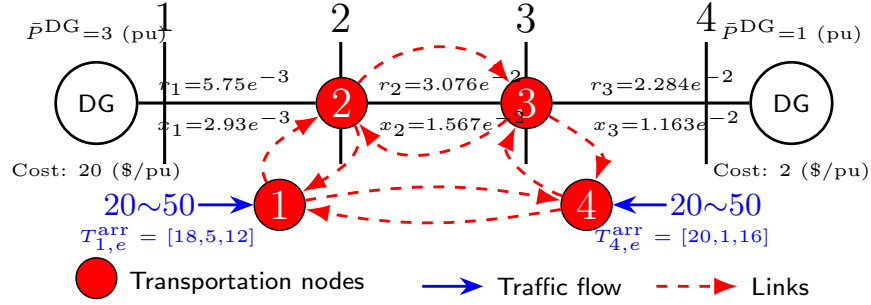
Figure 4.3: Four-node test system

The improvements in EV manufacturing shows that companies are developing EVs with higher battery capacities providing longer driving range [96]. Currently, Tesla offers the highest battery capacity on Model S with $\text{Cap} = 100$ kW, and a charging rate of 17.2 kWh [8]. In the future, EVs will have similar or higher capacities, and we assumed that EVs in our test system has the same characteristics as Tesla Model S.

EVs are in one of the three groups based on their SOC^{arr} ($\text{SOC}^{\text{arr}}_{r,e=1} = 0.2 \sim 0.4$, $\text{SOC}^{\text{arr}}_{r,e=2} = 0.4 \sim$

---

[3]The selected day is Sept. 2, 2021, from American Electric Power (AEP) zone

0.8, and $\mathrm{SOC}^{\mathrm{arr}}_{r,e=3} = 0.8 \sim 1$). In other words, EVs are groups based on their charging needs when they arrive at the CSs; group $e = 1$ having the highest and group $e = 3$ having the least charging requirements. The $\mathrm{SOC}^{\mathrm{arr}}$ of each group are selected from a random distribution in the defined ranges mentioned above [4]. We assume that EVs depart from the transportation nodes 1 and 4 with the incoming traffic selected from a normal distribution of integers in the range of $20 \sim 50$ EVs/hour. The arrival times of EVs are also from a random distribution at hours τ ($\in \mathcal{T}^{\mathrm{arr}}_{r,e}$) to either CSs. The generated random arrival times for EV groups are presented in Fig. 4.3. We consider losing line (1–2) unexpectedly at $t = 10$, disconnecting the DG at node 1 from the system, which has a higher production capacity. The line comes back on at $t = 20$. We consider two levels of $\mathrm{SOC}^{\mathrm{dep}} = 0.7$ and 0.5 to investigate the effects of different EV charging needs on DS support.

The load pickup graphs (Fig. 4.4) show that the system will firstly restore the high priority load at node 3 for both $\mathrm{SOC}^{\mathrm{dep}}$. With a lower $\mathrm{SOC}^{\mathrm{dep}}$, more low priority loads are picked up. The total load loss decrease from 3.822 pu to 2.651 pu when $\mathrm{SOC}^{\mathrm{dep}}$ decrease from 0.7 to 0.5. The power injection of CSs in Fig. 4.5a, 4.5b shows more participation of EVs in DS support during disruption periods with $\mathrm{SOC}^{\mathrm{dep}} = 0.5$ compared to $\mathrm{SOC}^{\mathrm{dep}} = 0.7$, because when EVs have lower charging demand, they are more flexible to charge/discharge.

Energy prices during the disruption increase drastically compared to normal periods for all the nodes (see Fig. 4.6a, 4.6b) because the system has to leverage more expensive energy sources during disruptions. By comparing the disruption periods for both $\mathrm{SOC}^{\mathrm{dep}}$ levels, we have slightly lower energy prices when EVs are more flexible to participate in restoring the load. Comparing Fig. 4.7a and Fig. 4.7b, EVs with lower required $\mathrm{SOC}^{\mathrm{dep}}$ receive higher incentives because they are more valuable for system support. In addition, we see higher incentives for group 2 departing from transportation node 1 than 4 because group 2 EVs departing from transportation node 1 will

---

[4]All the random numbers used in case studies are generated with random seed = 3

53
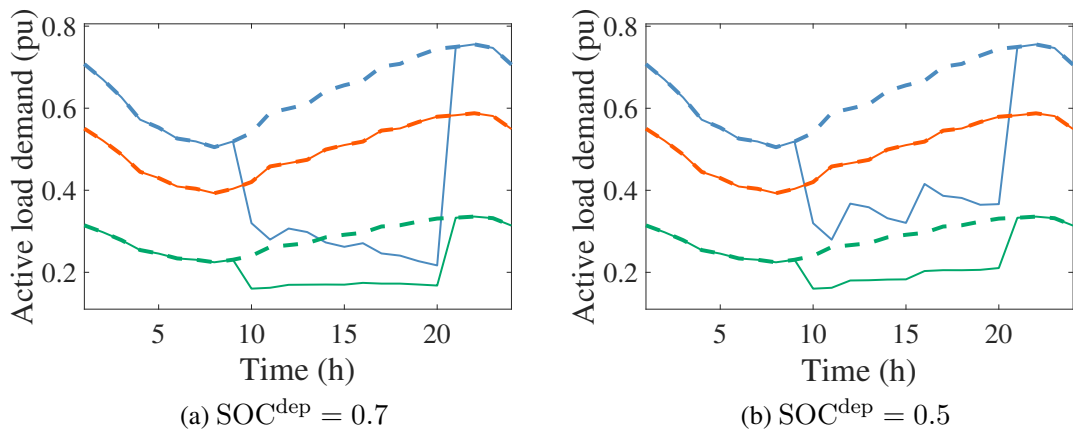
Figure 4.4: Expected (dashed lines) and picked up (solid lines) load; Nodes: — 2, — 3, — 4.
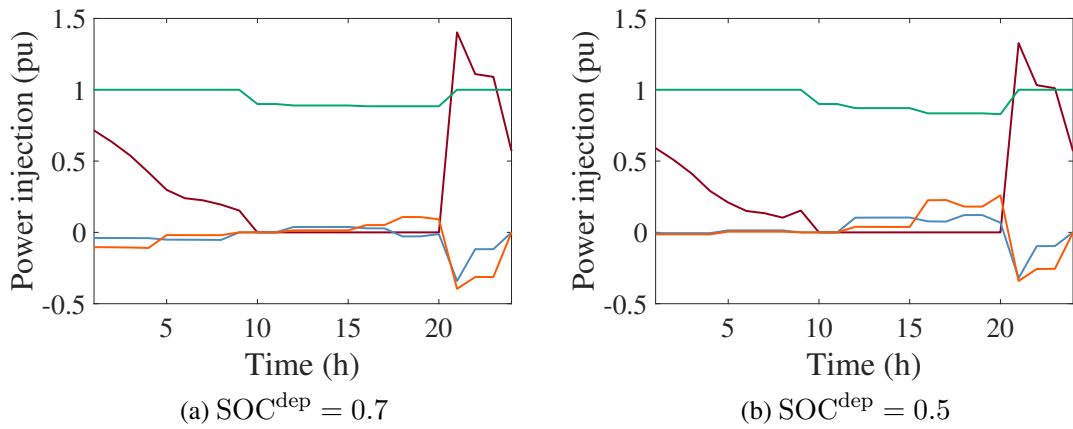
Figure 4.5: Nodal power injection; Nodes: — 1, — 2, — 3, — 4.

connect to DS from $t = 9$ to 13, during the period when the DS has high load pickup needs.

(a) $\text{SOC}^{\text{dep}} = 0.7$ (b) $\text{SOC}^{\text{dep}} = 0.5$
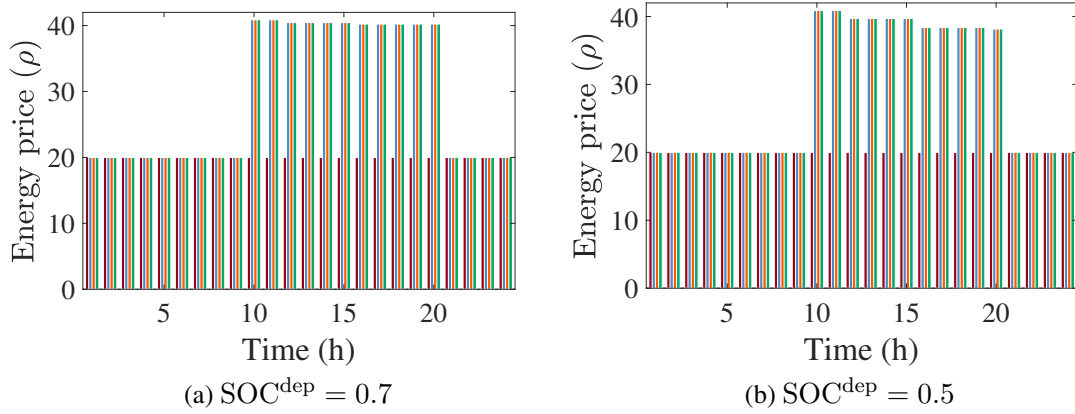
Figure 4.6: Nodal energy price; Nodes: ▮ 1, ▮ 2, ▮ 3, ▮ 4.

(a) $\text{SOC}^{\text{dep}} = 0.7$ (b) $\text{SOC}^{\text{dep}} = 0.5$
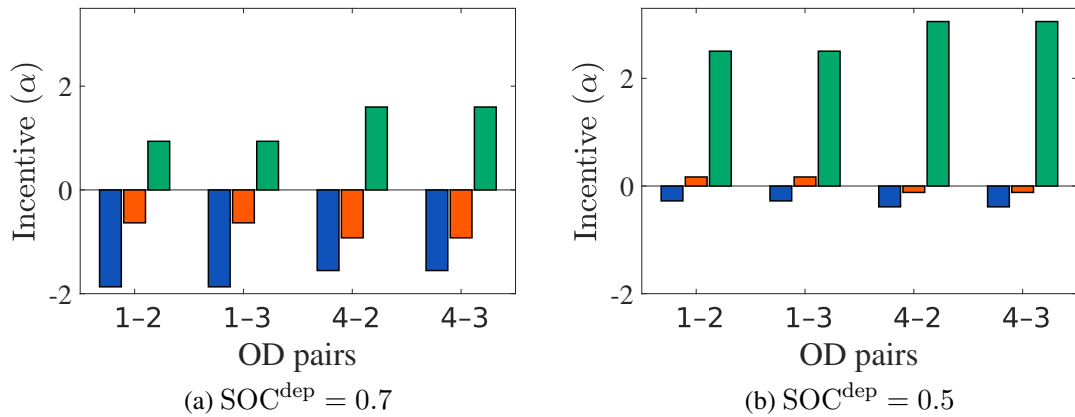
Figure 4.7: CS incentives for EVs; Groups: ▮ 1, ▮ 2, ▮ 3.

IEEE 33-node and Sioux Falls Test systems

We further test the proposed modeling and convex reformulation on larger systems, with IEEE 33-node as a benchmark test system [78] and Sioux Falls network [50] as a realistic transportation system. The computation times for solving the base case problem is 19.0 minutes. We note that the proposed model can be applied to larger test systems due to the convex reformulation. Since

problem (4.9) has a strictly convex objective function and linear constraints, this problem can be efficiently solved by general-purpose nonlinear programming solvers or classical methods such as the renowned Frank-Wolfe algorithm [97]. In the case study, the interior-point-based solver IPOPT is adopted to solve problem (4.9), and the computation time is acceptable for the purpose of this study. For extreme large-scale systems, two approaches can be considered to further enhance computational efficiency: 1) The network topology of both systems can be aggregated in a way that they still retain the main characteristics of each system without jeopardizing the macro-level conclusions for system analyses or policy-making. 2) Decomposition-based methods such as ADMM algorithms can be directly applied to solve the proposed convex model since model (4.9) is decomposable by systems once the clearing conditions (4.7) are relaxed. ADMM methods also allow each system to solve its problem without acquiring extensive parameters and measurements from the other systems.

Fig. 4.8 represents the characteristics of both test systems along with the sequences of the line outages. Hourly load demand and DG characteristics are obtained from the authors of [98]. Blue numbers on the DS diagram show the correspondence between the node indexes in the transportation system. To ensure the scale of the transportation network to be consistent with the 33-node DS, we reduce the total capacity of links to 1 %. Also, we assume 1 % of all the traffic from the Sioux Falls data [5] are EVs. Each EV group contains 1/3 of the traffic flow, and we used the same SOC^{arr} levels as the four-node test system for different EV groups. The SOC^{dep} of EVs is set to 0.5. We investigate the performance of the systems with and without EV participation.

Without EVs, we observe load loss on many nodes as illustrated in Fig. 4.9a; EV participation avoids load loss on nodes 21 and 26∼33 completely and increases the load served on nodes 20, 21, 22, 24, and 25 (see Fig. 4.9b). Nodes 21 and 22 still have load losses because these two nodes are

---

[5]Data: https://github.com/bstabler/TransportationNetworks/
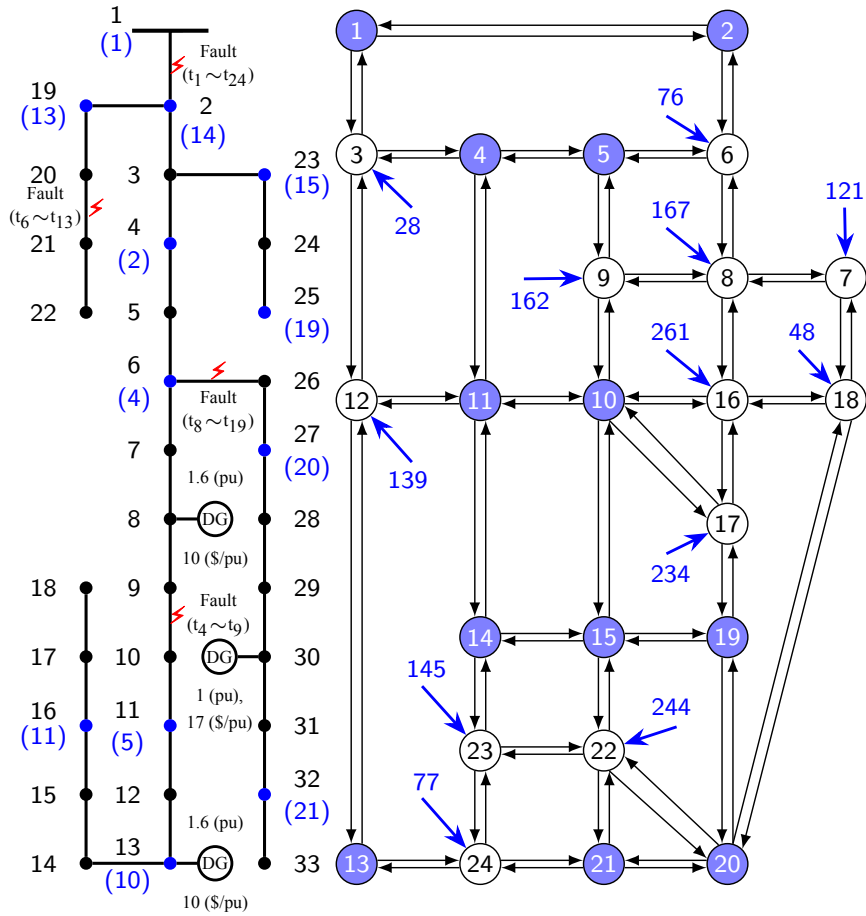
Figure 4.8: Test systems (a) 33-node DS ●: nodes; ●: corresponding nodes in transportation system (CSs); and ⚡: faults on lines. (b) Transportation system ○: origin nodes; ●: destination (CS) nodes; and →: EV incoming traffic flow.

completely isolated by line 20-21 outage. This suggests that CSs/DGs may need to be developed at these two locations from a system support perspective. The CSs at nodes 23 and 25 try to recover load at nodes 23~25. But node 25 has the highest load demand in the system, and both nodes 24 and 25 are far from DGs, making voltage and reactive power support difficult. These factors result in less load pickup at nodes 24 and 25. Overall, the daily load loss decreased from 7.899 pu to 5.426 pu with EV participating in system support.
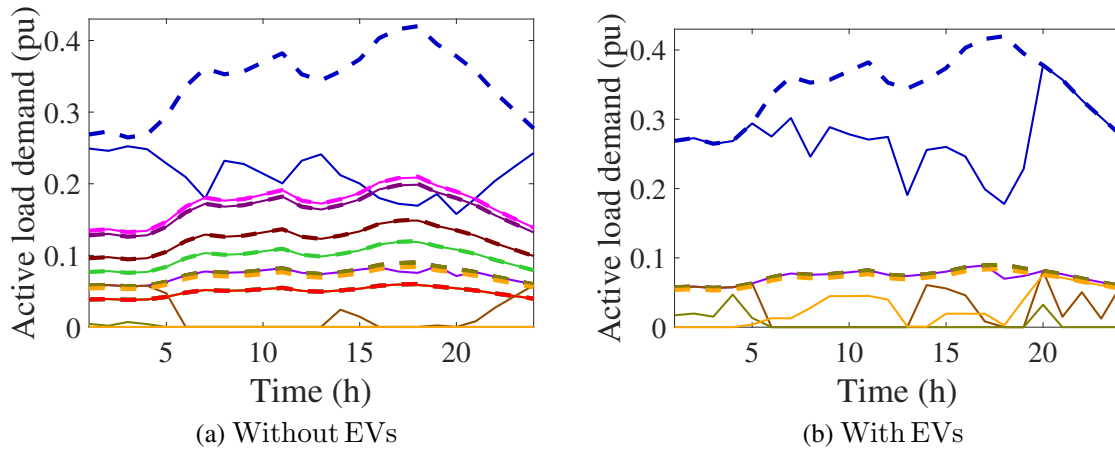
Figure 4.9: Expected (dashed lines) and picked up (solid lines) daily load profile of nodes with load loss; Nodes: —— 20, —— 21, —— 22, —— 24, —— 25, —— 26, —— 27, —— 28, —— 29, —— 30, —— 31, —— 32, —— 33.

The CS energy supply/demand is shown in Fig. 4.10. The discharged energy is to avoid load loss during line outages, and the charged energy is to satisfy the charging requirements of EVs. EVs can charge/discharge flexibly during their dwelling time at CSs as long as their SOCs meet the minimum SOC^{dep}. For example, the CS at node 27 charges at time steps $t = 4$ and 5 and discharges energy to the system at $t = 7$ to support the DS.

Fig. 4.11 shows that the participation of EVs decreases the energy prices at different nodes and time steps. The decrease in energy prices is an indicator of the system's ability to satisfy the load demand and avoid load loss with EVs. For example, the energy prices at nodes 8 and 11 drop at time steps $t_{20} \sim t_{24}$; the energy prices at nodes $27 \sim 32$ drop during $t_{17} \sim t_{18}$. The drop in energy prices is because of avoiding load loss at these nodes and the nodes nearby. For nodes where we still have large load loss (e.g., node 25), the energy price is still high but not as high as the system without EVs.

Similar to the four-node system, the CS incentives are negative or around zero for EVs who want
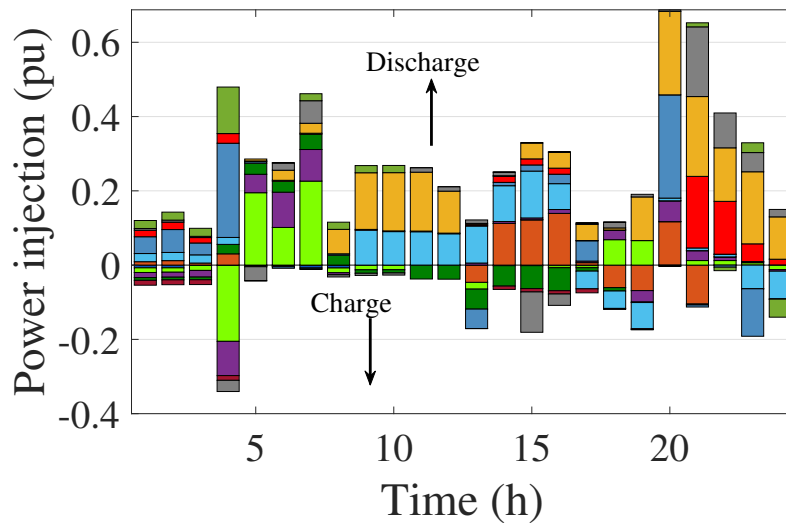
Figure 4.10: EV generation/load at CSs; Nodes: ■ 1, ■ 2, ■ 4, ■ 6, ■ 11, ■ 13, ■ 19, ■ 23, ■ 25, ■ 27, ■ 32.

to charge their cars ($e = 1$) and positive for EVs who want to participate in V2G program ($e = 2$ and 3) – see Fig. 4.12. Different CSs provide different incentives to EVs based on EVs' arrival time and DS's energy needs. For example, CS at transportation node 19, which corresponds to node 25 in DS, offers the highest incentives for group 3 EVs and charge the highest prices for group 1 EVs because energy shortage is severe around node 25, which nodes experience a high load loss (see Fig. 4.9). In other words, the CS at this node wants to attract EVs who can discharge and impose a penalty for EVs who want to charge at this location.

The CS selection of different EV groups is illustrated in Fig. 4.13. CS selection depends on a combination of the close proximity of the destination and the incentives of CSs. The impact of incentives can be seen at transportation node 19 (node 25 in DS). Drivers from origin node 17 would normally choose to go to destination node 19 based on its proximity. EV drivers of groups 2 and 3 have done just that but fewer drivers of group 1 have chosen this CS. This is because the corresponding node to transportation node 19 in DS (i.e., node 25) requires energy and has
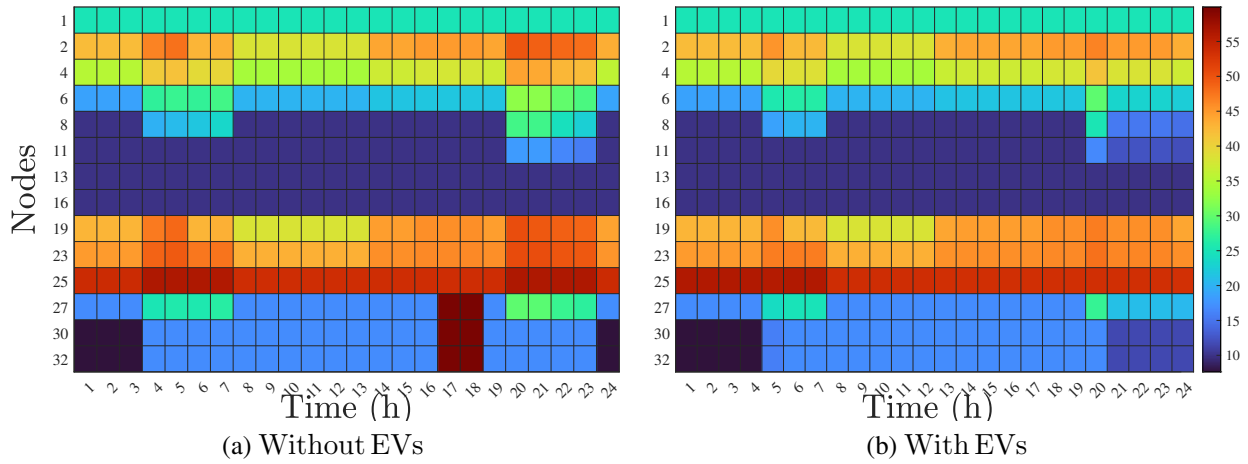
Figure 4.11: Energy price at DG ($\mathcal{I}^{DG}$) and CS ($\mathcal{I}^{CS}$) nodes.
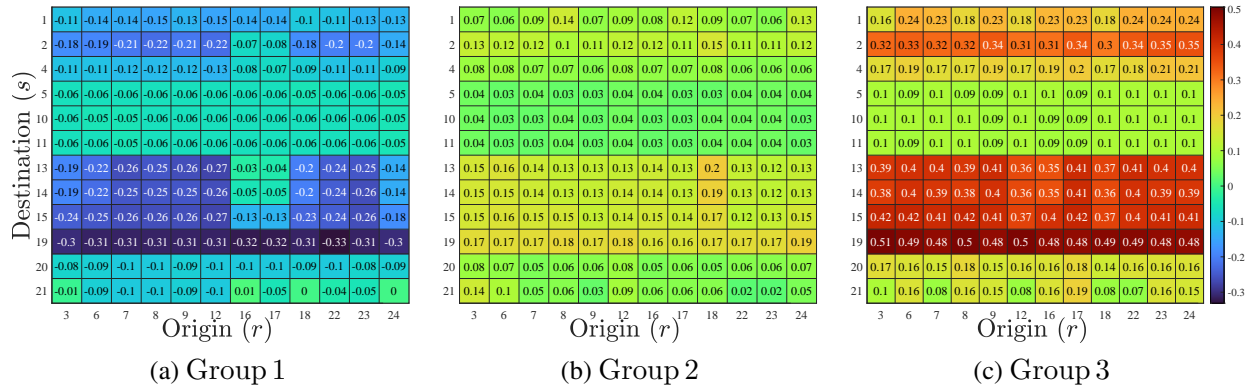
Figure 4.12: CS (s) incentives for EVs coming from different origins (r) and different EV groups.

a higher cost for EVs that need to charge. In general, EVs from group 1 slightly prefer to go to transportation nodes 5∼11 and try to avoid going to transportation nodes 13∼19 compared to groups 2 and 3 because charging costs are lower at transportation nodes 5∼11 compared to transportation nodes 13∼19 for group 1.

60

(a) Group 1   (b) Group 2   (c) Group 3
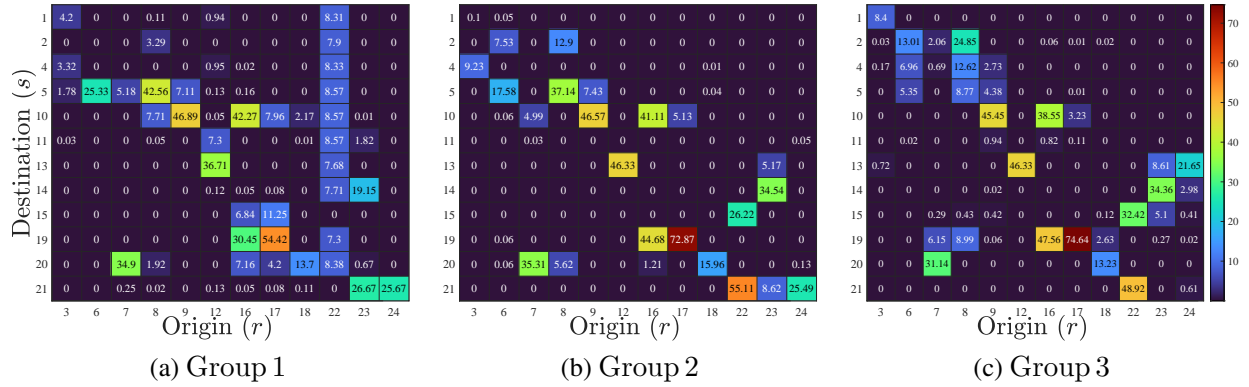
Figure 4.13: Traffic flow of EVs among origins (r) and CSs (s) for different EV groups.

Sensitivity analysis of model inputs

In this section, we analyze the sensitivity of data inputs on the model results. We focus on three input parameters: stress level (multiplying load demand by 0.8, 0.9, 1.1, 1.2), distribution line parameters (multiplying line resistance and reactance by 0.8, 0.9, 1.1, 1.2), and the total number of EVs (multiplying the number of EVs by 0.8, 0.9, 1.1, 1.2). The computation times for solving the problem with these different input parameters are consistently between 18.1 minutes to 21.7 minutes. Fig. 4.14 presents the load loss profile for these varying factors in the cases without and with EVs in the systems. As expected, with EVs in the systems, the total load losses will significantly decrease compared with the case without EVs for all the investigated factors.

Furthermore, from Fig. 4.14a, the load loss increases rapidly as the stress level increases for both with and without EV cases. The load loss difference between the two cases has been slightly increasing from 1.69 pu to 2.67 pu when the scaling factor increases from 0.8 to 1.1, which means when the system is not too congested, higher load demand provides more opportunities for EVs to provide grid services to avoid load losses. However, the additional load pick-up with EVs decreases significantly from 2.67 pu to 1.44 pu when the scaling factor increases from 1.1 to 1.2. This is
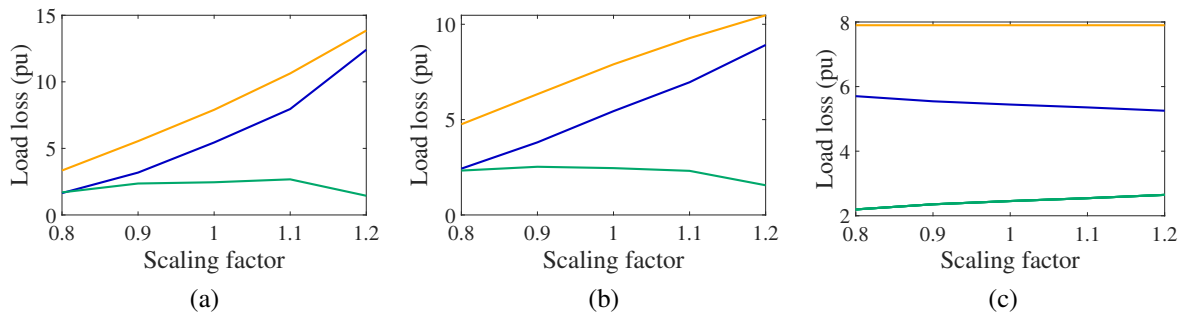
Figure 4.14: Sensitivity analysis on load loss with model inputs: (a) stress level, (b) line parameters, (c) total number of EVs; — without EVs, — with EVs, and — load loss difference between with and without EV cases.

because with load demand being too high, both line capacity and voltage constraints may restrict power distribution to the nodes downstream from the generation nodes, which reduces the potential of EVs to provide grid services. From Fig. 4.14b, the difference of load loss between without and with EVs cases decreases with the increase of distribution line resistance and reactance, meaning that increasing these DS parameters reduce the potential of EVs to provide grid services. This is because higher line resistance and reactance may result in higher voltage drops in the radial structure of the DS so that additional V2G power flow may not be allowed due to violation of voltage and line capacity constraints. From Fig. 4.14c, as the number of EVs grows, we observe less load loss in the system. Note that increasing the number of EVs also means higher charging demand. However, Fig. 4.14c indicates that the benefits of EVs' participation in system support have outweighed the additional charging demand, which shows the potential values of large-scale EV participation in DS support.

Conclusion

We investigate the impact of decentralized EVs on DS load pickup under stressed conditions in a network equilibrium framework, where each stakeholder, including DG owners, DSO, EV drivers, and CSA, maximizes its own objective in a coupled transportation and DSs. We reformulate the network equilibrium problem as an equivalent convex optimization problem, which can be efficiently solved by commercial nonlinear solvers. Numerical results on different test systems show that the participation of EVs helps to reduce the load loss during the line outage, and the system should provide different incentives to EVs based on their value for the DS to maximize system benefits. Moreover, the results reveal how the decision makings and requirements of each stakeholder affect the decision making of other stakeholders.

This work can be extended in multiple directions. First, the modeling framework can be used to design optimal incentives for EVs to participate in DS service supports. Second, this work can be used for transportation and DSs' upgrades considering potential future EV participation in grid services. Third, probabilistic modeling on renewable energy sources, line outages, EV characteristics (e.g., EVs' arrival and departure time and arrival/minimum departure SOC), and elastic EV participation can be further examined by extending the proposed modeling framework to a stochastic equilibrium problem. Fourth, decomposition-based algorithms can be developed combined with the proposed exact convex reformulation to facilitate computation for extreme large-scale systems facing high-dimensional uncertainties.

CHAPTER 5: PRIVATE ELECTRIC VEHICLES FOR EMERGENCY LOAD PICKUP: A MULTI-NETWORK STOCHASTIC EQUILIBRIUM APPROACH[1]

Introduction

Weather conditions can cause disruptions and outages in DSs operation resulting in societal and economical losses. As weather-related outages become more intense and more frequent, versatile energy sources are needed to increase DS resilience and reliability. Increasing market penetration of private electric vehicles (EVs) with their mobility and fast regulating characteristics provides new opportunities as flexible energy resources for enhancing power system resilience. EV owners have no obligations and most likely will not be able to participate in improving network resilience during extreme events. However, given sufficient incentives and charging station (CS) availability, they may be willing to provide restoration services after the event. EV participation will be more likely when the surrounding environment is safe or during events where no hazards endanger the safety of people, e.g., the 2021 Texas power crisis.

DSs face uncertainties from different sources, including EV participation, power supply, load demand, and line outage uncertainties, which can significantly impact the restoration process. We will extend our proposed model in the previous chapter to a stochastic equilibrium model to consider uncertainties in a coupled DS and transportation system, which is necessary to draw realistic insights on the interaction between these two systems. The interaction of stakeholders in coupled distribution and transportation systems will be modeled as a network-based multi-agent stochastic optimization problem with equilibrium constraints (N-MSOPEC). Distribution system operator

---

(DSO), DG owners, charging station aggregator (CSA), and EV owners are modeled explicitly as non-cooperative stakeholders to maximize their objectives during the restoration process. We consider stochastic line outages in weather related events and the number of EVs participating in DS restoration as uncertainty sources in DS and TS, respectively. Additionally, an exact convex reformulation technique has been developed for the proposed N-MSOPEC model, which significantly improves the computational efficiency to solve the high-dimensional complementarity problems. Study cases have been created to demonstrate the close coupling between distribution and transportation systems resulting from the decision making of stakeholders involved.

The remainder of this chapter is organized as follows: The overall modeling and scenario generation and reduction techniques are explained in Methodology Overview section. Mathematical Modeling section provides the detailed mathematical formulation and design of the developed N-MSOPEC model, followed by Convex Reformulation section for the solution strategies for the proposed model. Numerical Results section presents the results of implementing the model on a test system. Lastly, Conclusion section concludes the paper with the summary of findings and the future work.

The notation used in this chapter are similar to the notations of the previous chapter except for the addition of scenario indices (ξ) in a set of scenarios (Ξ).

Methodology Overview

The overall methodology of this study is illustrated in Figure 5.1. In the first step, the input data of DS, TS, and the weather condition (i.e., wind speed) are acquired. Monte-Carlo simulation (MCS) method is used in the next step to generate random scenarios for the number of EVs participating in restoration based on the normal distribution. Similarly, line outage scenarios are generated

65

based on a line fragility function and wind speed forecasts. A line fragility function provides the probability of a line outage w.r.t weather conditions (e.g., wind speed and temperature), used in multiple studies to simulate weather event outages in transmission and distribution systems [99–101].
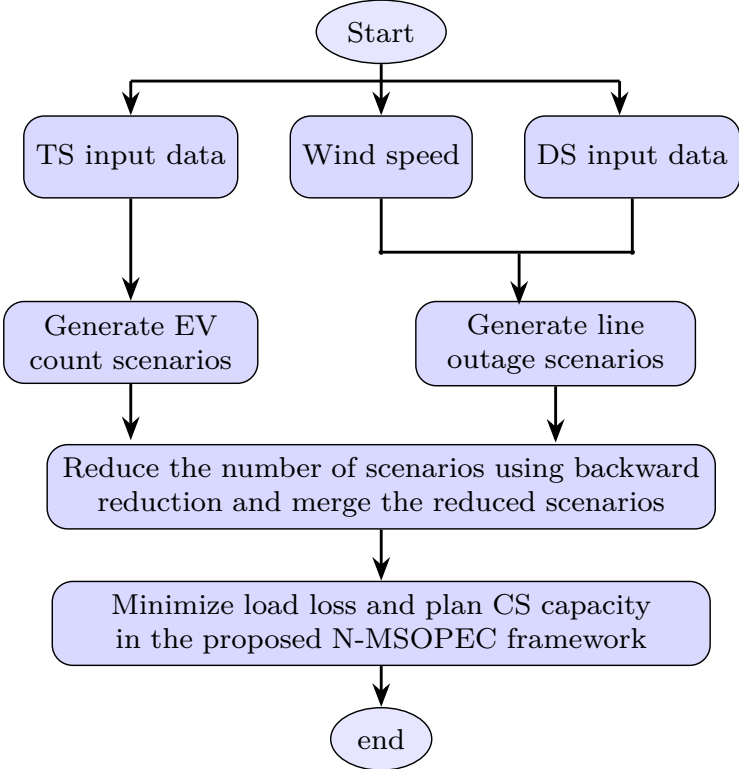
Figure 5.1: Proposed method

We adopt the line outage probability function proposed in [100], which suggests that the line outage probability is constant until the wind speed reaches a critical threshold (w^{critical}); afterward, the probability of line outage increases linearly, until the wind speed becomes strong enough (w^{collapse})

that the line would definitely collapse. This relation is summarized in equation (5.1) [100].

$$
\mathcal{P}_L = \begin{cases} \overline{\mathcal{P}} & w < w^{\text{critical}} \\ a \cdot w + \overline{\mathcal{P}} & w^{\text{critical}} \leq w < w^{\text{collapse}} \\ 1 & w \geq w^{\text{collapse}}. \end{cases} \tag{5.1}
$$

Note that the lines' fragility function based on other weather conditions can also be compounded in the same manner to calculate the total line outage probability. Here our focus is to model unexpected outages and analyze the impacts of EV participation on DS system support. We have considered outages due to windy weather conditions such as hurricanes and tornadoes, and we will leave the influence of other factors to future studies. In order to generate line outage scenarios, the regional hourly wind speed forecasts will be acquired, and the outage probability for each line at each hour will be calculated based on equation (5.1). Then, a large number of random numbers will be generated as scenarios in the range of $0 \sim 1$ for each line and time step. If the generated random number is less than the line outage probability, the line status would be disconnected (i.e., $\lambda = 0$). Once a line outage occurs at time step t, the line status will remain as $\lambda = 0$ for at least Δt time steps until the detection of the next line outage. Δt depends on the severity of weather conditions and repair time of the outage. On the other hand, we will model the uncertainty of available EVs by generating random numbers as the number of EVs who are starting their trip from similar origins. The parameters used for generating line outage and EV participation scenarios will be discussed in details in the case studies.

In the next step, the backward scenario reduction algorithm is implemented based on [102] to improve computational tractability and avoid an excessive number of scenarios. At each iteration of the algorithm, scenarios that are similar (close) to each other get replaced with one scenario, and its probability will equal the summation of the scenarios it has replaced. The iterations will
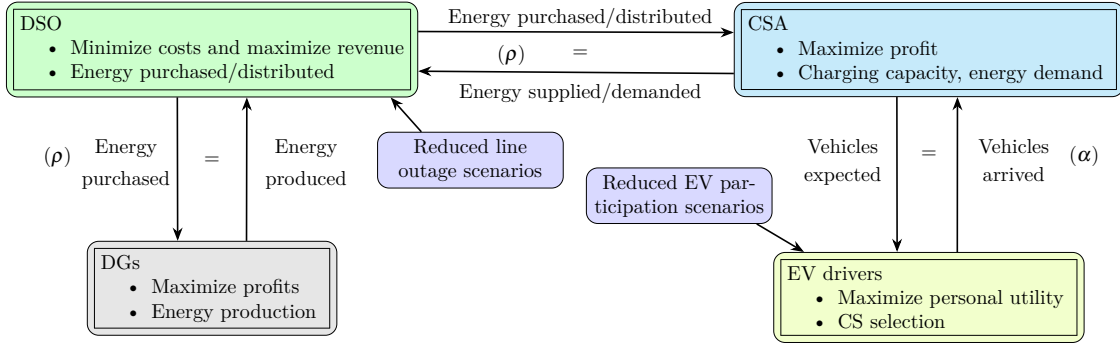
Figure 5.2: Stakeholder's interaction modeling, inputs, and objectives.

go on until the total number of remaining scenarios reach the desired count. For the step-by-step implementation of the algorithm please see [102]. Assuming that line outage and EV participation are two independent sources of uncertainties, the reduced number of scenarios can be easily merged by compounding the line outage scenarios with the scenarios of the EV number.

After reducing the scenarios to the desired number, we propose the N-MSOPEC method to capture the stakeholders' interaction. Figure 5.2 summarizes the proposed modeling framework, including the stakeholders' objectives, inputs, main decision variables, and their interactions. DSO receives the probable line outage scenarios as input and purchases energy from DGs and CSA to maximize load pickup and minimize its costs accordingly; DGs aim to maximize their profits by selling the generated energy to the DS. On the other hand, the CSA maximizes its profit by managing EV charging and energy exchange with the DSO. Note that CSA can either purchase energy from the system if it needs to charge the EVs or provide energy to DSO whenever EVs want to participate in DS system support by discharging their stored energy. The EVs' charging flexibility will determine the incentives they receive. A market clearing is enforced on the energy exchange in the system, which requires the supplied energy by CSA and DGs to be equal to the energy demanded by DSs (including load pickup and charging demand). Energy prices (ρ) are associated with this market clearing condition. The other main interaction is between the EV owners and CSA. EV drivers

who are willing to participate in the grid services will choose their plug-in locations based on their travel plan to maximize their personal utilities. A market clearing condition is considered in this interaction which balances the number of EVs selecting a CS with the number of EVs expected by CSA. This clearing condition is associated with the locational incentives (α) offered by CSs to EV drivers. The modeling details of the proposed N-MSOPEC are delineated in the next section providing the mathematical modeling for each of the stakeholders and market clearing conditions.

Mathematical Modeling

In this section, we will outline the mathematical modeling of each stakeholder, followed by the market clearing conditions and the developed convex reformulation technique to solve the problem.

DG Owners Modeling

DG owners determine their hourly generation quantity $p_{i,t,\xi}^{DG}$ to maximize profits (i.e., minimize negative profits) of selling energy based on energy price ρ. Because individual DG generation capacity is limited, we assume DG owners are perfectly competitive and do not have market power to influence the locational electricity prices. Therefore, the decision making of all DG owners can be aggregated into a single optimization problem, as formulated in model (5.2).

$$\min_{\boldsymbol{p}^{DG},\boldsymbol{p}^{R}\geq\boldsymbol{0}} \quad \sum_{\xi\in\Xi}\Omega_{\xi}\left[\sum_{i\in\mathcal{I}^{DG}}\sum_{t\in\mathcal{T}}\left(C_i(p_{i,t,\xi}^{DG})-\rho_{i,t,\xi}\,p_{i,t,\xi}^{DG}\right)\right] \quad (5.2a)$$

$$\text{s.t.} \quad \underline{P}_i^{DG}\leq p_{i,t,\xi}^{DG}\leq\bar{P}_i^{DG},\;\forall i\in\mathcal{I}^{DG},t\in\mathcal{T},\xi\in\Xi \quad (5.2b)$$

Objective (5.2a) minimizes the expectation of the negative profits of DG owners, calculated as the weighted sum of operation costs of scenarios $\sum_{\xi \in \Xi} \sum_{i \in \mathcal{I}^{DG}} \sum_{t \in \mathcal{T}} \Omega_\xi C_i(p_{i,t,\xi}^{DG})$ subtracting the revenue of energy exchange with the system $\sum_{\xi \in \Xi} \sum_{i \in \mathcal{I}^{DG}} \sum_{t \in \mathcal{T}} \Omega_\xi \rho_{i,t,\xi} p_{i,t,\xi}^{DG}$ where probabilities of scenarios ($\Omega_{i,t,\xi}$) are considered as weights. We assume $C_i(\cdot)$ to be convex function w.r.t $p_{i,t,\xi}^{DG}$ with different cost parameters for different DGs. This implies a non-decreasing marginal cost. Constraint (5.2b) determines the upper and lower bounds of total power generation at DG node i for time t and scenario ξ.

DSO Modeling

During outages and system disturbances, the main goal of the DSO is to restore energy services to the customers. Given the characteristics and application of the customers, some have higher priority, such as hospitals, emergency centers, etc. Here, we assume that the DSO intends to maximize serviced load demand or load pickup ($p_{i,t,\xi}^d$) based on their priorities ($\omega_{i,t}$) and minimize the total cost of purchased energy from either DG units or CSs while satisfying system constraints in all of the scenarios. Formulation defined in model (5.3) represents the optimization problem of DSO in the restoration process.

Objective (5.3a) maximizes the the load pickup $\sum_{t \in \mathcal{T}} \sum_{i \in \mathcal{I}^L} \omega_{i,t}\, p_{i,t,\xi}^d$, which is weighted by the load priority $\omega_{i,t}$, subtracting the cost of energy exchanges with DGs and CSs $\sum_{t \in \mathcal{T}} \sum \rho_{i,t,\xi}\, p_{i,t,\xi}^s$. The objectives of scenarios are weighted based on their probabilities Ω_ξ. Operational requirements of the DS are adopted from the Dist-Flow model [78] in (5.3b)-(5.3i). Active and reactive power flow balances are modeled in (5.3b) and (5.3c), respectively. Constraint (5.3f) limits power flow not exceeding line capacity with the uncertain binary line status parameter $\lambda_{l,\xi}$, where $\lambda_{l,\xi} = 0$ indicates line outage. Constraint (5.3g) and (5.3h) calculate the voltage at each node where M is a big number to model line outage when $\lambda_{l,t,\xi} = 0$. Lastly, constraint (5.3i) enforces the voltage

70

boundaries at each node.

$$\max_{\substack{\boldsymbol{p^d}, \boldsymbol{v} \geq 0, \\ \boldsymbol{p^s}, \boldsymbol{pf}, \boldsymbol{qf}}} \quad \sum_{\xi \in \Xi} \Omega_\xi \Bigg[\sum_{t \in \mathcal{T}} \Big(\sum_{i \in \mathcal{I}^L} \omega_{i,t}\, p^d_{i,t,\xi} - \sum_{i \in \mathcal{I}^{\mathrm{DG}} \cup \mathcal{I}^{\mathrm{CS}}} \rho_{i,t,\xi}\, p^s_{i,t,\xi} \Big) \Bigg] \tag{5.3a}$$

$$\text{s.t.} \quad \sum_{l \in \mathcal{L}} pf_{l,t,\xi} \cdot \mathrm{LT}_{l,i} - \sum_{l \in \mathcal{L}} pf_{l,t,\xi} \cdot \mathrm{LF}_{l,i} = p^d_{i,t,\xi} - p^s_{i,t,\xi}, \ \forall i \in \mathcal{I}, t \in \mathcal{T}, \xi \in \Xi \tag{5.3b}$$

$$\sum_{l \in \mathcal{L}} qf_{l,t,\xi} \cdot \mathrm{LT}_{l,i} - \sum_{l \in \mathcal{L}} qf_{l,t,\xi} \cdot \mathrm{LF}_{l,i} = q^d_{i,t,\xi} - q^s_{i,t,\xi}, \ \forall i \in \mathcal{I}, t \in \mathcal{T}, \xi \in \Xi \tag{5.3c}$$

$$0 \leq p^d_{i,t,\xi} \leq \bar{P}^d_{i,t}, \ \forall i \in \mathcal{I}^l, t \in \mathcal{T}, \xi \in \Xi \tag{5.3d}$$

$$q^d_{i,t,\xi} = (\bar{Q}^d_{i,t} / \bar{P}^d_{i,t}) \cdot p^d_{i,t,\xi}, \ \forall i \in \mathcal{I}^l, t \in \mathcal{T}, \xi \in \Xi \tag{5.3e}$$

$$pf^2_{l,t,\xi} + qf^2_{l,t,\xi} \leq \lambda_{l,t,\xi} \cdot (S^{\mathrm{max}}_l)^2, \ \forall l \in \mathcal{L}, t \in \mathcal{T}, \xi \in \Xi \tag{5.3f}$$

$$v_{\mathrm{FN}_l,t,\xi} - v_{\mathrm{TN}_l,t,\xi} \leq (1 - \lambda_{l,t,\xi}) \cdot M + 2 \cdot (r_l \cdot pf_{l,t,\xi} + x_l \cdot qf_{l,t,\xi}), \ \forall l \in \mathcal{L}, t \in \mathcal{T}, \xi \in \Xi \tag{5.3g}$$

$$v_{\mathrm{FN}_l,t,\xi} - v_{\mathrm{TN}_l,t,\xi} \geq (\lambda_{l,t,\xi} - 1) \cdot M + 2 \cdot (r_l \cdot pf_{l,t,\xi} + x_l \cdot qf_{l,t,\xi}), \ \forall l \in \mathcal{L}, t \in \mathcal{T}, \xi \in \Xi \tag{5.3h}$$

$$(V^{\mathrm{min}}_i)^2 \leq v_{i,t,\xi} \leq (V^{\mathrm{max}}_i)^2, \ \forall i \in \mathcal{I}, t \in \mathcal{T}, \xi \in \Xi \tag{5.3i}$$

CSA Modeling

In this study, we assume a CSA, who is private entity responsible for planning charging station capacity and scheduling the charging and discharging for EV drivers while satisfying their energy needs. The CSA aims to maximize its profits [82] while maintaining the required charging demand of EVs in all of the scenarios. The decision making of the CSA is formulated in model (5.4). CSs determine their total capacity (p^{CC}_i) as their planning decision variable to fulfill charging demand reliably for all of the scenarios. Additionally, we assume that CSs will be providing incentives α for attracting drivers to charge/discharge at their locations. Incentives can be negative

or positive based on the charging requirements of the EVs. Negative values represent the charging cost for the EVs, and positive values represent the revenue of EVs for discharging and providing energy back to the system (i.e., vehicle-to-grid). The amount of the incentives will depend on the supply-demand relationship at the time of charging/discharging. For example, EVs that discharge during the emergency time of the system when the supply is significantly lower than the demand, will get more incentives compared with EVs that discharge during normal operation hours. The Objective (5.4a) minimizes the CSA's negative expected profits, which is calculated as the cost of the capacity investment of CSs $\sum_{i \in \mathcal{I}^{\mathrm{CS}}} F_i(p_i^{\mathrm{CC}})$, and the weighted sum of the negative profits and the operational costs at each scenario. Operational costs are calculated as the summation of the costs of providing incentives for EVs $\sum_{r \in \mathcal{R}} \sum_{i \in \mathcal{I}^{\mathrm{CS}}} \sum_{e \in \mathcal{E}} \alpha_{ri,\xi}^e q_{ri,\xi}'^e$ and battery degradation costs $\sum_{r \in \mathcal{R}} \sum_{t \in \mathcal{T}} \sum_{e \in \mathcal{E}} C_{i,r,t,\xi}^{\mathrm{deg},e}$. The revenue of the CSA is calculated as selling electricity to DS based on locational marginal prices $\sum_{i \in \mathcal{I}^{\mathrm{CS}}} \sum_{t \in \mathcal{T}} -\rho_{i,t,\xi}\, p_{i,t,\xi}^{\mathrm{CS}}$. The power output of CSs ($p_{i,t,\xi}^{\mathrm{CS}}$) will be positive when discharging and negative for charging instances. Energy prices (ρ) and incentives (α) will be calculated endogenously on the market, which is discussed further in Market Clearing Conditions.

EVs will be categorized into different homogeneous groups e based on their travel and charging characteristics, including arriving/departing time $T_{r,e}^{\mathrm{arr}}/T_{r,e}^{\mathrm{dep}}$, $\mathrm{SOC}_{r,e}^{\mathrm{arr}}$, and minimum $\mathrm{SOC}_{r,e}^{\mathrm{dep}}$. In other words, EVs with similar charging requirements and temporal behavior will be at the same group [75]. This will facilitate the incentives design and EV charging scheduling for DS support.

$$
\min_{\substack{\boldsymbol{p}^{\mathrm{CS}},\boldsymbol{q}', \\ p^{CC},\mathrm{soc}}} \quad \sum_{i\in\mathcal{I}^{\mathrm{CS}}} F_i(p_i^{\mathrm{CC}}) + \sum_{\xi\in\Xi}\Omega_\xi\left[\sum_{i\in\mathcal{I}^{\mathrm{CS}}}\sum_{t\in\mathcal{T}} -\rho_{i,t,\xi}\,p_{i,t,\xi}^{\mathrm{CS}} + \sum_{r\in\mathcal{R}}\sum_{i\in\mathcal{I}^{\mathrm{CS}}}\sum_{e\in\mathcal{E}} \alpha_{ri,\xi}^e q_{ri,\xi}'^e \right.
$$

$$
\left. + \sum_{i\in\mathcal{I}^{CS}}\sum_{r\in\mathcal{R}}\sum_{t\in\mathcal{T}}\sum_{e\in\mathcal{E}} C_{i,r,t,\xi}^{\mathrm{deg},e} \right] \tag{5.4a}
$$

s.t. (5.5)

$$
\mathrm{soc}_{i,r,t,\xi}^e = \mathrm{soc}_{i,r,t-1,\xi}^e - p_{i,r,t,\xi}^e, \ \forall i\in\mathcal{I}^{\mathrm{CS}}, r\in\mathcal{R}, e\in\mathcal{E}, t\in(T_{r,e}^{\mathrm{arr}},T_{r,e}^{\mathrm{dep}}], \xi\in\Xi \tag{5.4b}
$$

$$
q_{ri,\xi}'^e\underline{\mathrm{SOC}}^e \le \mathrm{soc}_{i,r,t,\xi}^e \le q_{ri,\xi}'^e\overline{\mathrm{SOC}}^e, \ \forall i\in\mathcal{I}^{\mathrm{CS}}, r\in\mathcal{R}, e\in\mathcal{E}, t\in[T_{r,e}^{\mathrm{arr}},T_{r,e}^{\mathrm{dep}}], \xi\in\Xi
$$
$$
\tag{5.4c}
$$

$$
\mathrm{soc}_{i,r,T_{r,e}^{\mathrm{arr}},\xi}^e = q_{ri,\xi}'^e\mathrm{SOC}_{r,e}^{\mathrm{arr}}, \ \forall i\in\mathcal{I}^{\mathrm{CS}}, r\in\mathcal{R}, e\in\mathcal{E}, \xi\in\Xi \tag{5.4d}
$$

$$
\mathrm{soc}_{i,r,T_{r,e}^{\mathrm{dep}},\xi}^e \ge q_{ri,\xi}'^e\mathrm{SOC}_{r,e}^{\mathrm{dep}}, \ \forall i\in\mathcal{I}^{\mathrm{CS}} r\in\mathcal{R}, e\in\mathcal{E}, \xi\in\Xi \tag{5.4e}
$$

$$
p_{i,t,\xi}^{\mathrm{CS}} = \sum_{r\in\mathcal{R}}\sum_{e\in\mathcal{E}} \frac{p_{i,r,t,\xi}^e}{S^{\mathrm{base}}}, \ \forall i\in\mathcal{I}^{\mathrm{CS}}, t\in[T_{r,e}^{\mathrm{arr}},T_{r,e}^{\mathrm{dep}}], \xi\in\Xi \tag{5.4f}
$$

$$
-p_i^{\mathrm{CC}} \le p_{i,t,\xi}^{\mathrm{CS}} \le p_i^{\mathrm{CC}} \ \forall i\in\mathcal{I}^{\mathrm{CS}}, t\in[T_{r,e}^{\mathrm{arr}},T_{r,e}^{\mathrm{dep}}], \xi\in\Xi \tag{5.4g}
$$

CSA needs to fulfill the charging requirements of EVs. EVs' state of charge (SOC) transition are modeled in (5.4b)-(5.4g). Constraint (5.4b) models the SOC dynamics of EVs coming from origin node r and charge at CS location i. Constraint (5.4c) enforces the acceptable range for the SOC of each EV group. Constraint (5.4d) enforces the initial SOC of EVs when they arrive a CS. Constraint (5.4e) specifies the expected minimum departure SOC for each EV group at charging location i when they leave the CS. The total hourly power supply/demand of a CS is calculated in (5.4f) as the summation of the normalized discharging/charging of EVs at each station. Lastly, Constraint (5.4g) ensures that the total hourly power output of each CS does not exceed the total charging/discharging capacity of the CS.

In addition, one factor that discourages the participation of EV drivers in system services is battery degradation as the result of frequent charging and discharging. Here, we assume that CSA is responsible for the costs of battery degradation of vehicles to provide DS services. The Ah-throughput counting model [86] is commonly used for modeling the shelf and cycle degradation types [85]. We formulated the degradation cost of EVs $C_{i,r,t}^{\text{deg},e}$ in model (5.5), adapted from [50,75] to consider battery degradation for different EV groups, time index, and scenarios.

$$z_{i,r,t,\xi}^e \geq p_{i,r,t,\xi}^e \ \forall i \in \mathcal{I}^{\text{CS}}, r \in \mathcal{R}, e \in \mathcal{E}, t \in \mathcal{T}, \xi \in \Xi \tag{5.5a}$$

$$z_{i,r,t,\xi}^e \geq -p_{i,r,t,\xi}^e \ \forall i \in \mathcal{I}^{\text{CS}}, r \in \mathcal{R}, e \in \mathcal{E}, t \in \mathcal{T}, \xi \in \Xi \tag{5.5b}$$

$$\text{cap}_{i,r,t,\xi}^{\text{loss},e} = \zeta^e \cdot z_{i,r,t,\xi}^e \cdot \Delta T, \ \forall i \in \mathcal{I}^{CS}, r \in \mathcal{R}, t \in [T_r^{\text{arr}}, T_{r,e}^{\text{dep}}], \xi \in \Xi \tag{5.5c}$$

$$d_{i,r,t,\xi}^{\text{cycle},e} = \frac{\text{cap}_{i,r,t,\xi}^{\text{loss},e}}{1 - \text{Cap}^{\text{end},e}}, \ \forall i \in \mathcal{I}^{CS}, r \in \mathcal{R}, e \in \mathcal{E}, \ t \in [T_{r,e}^{\text{arr}}, T_{r,e}^{\text{dep}}], \xi \in \Xi \tag{5.5d}$$

$$d_{i,r,t,\xi}^e = \max\{d_{i,r,t,\xi}^{\text{cycle},e}, d^{\text{shelf},e}\}, \ \forall i \in \mathcal{I}^{CS}, r \in \mathcal{R}, e \in \mathcal{E}, t \in [T_r^{\text{arr}}, T_{r,e}^{\text{dep}}], \xi \in \Xi \tag{5.5e}$$

$$C_{i,r,t,\xi}^{\text{deg},e} = d_{i,r,t,\xi}^e (C^{\text{rep},e} - C^{\text{res},e}) \text{Cap}^e, \ \forall i \in \mathcal{I}^{CS}, r \in \mathcal{R}, e \in \mathcal{E}, t \in [T_r^{\text{arr}}, T_{r,e}^{\text{dep}}], \xi \in \Xi \tag{5.5f}$$

EV Drivers Modeling

Routing and CS selection of EVs in transportation networks will be modeled in this section. We assume that drivers will select a CS that maximizes their own utility depending on four main factors including locational attractiveness $\beta_{0,s}$, travel time $-\beta_1 tt_{rs}$, charging cost/revenue from charging/discharging $\beta_2 \alpha_{rs}^e$, and a random term ϵ. These factors are included in the utility function of the driver formulated in (5.6) [50,67]. Other exogenous factors can also be included in (5.6) without affecting the modeling and computational strategies proposed in this paper.

$$U_{rs,\xi}^e = \beta_{0,s} - \beta_1 tt_{rs,\xi} + \beta_2 \alpha_{rs,\xi}^e + \epsilon. \tag{5.6}$$

The path travel time and CS selection of the drivers are interrelated as the destination selection of the drivers depends on path travel time and will impact the travel demand distribution of the system, which will eventually affect the travel time of all the drivers. Here, we have adopted the combined distribution and assignment (CDA) model to capture the interrelated CS selection and travel time of the EV drivers as formulated in (5.7). Notice that the CDA_τ model will be solved for any $\tau \in \mathcal{T}^{\text{arr}}$ to estimate the drivers' CS selection at each time step.

The first part of the objective function (5.7a) is the summation of the area under all the link travel cost functions $tt_a(\cdot)$ (e.g., Bureau of Public Roads (BPR) function) and the second part is the entropy of traffic distribution $q_{rs}^e (\ln q_{rs}^e - 1)$ and utility terms (excluding time) in (5.6). The technical proofs discussed in [87] prove that the solution of (5.7) guarantees the first Wardrop principal [89] and the multinomial logit destination choice assumption. Constraint (5.7b) calculates link flows by summing link flows of EVs (x_{rs}^τ) and conventional vehicles ($\bar{x}_{rs}^\tau$) travelling at the same time period τ over all origin and destination pairs. Constraints (5.7c-5.7d) are the vehicle flow conservation at each node for EV travel demand q_{rs}^e and conventional vehicle travel demand $\bar{q}_{rs}^\tau$, respectively. Constraint (5.7e) guarantees the summation of EV traffic flow distribution to each s (q_{rs}^e) equals the total EV travel demand from r, (Q_r^e).

$$\min_{\boldsymbol{x},\bar{\boldsymbol{x}},\boldsymbol{q}\geq 0} \quad \sum_{a\in\mathcal{A}}\int_0^{v_a^\tau} tt_a(u)\mathrm{d}u + \frac{1}{\beta_1}\sum_{\xi\in\Xi}\sum_{r\in\mathcal{R},s\in\mathcal{S}}\sum_{e\in\mathcal{E}^\tau} q_{rs,\xi}^e\left(\ln q_{rs,\xi}^e - 1 - \beta_2\alpha_{rs,\xi}^e - \beta_{0,s}\right) \quad (5.7a)$$

$$\text{s.t.} \quad \boldsymbol{v}^\tau = \sum_{r\in\mathcal{R},s\in\mathcal{S}}\boldsymbol{x}_{rs}^\tau + \sum_{r\in\bar{\mathcal{R}},s\in\bar{\mathcal{S}}}\bar{\boldsymbol{x}}_{rs,\xi}^\tau, \ \forall\tau\in\mathcal{T}^{\mathrm{arr}},\xi\in\Xi \quad (5.7b)$$

$$(\boldsymbol{\eta}_{rs}^\tau) \quad A\boldsymbol{x}_{rs,\xi}^\tau = \sum_{e\in\mathcal{E}^\tau} q_{rs,\xi}^e E_{rs}, \ \forall r\in\mathcal{R}, s\in\mathcal{S}, \tau\in\mathcal{T}^{\mathrm{arr}}, \xi\in\Xi \quad (5.7c)$$

$$A\bar{\boldsymbol{x}}_{rs}^\tau = \bar{q}_{rs}^\tau E_{rs}, \ \forall r\in\bar{\mathcal{R}}, s\in\bar{\mathcal{S}}, \tau\in\mathcal{T}^{\mathrm{arr}} \quad (5.7d)$$

$$\sum_{s\in\mathcal{S}} q_{rs,\xi}^e = Q_{r,\xi}^e, \forall r\in\mathcal{R}, e\in\mathcal{E}^\tau, \xi\in\Xi \quad (5.7e)$$

Market Clearing Conditions

The interaction of stakeholders are modeled as two main clearing conditions here. The power exchange among the DSO, DGs, and CS should be balanced in a way that the power purchased by DSO needs to be balanced with locational power generation. Additionally, the number of EVs selecting a CS should be equal to the expected number of EVs by CSA. These conditions are stated in the hourly market clearing conditions as equation (5.8). Equation (5.8a) guarantees that the total energy purchased by DSO is equal to the total energy generated at each node including DGs and CSs, and equation (5.8b) ensures that the number of EVs selecting a CS is equal to the number of EVs demanded by CSA. Locational prices of electricity $\rho_{i,t,\xi}$ and incentives for EVs $\alpha_{rs,\xi}^e$ can be interpreted as dual variables for the market clearing conditions. Since the objective functions are scaled with scenarios' probabilities Ω_ξ, we have scaled the clearing conditions with the same factor to derive the true prices after solving the optimization problem by evaluating the dual variables of

76

these conditions.

$$(\rho_{i,t,\xi}) \qquad \Omega_\xi \, p^s_{i,t,\xi} = \Omega_\xi \, p^{DG}_{i,t,\xi} + \Omega_\xi \, P^{CS}_{i,t,\xi}, \ \forall i \in \mathcal{I}^{DG} \cup \mathcal{I}^{CS}, \ \forall t \in \mathcal{T}, \xi \in \Xi \qquad (5.8a)$$

$$(\alpha^e_{rs,\xi}) \qquad \Omega_\xi \, q'^e_{rs,\xi} = \Omega_\xi \, q^e_{rs,\xi}, \ \forall r \in \mathcal{R}, s \in \mathcal{S}, e \in \mathcal{E}, \xi \in \Xi \qquad (5.8b)$$

<div align="center">Convex Reformulation</div>

The individual models of stakeholders defined in Section (5)∼(5) are interdependent and need to be solved simultaneously considering the market clearing conditions in equation (5.8), forming the N-MSOPEC model. Direct combination of these models results in a large-scale, highly non-convex complementarity problem, which is challenging to solve. We will extend our proposed reformulation technique in [75] from deterministic to stochastic settings to form an exact convex formulation of the N-MSOPEC framework developed here. We observe that models (5.2)∼(5.4) are convex optimization problems with constraints completely separable. The objective functions of these models are almost separable except for the multiplication terms of primal and dual variables in market clearing conditions (5.8) (i.e., $\rho_{i,t}p^s_{i,t}$, $\rho_{i,t}p^{DG}_{i,t}$, $\rho_{i,t}P^{CS}_{i,t}$, $\alpha^e_{rs,\xi}q'^e_{rs,\xi}$, $\alpha^e_{rs,\xi}q^e_{rs,\xi}$). This type of problem can be reformulated by linearly combining all the (scaled) objective functions and intersecting all the constraint sets in (5.2)∼(5.4). Then, we apply the reverse procedures of Lagrangian relaxation to the market clearing conditions (5.8) [103]. Accordingly, the N-MSOPEC (i.e., (5.2)∼(5.4) and (5.8)) can be equivalently reformulated as a single convex optimization problem (5.9), which can be efficiently solved by commercial nonlinear solvers (e.g., IPOPT). For proof, one can reformulate (5.2)∼(5.4), and (5.8) as variational inequalities (VIs), which can be shown to be equivalent with the VIs for (5.9) (see [75] for details). After solving the problem defined in (5.9), we can derive the locational energy prices ($\rho_{i,t}$) and charging prices ($\beta_{i,t,y}$) by

retrieving the dual variables corresponding to constraints (5.8). Note that model (5.9a) is a classic two-stage stochastic programming problem, which can be further decomposed by system, scenario, and stage to improve computational efficiency for extremely large cases. Since the main focus of this study is not on an extremely large case investigation, we will leave the advanced algorithm design for the future.

$$\min_{\boldsymbol{p}^{\text{CS}}, \boldsymbol{soc}} \sum_{i \in \mathcal{I}^{\text{CS}}} F_i(p_i^{\text{CC}}) + \sum_{\xi \in \Xi} \Omega_\xi \left[\sum_{t \in \mathcal{T}} \left(\sum_{i \in \mathcal{I}^{\text{DG}}} C_i(p_{i,t,\xi}^{\text{DG}}) - \sum_{i \in \mathcal{I}^l} \omega_{i,t} p_{i,t,\xi}^d + \sum_{i \in \mathcal{I}^{CS}} \sum_{r \in \mathcal{R}} \sum_{e \in \mathcal{E}} C_{i,r,t,\xi}^{\text{deg},e} \right) \right.$$

$$\left. + \frac{\beta_1}{\beta_2} \sum_{a \in \mathcal{A}, \tau \in \mathcal{T}^{\text{arr}}} \int_0^{v_a^\tau} tt_a(u) \mathrm{d}u + \frac{1}{\beta_2} \sum_{\tau \in \mathcal{T}^{\text{arr}}} \sum_{r \in R, s \in S} \sum_{e \in \mathcal{E}^\tau} q_{rs,\xi}^e \left(\ln q_{rs,\xi}^e - 1 - \beta_0^s \right) \right] \quad (5.9a)$$

s.t. $(5.2b), (5.3b) \sim (5.3i), (5.4b) \sim (5.4g), (5.5), (5.7b) \sim (5.7e), (5.8)$ \hfill (5.9b)

Numerical Results

In this section, the effectiveness of the proposed model will be investigated based on a small test system coupling DS and TS. The results are mainly used to get meaningful insights into the system interactions and the impact of stochasticity on the systems. For notation simplicity, the term *node* is referred to as a DS node unless declared as a TS node explicitly throughout this section.

Four-node Test System

A small four-node test system (see Figure 5.3) is considered here for deriving insights and evaluating the interdependencies of the systems. Nodes are shown with black lines and numbers, and red

circles show the TS nodes. Distribution lines have the capacity of 2 (pu), and each lines' characteristics (r, x) are included in Figure 5.3. Nodes 1 and 4 are generation nodes connecting to DGs. The generation cost functions for DGs ($C_i(\cdot)$) are assumed to be linear functions w.r.t p^{DG} and the constant cost coefficients for each DG is included in Figure 5.3. Nodes $2 \sim 4$ are load nodes with daily load profiles shown with dashed lines in Figure 5.5. We assumed that loads at node 3 have higher priority of load pickup ($\omega_3 = 60$) compared to nodes 2 and 4 ($\omega_2 = \omega_4 = 50$). The TS nodes 1 and 4 are origin nodes of EVs, and TS nodes 2 and 3 are their candidate charging locations – coupling with the DS. The charging capacity cost function $F_i(\cdot)$ is assumed to be a linear function w.r.t p^{CC} and the cost coefficient for CS at nodes 2 and 3 is 20($/pu).
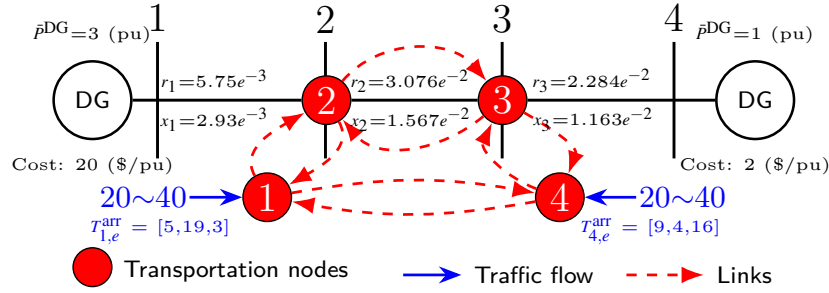
Figure 5.3: Four-node test system

All the transportation links have a capacity parameter in the 4th-order BPR function of 20 vehicles/hour. The incoming traffic of EVs are in one of the three groups based on their $\mathrm{SOC}^{\mathrm{arr}}$ ($\mathrm{SOC}^{\mathrm{arr}}_{r,e=1} = 0.3$, $\mathrm{SOC}^{\mathrm{arr}}_{r,e=2} = 0.6$, and $\mathrm{SOC}^{\mathrm{arr}}_{r,e=3} = 0.8$). We assume that EVs from each origin node are divided evenly between these three groups to consider different charging requirements, e.g., if 30 EVs depart from TS node 1, each group will have 10 EVs. The arrival time of each group to CSs departing from TS origin nodes 1 and 4 ($\tau \; (\in \mathcal{T}^{\mathrm{arr}}_{r,e})$) are selected randomly from a uniform distribution, as reported in Figure 5.3[2].

---

[2]All the random numbers in this paper are generated with random seed=1
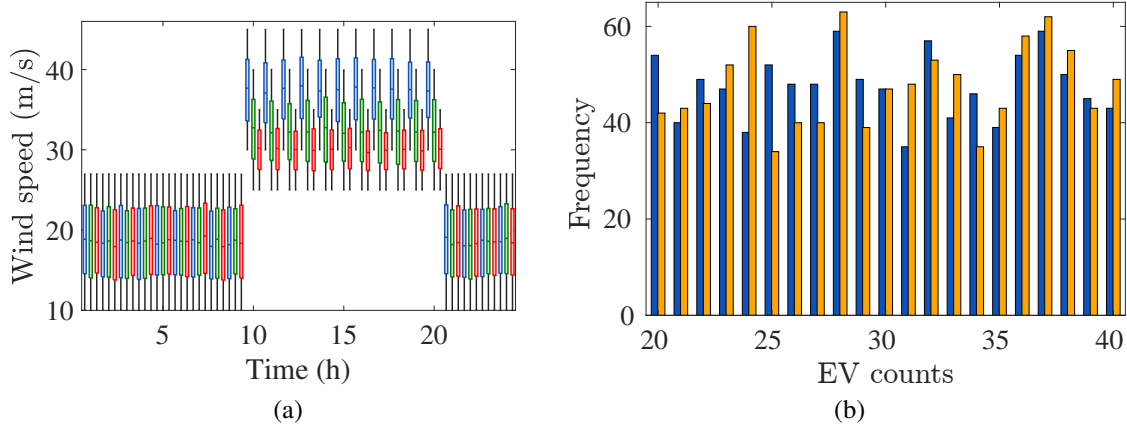
Figure 5.4: Generated scenarios for (a) forecasted day ahead wind speed at lines: ■ 1, ■ 2, and ■ 3; (b) number of occurrences for EV counts from each origin nodes: ■ 1 and ■ 4.

Scenarios are generated based on the methodology discussed in Methodology Overview section. The critical and collapse wind speeds for lines are set as w^{critical}= 30 (m/s) and w^{collapse}= 50 (m/s), respectively [100]. It is assumed that a severe wind condition will hit the area during t= 10∼20 (h). To model this weather condition, wind speed for the area of lines 1, 2, and 3 is selected randomly in the range of w= 30 ∼ 45 (m/s), w= 25 ∼ 40 (m/s), and w= 25 ∼ 35 (m/s), respectively for each hour during that period. Additionally, for other time steps, the wind speed is assumed to be less than the w^{critical} for all the lines. We generated 1000 scenarios of wind speed for each line and time step as reported in Figure 5.4a Then, the line outage probability was calculated based on equation (5.1) with $\bar{\mathcal{P}}$ = 0.003. We assumed that once a lone outage occurs, the line status remain 0 for at least Δ = 3 hours (considering the repair time). We generated 1000 line outage scenarios based on the calculated probabilities and reduced the number of scenarios to 5 for all the lines. The same number of scenarios were generated for the number of EVs as random integers with uniform distributions in the range of 20∼40 for each origin node. Figure 5.4b shows the generated scenarios of EV counts for the two origin nodes. These scenarios were also reduced to 5 scenarios. As mentioned, we assumed that the total number of EVs departed from each origin will be divided

TABLE 5.1 REDUCED LINE OUTAGE AND EV PARTICIPATION SCENARIOS

Scenario ξ	Line outage		Ω	EV counts (Q_r^e)	Ω
	Line	Duration			
1	1	9∼21	0.256	$Q_1^1 = 7.33$, $Q_1^2 = 6.59$, $Q_1^3 = 7.33$ $Q_4^1 = 10$, $Q_4^2 = 10$, $Q_4^3 = 9$	0.173
	2	9∼17			
	3	11∼13			
2	1	9∼21	0.204	$Q_1^1 = 9.33$, $Q_1^2 = 8.39$, $Q_1^3 = 9.33$ $Q_4^1 = 7.66$, $Q_4^2 = 7.66$, $Q_4^3 = 6.89$	0.218
	2	11∼20			
3	1	10∼21	0.311	$Q_1^1 = 9.33$, $Q_1^2 = 8.39$, $Q_1^3 = 9.33$ $Q_4^1 = 12.33$, $Q_4^2 = 12.33$, $Q_4^3 = 11.09$	0.239
	2	13∼15			
4	1	12∼21	0.122	$Q_1^1 = 12$, $Q_1^2 = 10.8$, $Q_1^3 = 12$ $Q_4^1 = 11$, $Q_4^2 = 11$, $Q_4^3 = 9.9$	0.237
	2	9∼20			
5	1	12∼21	0.105	$Q_1^1 = 12.66$, $Q_1^2 = 11.39$, $Q_1^3 = 12.66$ $Q_4^1 = 7.66$, $Q_4^2 = 7.66$, $Q_4^3 = 6.89$	0.133

evenly into three groups (e) to represent EVs with different charging requirements. Table 5.1 shows the number of EVs for each group on the reduced scenarios along with the reduced scenarios of line outages. Note that high winds will also impact the transportation demand and relative highway capacities (41). Here, we will consider a more drastic impact by considering a 10% decrease in travel demand of EVs who have an arrival time during the high wind forecast ($t = 10\sim20$) (i.e., group $e = 2, 3$ EVs from origin nodes 1 and 2, respectively, as these EVs have an arrival time of $T_{r,e}^{\mathrm{arr}} = 19$ and 16 (see Figure 5.3)). Lastly, the reduced scenarios were merged into 25 total scenarios as discussed in Methodology Overview section. In the upcoming subsections, we will delve into power and transportation interdependencies in case analysis and investigate stochastic metrics the stochastic analysis.

Case analysis

To investigate system interdependencies and conduct sensitivity analyses, we designed three cases. In case 1 (base case), the line outage and EV count scenarios are considered with the above-mentioned system characteristics. In case 2, the capacity of the distribution line connecting nodes

3 to 4 is reduced to 0.5 (pu) to evaluate the impact of DS congestion on the overall performance of the model. In case 3, the transportation link capacity of the link connecting TS nodes 1 to 2 is reduced to 2 (vehicle/hour), and the other system characteristics remain the same as in case 1.

(a) Case 1   (b) Case 2   (c) Case 3
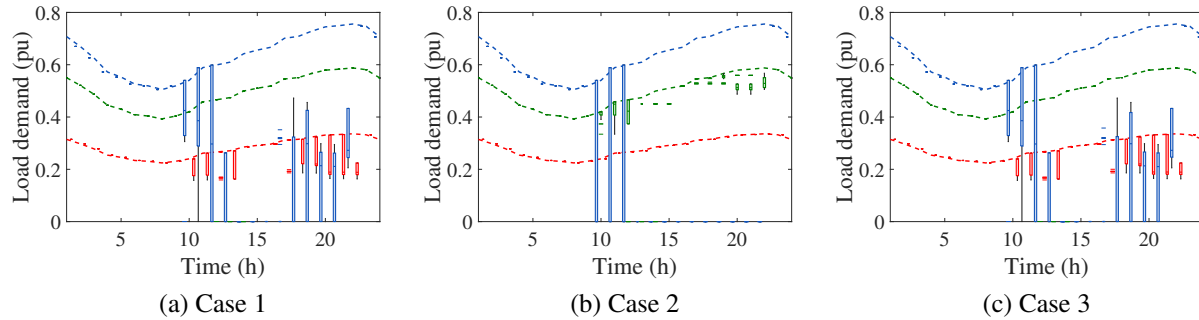
Figure 5.5: Load pickup profile: - - - expected load demand; ▮ node 2, ▮ node 3 , and ▮ node 4.

The load pickup pattern in Figure 5.5 shows that the system was able to manage energy generation from DGs and CSs to fulfill the expected energy demand (dashed lines) for the higher priority load (node 3) in cases 1 and 3 but experience load losses in the other nodes because the line outages limit energy transmission toward these nodes. More load loss occurs at node 2 (Figure 5.5b) because the capacity of distribution line 3–4 has reduced, limiting the energy transmission toward nodes 2 and 3. But in case 2, the system was able to provide the load demand at node 4 since DG at node 4 has enough generation capacity for node 4. On the other hand, the reduced link capacity connecting TS nodes 1–2 did not cause major changes in the load pickup (see Figure 5.5c) because this limitation changes the distribution of EVs to different CSs only (further illustrated in Figure 5.8) and the total EV charging demand/support remains similar to case 1 (illustrated in Figure 5.7).

Figure 5.6 and 5.7 represent the power output of DG and CS nodes respectively for the defined cases. DG at node 4 has provided the highest generation during the day because it has a lower generation cost compared to the DG at node 1. Generation at node 4 decreases when system

82
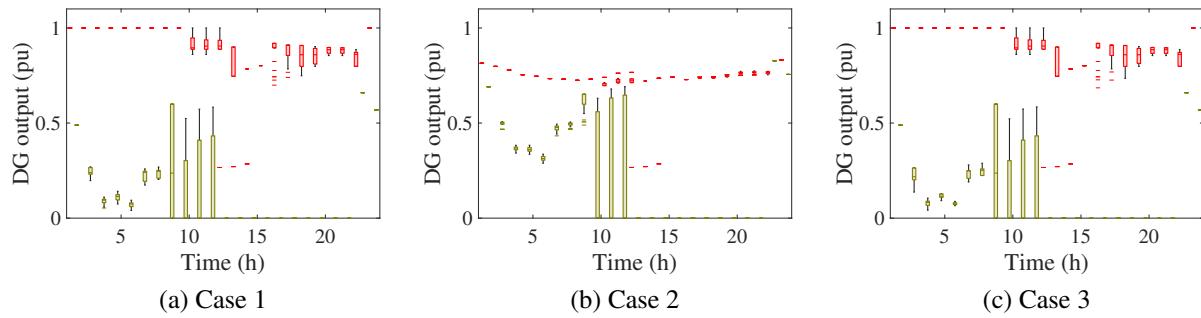
Figure 5.6: Power output of DGs: ▨ node 1 and ▨ node 4.
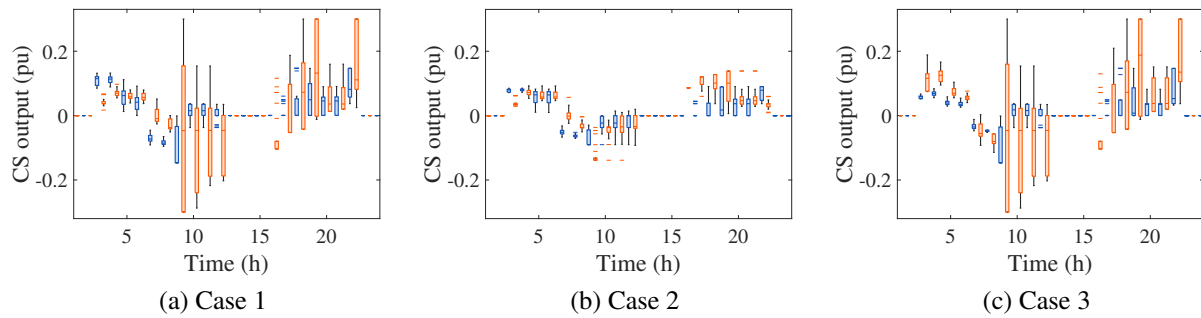
Figure 5.7: Power output of CSs: ▨ node 2 and ▨ node 3.

requirements (e.g., voltage constraints) propel DG at node 1 to provide energy or when CSs can provide energy back to the system (see Figure 5.6). The positive power output at CS nodes 2 and 3 shows the V2G support from EVs at CSs when EVs have sufficient and flexible stored energy; and the negative values represent the charging demand of the EVs (see Figure 5.7). For example, in case 1 (Figure 5.7a), we observe that EVs provide more energy services to the system to prevent load loss at nodes 2 and 3 especially during night time. The power injection patterns in cases 2 and 3 (Figures 5.7b and 5.7b) show the influence of the DS and TS on the decision making of stakeholders in both systems. Without the possibility of energy transmission to node 2 in case 2, the energy output of CS at node 3 has been reduced, which also caused the major reduction of

the CD at node 2 (Figure 5.7b). For example, charging demand at nodes 3 and 2 has significantly decreased during $t = 8{\sim}13$ compared to case 1 to avoid consuming more distribution capacity and causing more load losses. As a consequence, the power injection at node 3 for system support during $t = 17{\sim}22$ is lower compared to case 1 because not enough energy has been charged for EVs in the earlier time periods. In case 3, where the reduced TS link capacity causes congestion for EVs going to node 2 (see Figure 5.8c), we observe that charging demand and system support have shifted from node 2 to node 3 during $t = 3{\sim}7$ and later during $t = 19{\sim}22$ compared to case 1 (see Figure 5.5a). This shift reflects the arrival time of the vehicles departing from nodes 1 to 3. Since the shift in CS outputs has not occurred during the line outage period, it did not cause major changes in load pickup (Figure 5.5c) and incentives (Figure 5.9c). Other time steps with no significant shifts represent the arrival time of EVs departing from node 4 or the EVs from node 1 that have not changed their CS selection compared to case 1 (compare Figure 5.8c and 5.8a).
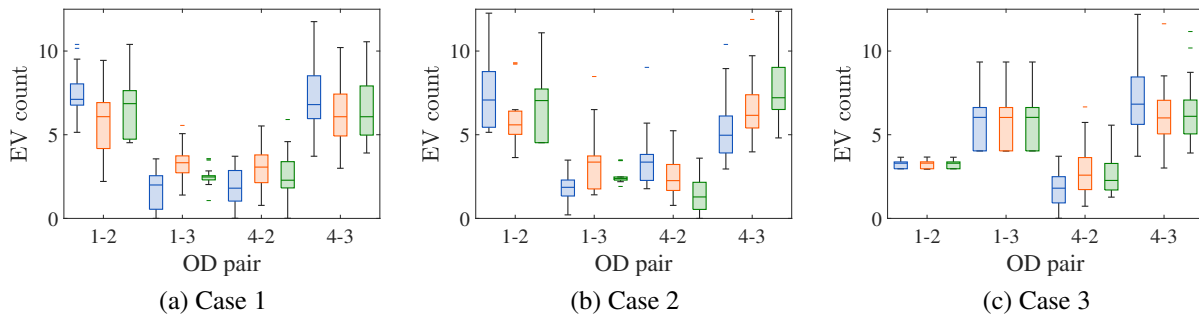
Figure 5.8: EVs' CS selection: ▇ group 1, ▇ group 2, and ▇ group 3.

EV drivers' CS choices are shown in Figure 5.8 as the number of EVs from each group for each OD pair. EVs CS selection co-relates with both the proximity of the charging location and provided incentives by the CSs. EVs with the availability to participate in system support are offered higher incentives (Figure 5.9) and attracted toward the nodes having more generation service needed (Figure 5.8). More system support urgency in case 2 resulted in higher charging costs and higher

incentives for EVs' system support (Figure 5.9b). Consequently, node 2 has attracted more EVs with charging requirements (group 1), which has lower charging costs, and EVs with less charging requirements (groups 2 and 3) are attracted to node 3 in case 2, which offers more system support (Figure 5.8b). This is another indicator that our model could capture close coupling between the coupled systems. The reduced TS link capacity in case 3 increases the travel time from origin node 1 to 2 due to congestion and encourages drivers departing from node 1 to choose the CS at node 3 instead of node 2 (see Figure 5.8c). This shift in CS selection is also reflected in the CS power output shown in Figure 5.6c, which we have discussed previously.

(a) Case 1   (b) Case 2   (c) Case 3
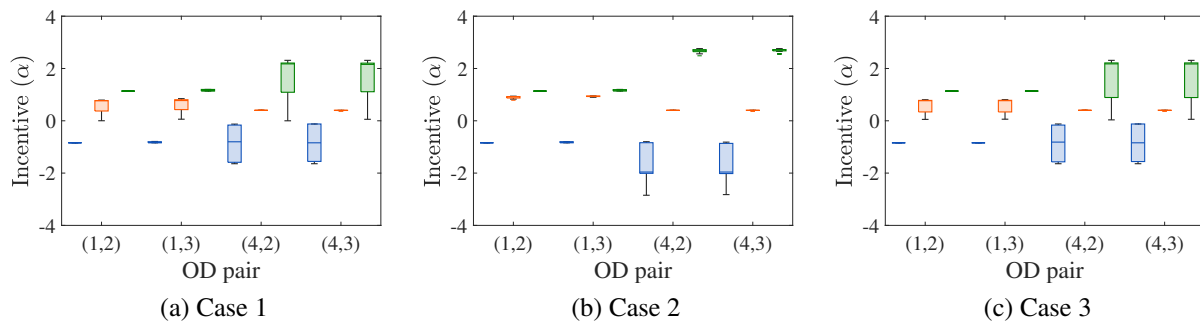
Figure 5.9: CS incentives for EVs: ▬ group 1, ▬ group 2, and ▬ group 3.

We calculated the incentives given to EV drivers by CSA as the dual variables of the clearing conditions discussed in Market Clearing Conditions. Figure 5.9 shows these values for different EV groups in the three cases. The incentives reflect the value of different EV groups to CSA. Negative incentives for group 1 EVs represent charging costs for the drivers as this EV group has higher charging demand, and positive incentives for groups 2 and 3 EVs represent the revenue for those drivers since they have lower charging demand and have the flexibility to provide DS support. EVs with lower charging requirements are offered higher incentives (Figure 5.9) because of their availability to participate in system support during line outages. In case 1 (Figure 5.9a), group 3 EVs departing from TS node 4 receive higher incentives compared to the group 3 EVs departing

from node 1. This is because EVs from TS node 4 arrive at CSs during the time when the system needs more support to avoid load losses. The same reasoning applies for the higher charging cost for group 1 EVs from origin node 4. Incentives for group 3 EVs from origin node 4 have increased in case 2 (see Figure 5.9b) because DS is experiencing higher load losses compared to case 1 (see Figure 5.5) during the dwelling time of these EVs at the CSs. The reduced TS link capacity in case 3 does not change the incentives compared with case 1. This is because although more EVs from node 1 will choose CS at node 3 to avoid congestion in case 3, the power from EVs can be freely transferred between node 2 and 3 since there is no congestion in DS.

Stochastic analysis

First, we calculate the value of the stochastic solution (VSS) by comparing the impacts of using the proposed stochastic modeling with the results of deterministic modeling. The deterministic modeling results are achieved by solving a deterministic problem using the expected value of the uncertain parameters (weighted average value of uncertain parameters based on the probability of scenarios) as its only scenario. In the proposed N-MSOPEC, we can compare the objective function value of each stakeholder in stochastic and deterministic models to evaluate how each stakeholder has benefited from the stochastic modeling compared to the case where they have only considered the expected value of the uncertain parameters.

Second, we compute the expected value of perfect information (EVPI) for each stakeholder. In the single-agent stochastic optimization models, the decision maker can always benefit from knowing the exact realization of the uncertain parameters [104]. In a multi-agent setting, however, agents compete with each other for their own benefits. If all the agents had access to the perfect information, the perfect information may not benefit all the agents. To simulate the case with perfect information, we will allow the planning variable (CS capacity p^{CC}) to be scenario dependent.

Therefore, the objective function of CSA (5.4a) can be reformulated as (5.10) and the bounds of CS capacity constraint (5.4g) will be scenario dependant.

$$
\min_{\substack{p^{\mathrm{CS}},q', \\ p^{\mathrm{CC}},soc}} \quad \sum_{\xi \in \Xi} \Omega_\xi \Big[\sum_{i \in \mathcal{I}^{\mathrm{CS}}} \Big(F_i(p_{i,\xi}^{\mathrm{CC}}) + \sum_{t \in \mathcal{T}} -\rho_{i,t,\xi}\, p_{i,t,\xi}^{\mathrm{CS}} \Big) + \sum_{r \in \mathcal{R}} \sum_{i \in \mathcal{I}^{\mathrm{CS}}} \sum_{e \in \mathcal{E}} \alpha_{ri,\xi}^e q_{ri,\xi}'^e
$$
$$
+ \sum_{i \in \mathcal{I}^{CS}} \sum_{r \in \mathcal{R}} \sum_{t \in \mathcal{T}} \sum_{e \in \mathcal{E}} C_{i,r,t,\xi}^{\mathrm{deg},e} \Big] \tag{5.10}
$$

Accordingly, the charging capacity term in the objective function of the convex reformulation (5.9a) will also be scenario-dependant, and the problem with perfect information can be defined as (5.11). This combined problem can be decomposed by scenario. To calculate the EVPI for each stakeholder, we just need to solve both problems (5.9a) and (5.11) and evaluate the differences in the objective functions of each stakeholder.

$$
\min_{p^{\mathrm{CS}},soc} \quad \sum_{\xi \in \Xi} \Omega_\xi \Big[\sum_{i \in \mathcal{I}^{\mathrm{CS}}} F_i(p_{i,\xi}^{\mathrm{CC}}) + \sum_{t \in \mathcal{T}} \Big(\sum_{i \in \mathcal{I}^{\mathrm{DG}}} C_i(p_{i,t,\xi}^{\mathrm{DG}}) - \sum_{i \in \mathcal{I}^l} \omega_{i,t} p_{i,t,\xi}^d + \sum_{i \in \mathcal{I}^{\mathrm{CS}}} \sum_{r \in \mathcal{R}} \sum_{e \in \mathcal{E}} C_{i,r,t,\xi}^{\mathrm{deg},e} \Big)
$$
$$
+ \frac{\beta_1}{\beta_2} \sum_{a \in \mathcal{A}, \tau \in \mathcal{T}^{\mathrm{arr}}} \int_0^{v_a^\tau} tt_a(u)\mathrm{d}u + \frac{1}{\beta_2} \sum_{\tau \in \mathcal{T}^{\mathrm{arr}}} \sum_{r \in R, s \in S} \sum_{e \in \mathcal{E}^\tau} q_{rs,\xi}^e \big(\ln q_{rs,\xi}^e - 1 - \beta_0^s \big) \Big]
$$
$$
\tag{5.11a}
$$

s.t. $\quad (5.2b), (5.3b) \sim (5.3i), (5.4b) \sim (5.4g), (5.5), (5.7b) \sim (5.7e), (5.8)$ $\tag{5.11b}$

Figure 5.10 shows the objective values of stakeholders in three types of modeling, i.e., stochastic, deterministic, and perfect information. Note that the objective of DGs and CSA, as defined in (2a) and (5.4a), are minimization problems, and the objective of DSO (3a) is a maximization problem. In other words, lower objective values are favorable for DGs and CSA, and a higher
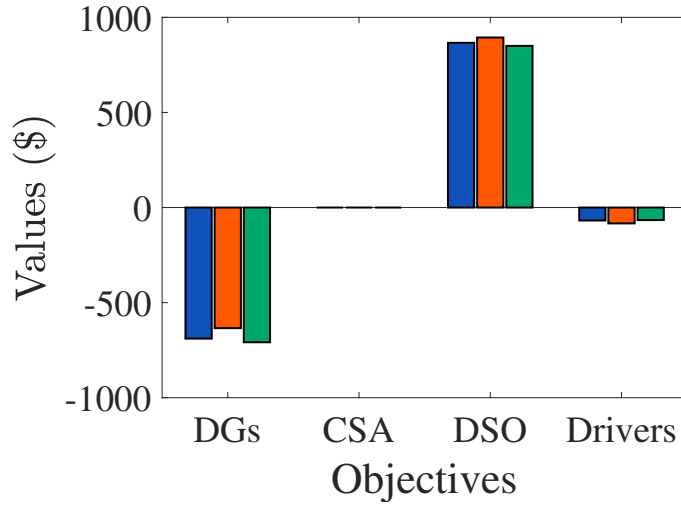
Figure 5.10: Stakeholders' objectives

objective value is favorable for DSO. As for the EV drivers, the objective is defined as the total expected utility ($\mathbb{E} \sum u_{rs}^e q_{rs}^e$). The difference between stochastic and deterministic objective values represents VSS. We observed that stochastic modeling was more beneficial for DGs and the drivers where they achieved lower objectives/higher utility compared to the deterministic problem. This is because considering uncertainty will reflect the extreme energy shortage scenarios, where energy prices and EV incentives are higher for DGs and EV drivers. However, the DSO had better objective values in the deterministic modeling. The CSA acted as a non-beneficiary entity in the equilibrium model and had an objective function value close to zero in all three types of modelings. This is because the objective function of CSA is linear to energy prices and EV incentives, which are both determined by market clearing conditions. These results show that, in the multi-agent framework, stakeholders may benefit differently by adopting a stochastic modeling approach compared with deterministic models.

Comparing the objective values of stochastic and perfect information problems will give us the EVPI. We observed that DGs and EV drivers benefited from having access to perfect information,

reduced their costs and increase their utility, respectively. This is because perfect information allows the CSA to make scenario-dependent investments avoiding over-investment, which will increase the locational energy prices and EV incentives. On the other hand, the DSO has incurred less objective value. The results show that, unlike centralized problems where a central entity would benefit from perfect information, in mutli-agent framework, all decision makers will respond to perfect information, and their decisions are impacting the benefits of each other. The aggregate impacts of more information on each decision maker will include both the impacts brought by more information to the system and the secondary impacts brought by the response of other decision makers to more information.

Additionally, we investigated the total expected load loss in the three types of modeling. The load loss decreased from 7.6788 pu in deterministic modeling to 7.2199 pu in stochastic modeling, and perfect information helped further reduce the total load loss to 7.1232 pu. The reason is that a deterministic approach overlooks the potential extreme supply shortage scenarios, which have a higher return and under-investment. Also, the system improved load pickup with perfect information as the CSA could plan independently for each scenario of outages to allow DSO to operate more efficiently, resulting in better load pick-up opportunities for EVs and DGs.

Conclusion

We explored the potential value of private electric vehicles (EVs) for load pickup in a coupled power distribution and transportation system with uncertainties of line outage and EV participation. We developed a network-based multi-agent stochastic optimization problem with equilibrium constraints (N-MSOPEC) framework to capture the decision making of decentralized stakeholders in both distribution and transportation systems incentivizing EV participation. A large number of line outages and EV participation scenarios were generated and further reduced to high probable

scenarios to reflect the stochastic nature of the system while ensuring computational tractability. We then propose an exact convex reformulation to the N-MSOPEC, so that the highly non-convex N-MSOPEC problem can be effectively solved by commercial non-linear solvers with guaranteed global convergence. The simulation results on a small test system and designed case studies provided insights into the value of private EVs on distribution system support during line outages. The results showed that our model could capture the interactions between key stakeholders to quantify the value of EVs' DS system support. Some key takeaways from the numerical studies are: 1) EV participation along with DG generations can help fulfill the high-priority loads and reduce total load loss. 2) The incentives offered by the CSs depend on the flexibility of EV charging, the needs of DS load pickup, and the accessibility of CSs. 3) Characteristics of both power and transportation systems influence the decision making of stakeholders, and a holistic modeling approach is necessary to capture these complex couplings.Additionally, we found out that stochastic modeling or perfect information does not necessarily benefit all stakeholders. The proposed multi-agent modeling framework can be an effective tool to quantify the impacts of stochasticity and information on individual stakeholders.

The proposed methodology can be used by transportation and distribution system planners for evaluating alternative system upgrade plans considering a large-scale EV adoption in the future. In addition, charging station aggregators can leverage the proposed models to guide their incentive design to attract EVs to provide distribution system services at the right time and locations. For the government, this model can be used to evaluate regulations on the V2G market and policies on promoting EV adoption and V2G participation. To enable a real world large-scale study, decomposition based methods can be further developed to the reformulated convex optimization model as a nature extension to improve the computational efficiency. Additionally, the modeling can be extended to consider other weather-related events, such as extreme temperatures and flooding rains, by incorporating additional line fragility functions for each weather condition.

CHAPTER 6: MULTI-STAGE CHARGING STATION AND DISTRIBUTED GENERATOR CAPACITY EXPANSION IN DECENTRALIZED POWER DISTRIBUTION AND TRANSPORTATION SYSTEMS[1]

Introduction

As worldwide environmental concerns have propelled governments to issue long-term plans for the transportation sector to become fully electric, we are observing an increasing EV adoption pattern. The pathways towards transitioning to EVs requires a reliable charging infrastructure, providing the CD of EVs. The prerequisite for such infrastructure requires a long-term plan from both power and transportation systems. From the perspective of the power distribution system operator (DSO), the distribution system (DS) will need to accommodate a combination of the growing EV CD and the existing load profiles. Therefore, the capacity of CSs and generation units need to be carefully planned spatially and temporally to fulfill the charging needs while minimizing grid impacts. DGs are the key energy sources in DSs that need to plan for the growing CD of EVs along with the CSs. One important aspect of this long-term plan is how to model the independent stakeholders in the coupled DTSs where the decision making of each stakeholder will impact the others. Here, we have formulated the CS and DG capacity planning problem as a multi-stage multi-agent optimization problem where the non-cooperative stakeholders make decisions to fulfill their own objectives in coupled DTSs. The proposed model provides a practical framework for better understanding the interaction of private investors and better preparing for a large number of EVs. The proposed model incorporates both long-term planning actions and

---

[1]This chapter is developed based on an article currently under 2nd round peer-review process at the journal of IEEE Systems Journal

short-term operational decision makings. Feedback effects of CS availability and EV adoption can be explicitly captured and locational electricity prices can be endogenously determined. The original formulation is a high-dimensional non-convex problem, which is further reformulated as a convex problem that can be solved efficiently. In summary, the main contribution is that we have developed a computational tractable multi-stage multi-agent joint CS and DG capacity planning model that can capture the decentralized decision making of different stakeholders from both TS and DSs and identify plausible paths of system evolvement to achieve a target EV penetration level.

The remainder of this chapter is organized as follows: the Mathematical Modeling section summarizes the overall problem followed by the detailed modeling and reformulation strategies. Results section discusses the outcomes obtained from solving the proposed model on test systems and sensitivity analyses on important parameters. Conclusion section concludes the paper with a summary of findings and potential future research directions.

The following list provides the definition of all the notations and indices used for the problem modeling in this chapter.

Sets and Indices

- $\mathcal{E}$: Set of EV groups, indexed by e
    - $\mathcal{E}^\tau$: set of EV groups arriving at CSs at time τ

- $\mathcal{I}$: Set of distribution system nodes, indexed by i or j
    - $\mathcal{I}^{\mathrm{CS}}$: set of charging station nodes
    - $\mathcal{I}^{\mathrm{DG}}$: set of distributed generation nodes
    - $\mathcal{I}^L$: set of load nodes

- $\mathcal{L}$: Set of distribution lines, indexed by l

- $\mathcal{R}$: Set of vehicle origin nodes in transportation network, indexed by r

92

- $\mathcal{S}$: Set of charging locations in transportation network, indexed by s

- $\mathcal{T}$: Set of time periods in one day, indexed by t or τ

- $\mathcal{Y}$: Set of years in planning horizon, indexed by y

Parameters

- α: Discount factor

- $\gamma_{i,t,y}$: Charging cost for EVs at CS i time t of year y

- δ_r^e: Fraction of total number of EVs for group e EVs

- ω_r^y: Predicted EV growth rate for each year y departing from r

- $b_0/b_1/b_2$: Drivers' utility function coefficients

- B_y^{CS}: CS upgrade budget in year y

- $B_{i,y}^{\mathrm{DG}}$: DG upgrade budget for DG i in year y

- $C_i^1/C_i^2/C_i^3$: Generation upgrade /maintenance/production cost functions for DG i

- Cap^e: Total battery capacity of group e EVs.

- F_i^1/F_i^2: Capacity upgrade/maintenance cost functions for CS i

- $\mathrm{FN}_l/\mathrm{TN}_l$: Start/end nodes of line l

- k: Yearly EV adoption coefficient based on available total charging capacity

- $\mathrm{LF}_{l,i}/\mathrm{LT}_{l,i}$: Incidence matrices with element l, i: equals to 1 if line l starts/connects from/to node i and zero otherwise

- $\bar{P}_{r,e}^{\mathrm{ch}}$: Maximum charge rate of group e EVs departing from r

- $\underline{P}_i^{\mathrm{DG}}$: Minimum active generation capacity of DG i

- $P_{i,t,y}^d/Q_{i,t,y}^d$: Active/reactive load demand at node i and time t of year y

- pr_{rs}^y: Probability of a driver departing from r to select a CS at location s at year y

- $\bar{Q}_{rs}^y$: Predicted EV traffic flow from r to s at year y

- r_l/x_l: Resistance/reactance of line l

- S^{base}: The nominal apparent power of the DS

- S_l^{max}: Maximum apparent power of line l

- $\mathrm{SOC}_{r,e}^{\mathrm{arr}}/\mathrm{SOC}_{r,e}^{\mathrm{dep}}$: Arrival/minimum required departure SOC of group e EVs departing from node r

- $\underline{\mathrm{SOC}}^e/\overline{\mathrm{SOC}}^e$: Minimum/maximum SOC permissible for group e EVs

- $T_{r,e}^{\mathrm{arr}}/T_{r,e}^{\mathrm{dep}}$: Arrival/departure time of group e EVs to/from CSs traveling from r

- U_{rs}^y: Utility of a driver at origin node r selecting a CS at destination node s of year y

- $V_i^{\mathrm{min}}/V_i^{\mathrm{max}}$: Minimum/maximum voltage at node i

Variables

- $\beta_{i,t,y}$: Charging/service cost for CSA/users at node i and time t of year y

- $\rho_{i,t,y}$: Electricity price at node i and time t of year y

- $A_{i,y}$: Additional generation capacity for DG i in year y

- $D_{i,y}$: Additional charging capacity for CS i in year y

- $p_{i,r,t}^{e,y}$: Aggregated CD of group e EVs at CS $i(s)$, traveling from r at time t of year y

- $p_{i,t,y}^{\mathrm{CS}}$: Aggregated CD at CS $i(s)$ at time t of year y

- $p_{i,t,y}^{\mathrm{DG}}/q_{i,t,y}^{\mathrm{DG}}$: Active/reactive power generation of DG at node i and time t of year y

- $p_{i,t,y}^{d}$: CD satisfied by DSO at node i and time t of year y

- $p_{i,t,y}^{s}/q_{i,t,y}^{s}$: Active/reactive power purchased by DSO at node i and time t of year y

- $p_{i,y}^{\mathrm{CC}}$: Total charging capacity of CS i in year y

- $q_{rs}^{e,y}$: Travel demand of group e EVs from r to s in year y

- $Q_{r}^{e,y}$: Total number of group e EVs departing from r in year y

- $\mathcal{Q}_{r}^{y}$: Total number of EVs departing from r in year y

- $\bar{S}_{i,y}^{DG}$: The generation capacity of DG at node i of year y

- $\mathrm{soc}_{i,r,t}^{e,y}$: SOC of group e EVs departing from r at CS $i(s)$ and time t of year y

- $v_{i,t}$: Squared voltage magnitude at node i and time t

Mathematical Modeling

On one hand, the increasing EV adoption and charging demand require effective planning of CS and DG generation; on the other hand, the planning of CSs and DGs influences the charging availability and electricity costs, which affects the future EV adoption and charging demand distribution. We will model the multi-stage CS and DG planning for a growing number of EVs over years considering these closed coupling. Our objective is to determine the equilibrium investment patterns of CSs and DGs capacity for each year considering key stakeholders' own interests while reaching the desired target level of EV adoption at the end of the planning horizon.

We consider three key decentralized decision makers that are involved in the CS and DG planning problem: 1) DSO, 2) CSA, and 3) DG owners. In this section, we will present the mathematical modeling of the proposed network-based multi-stage multi-agent optimization problems with equilibrium constraints (NM-MOPEC) framework, in which we model the decentralized decision-making of each stakeholder and equilibrium conditions in a coupled distribution and transportation system. In addition, to mitigate the computational challenges brought by non-convexity, we propose an exact convex reformulation to solve the NM-MOPEC efficiently.

DG Owners Modeling

Each DG i ($\in \mathcal{I}^{DG}$) determines its hourly generation quantity $p_{i,t,y}^{DG}$ and yearly added capacity $U_{i,y}^{DG}$ to minimize net costs (i.e., maximize profits). We assume that DG owners are perfectly competitive since each DG owner has limited capacity and does not have the market power to influence the locational electricity prices $\rho_{i,t,y}$ [67]. Therefore, the decision making of all DG owners can be aggregated and formulated in model (6.1).

$$\min_{\substack{p^{DG},q^{DG}, \\ \bar{S}^{DG},U^{DG}\geq 0}} \quad \sum_{y\in\mathcal{Y}} \alpha^y \Bigg[\sum_{i\in\mathcal{I}^{DG}} \Big[C_i^1(U_{i,y}) + C_i^2(\bar{S}_{i,y}^{DG}) + \sum_{t\in\mathcal{T}} \big(C_i^3(p_{i,t,y}^{DG}) - \rho_{i,t,y} p_{i,t,y}^{DG} \big) \Big] \Bigg] \quad (6.1a)$$

$$\text{s.t.} \quad p_{i,t,y}^{DG\,2} + q_{i,t,y}^{DG\,2} \leq (\bar{S}_{i,y}^{DG})^2,$$

$$\forall i \in \mathcal{I}^{DG}, t \in \mathcal{T}, y \in \mathcal{Y} \quad (6.1b)$$

$$p_{i,t,y}^{DG} \geq \underline{P}_i^{DG}, \ \forall i \in \mathcal{I}^{DG}, t \in \mathcal{T}, y \in \mathcal{Y} \quad (6.1c)$$

$$\bar{S}_{i,0}^{DG} = \bar{S}_i^{\text{Init}} \quad (6.1d)$$

$$\bar{S}_{i,y}^{DG} = \bar{S}_{i,y-1}^{DG} + U_{i,y}^{DG}, \ \forall i \in \mathcal{I}^{DG}, y \in \mathcal{Y}/\{0\} \quad (6.1e)$$

$$C_i^1(U_{i,y}) \leq B_{i,y}^{DG}, \ \forall i \in \mathcal{I}^{DG}, y \in \mathcal{Y} \quad (6.1f)$$

Objective (6.1a) minimizes the cost of DG owners, calculated as the total cost of additional generation capacity $\sum_{y\in\mathcal{Y}} \alpha^y \sum_{i\in\mathcal{I}^{DG}} C_i^1(U_{i,y})$, total cost of yearly maintenance with respect to total installed generation capacity $\sum_{y\in\mathcal{Y}} \alpha^y \sum_{i\in\mathcal{I}^{DG}} C_i^2(\bar{S}_{i,y})$, and total costs of energy production $\sum_{i\in\mathcal{I}^{DG}} \sum_{t\in\mathcal{T}} C_i^3(p_{i,t}^{DG})$ subtracting the total revenue from energy sales $\sum_{i\in\mathcal{I}^{DG}} \sum_{t\in\mathcal{T}} \rho_{i,t} p_{i,t}^{DG}$. We assume $C_i^k(\cdot)$ to be convex functions [77] with respect to $U_{i,y}$, $\bar{S}_{i,y}$, and $\bar{p}_{i,y}^{DG}$, respectively, with different cost parameters for different DGs. This implies non-decreasing marginal costs. Note that, the energy prices $\rho_{i,t,y}$ are determined endogenously in our modeling framework based on energy supply and demand balancing, which will be discussed in Section 6. Constraint (6.1b) specifies the upper bounds of total power generation for each DG at each time step. Constraint (6.1c) restricts the minimum generation output of DGs. Constraint (6.1d) sets the initial capacity of DGs. Constraint (6.1e) calculates the total DG capacity at each year based on the added capacity $U_{i,y}$ at year y and the existing capacity in the previous year $y-1$. Moreover, we consider each DG investor may have limited annual budget for upgrading its generation capacity, as formulated in constraint (6.1f).

DSO Modeling

The DSO intends to minimize the total operation costs while satisfying system operational constraints, which can be formulated as model (6.2). Objective (6.2a) minimizes the total cost of purchased energy from DG generators and upstream substation $\sum_{y\in\mathcal{Y}} \left(\alpha^y \sum_{i\in\mathcal{I}^{DG}} \sum_{t\in\mathcal{T}} \rho_{i,t,y} p_{i,t,y}^s \right)$ subtracting the revenue from supplying energy to CSs $\sum_{y\in\mathcal{Y}} \left(\alpha^y \sum_{i\in\mathcal{I}} \sum_{t\in\mathcal{T}} \beta_{i,t,y} p_{i,t,y}^s \right)$. Operational constraints are formulated in (6.2b)-(6.2f), which are adapted based on the Dist-Flow equations proposed in [78]. Active (including charging demand) and reactive power flow balances are modeled in (6.2b) and (6.2c), respectively. Constraint (6.2d) limits power flow not exceeding line capacity. Constraint (6.2e) calculates the voltage at each node while constraint (6.2f) defines the acceptable voltage range at each node.

$$\min_{\substack{\boldsymbol{v} \geq \boldsymbol{0}, \\ \boldsymbol{p^s}, \boldsymbol{pf}, \boldsymbol{qf}}} \quad \sum_{y \in \mathcal{Y}} \alpha^y \Big[\sum_{i \in \mathcal{I}^{\mathrm{DG}}} \sum_{t \in \mathcal{T}} \rho_{i,t,y} p^s_{i,t,y} - \sum_{i \in \mathcal{I}} \sum_{t \in \mathcal{T}} \beta_{i,t,y} p^d_{i,t,y} \Big] \tag{6.2a}$$

$$\text{s.t.} \quad \sum_{l \in \mathcal{L}} pf_{l,t,y} \cdot \mathrm{LT}_{l,i} - \sum_{l \in \mathcal{L}} pf_{l,t,y} \cdot \mathrm{LF}_{l,i} = P^d_{i,t,y} + p^d_{i,t,y} - p^s_{i,t,y}, \ \forall i \in \mathcal{I}, t \in \mathcal{T}, y \in \mathcal{Y}$$

$$\tag{6.2b}$$

$$\sum_{l \in \mathcal{L}} qf_{l,t,y} \cdot \mathrm{LT}_{l,i} - \sum_{l \in \mathcal{L}} qf_{l,t,y} \cdot \mathrm{LF}_{l,i} = Q^d_{i,t,y} - q^s_{i,t,y}, \ \forall i \in \mathcal{I}, t \in \mathcal{T}, y \in \mathcal{Y} \tag{6.2c}$$

$$pf^2_{l,t,y} + qf^2_{l,t,y} \leq (S^{\max}_l)^2, \ \forall l \in \mathcal{L}, t \in \mathcal{T}, y \in \mathcal{Y} \tag{6.2d}$$

$$v_{\mathrm{FN}_l,t,y} - v_{\mathrm{TN}_l,t,y} = 2 \cdot (r_l \cdot pf_{l,t,y} + x_l \cdot qf_{l,t,y}), \forall l \in \mathcal{L}, t \in \mathcal{T}, y \in \mathcal{Y} \tag{6.2e}$$

$$V^{\min 2}_i \leq v_{i,t,y} \leq V^{\max 2}_i, \ \forall i \in \mathcal{I}, t \in \mathcal{T}, y \in \mathcal{Y} \tag{6.2f}$$

Drivers charging choice modeling

To model drivers' choices of charging locations in the transportation system, we adopt a logit model, where drivers choose the CS locations that maximize their own utility. Denote set $r \in \mathcal{R}$ is the location of EV drivers and set $s \in \mathcal{S}$ is candidate charging locations. The utility function U_{rs} of a driver selecting location s from r is formulated in (6.3) [50, 67, 105]. We assume that EV drivers make charging location choices based on four factors: locational attractiveness $b_{0,s}$, travel time $-b_1 tt_{rs}$, charging cost $-b_2 \gamma^e_{rs}$, and a random term ϵ. Other exogenous factors can also be included in (6.3) without affecting the modeling and computational strategies proposed in this chapter. Note that travel time incorporates travel distance, congestion, and other traffic incidents, which are important factors in the decision-making of drivers.

$$U^y_{rs} = b_{0,s} - b_1 tt_{rs} - b_2 \gamma_{s,y} + \epsilon. \tag{6.3}$$

Then, the probability of a driver (pr_{rs}) choosing CS s departing from r can be calculated as a function of U_{rs} using (6.4).

$$\text{pr}_{rs}^y = \frac{e^{U_{rs}^y}}{\sum_{s \in S} e^{U_{rs}^y}}. \tag{6.4}$$

The calculated probability can be used as the expected percentage of the drivers who start from r and charge at location s. We will use this probability to distribute the total traffic flow of EVs from each origin node to the candidate CS nodes in the next section.

CSA Modeling

A CSA is a private entity managing charging infrastructure and EV charging activities. The CSA aims to minimize its costs (i.e., maximize its profits) [82] while satisfying the charging requirements of EVs. The decision making of the CSA is formulated in model (6.5). Objective (6.5a) minimizes the CSA's present value of costs, which is calculated as summing the discounted costs of (1) adding new charging capacity $\sum_{y \in \mathcal{Y}} \alpha^y \sum_{i \in \mathcal{I}} F_i^1(D_{i,y})$, (2) maintaining the existing CS based on its total charging capacity $\sum_{y \in \mathcal{Y}} \alpha^y \sum_{i \in \mathcal{I}} F_i^2(p_{i,y}^{CC})$, (3) purchasing energy from the system $\sum_{y \in \mathcal{Y}} \alpha^y \sum_{i \in \mathcal{I}} \sum_{t \in \mathcal{T}} \beta_{i,t,y}(p_{i,t,y}^{CS})$, and subtracting the revenue received from charging EVs $\sum_{y \in \mathcal{Y}} \alpha^y \sum_{i \in \mathcal{I}} \sum_{t \in \mathcal{T}} \gamma_{i,t,y}(p_{i,t,y}^{CS})$. Similar with electricity purchasing cost from DG ($\rho_{i,t,y}$), electricity cost for CSA ($\beta_{i,t,y}$) will be determined endogenously by the market electricity supply and demand, as discussed in Section 6.

In this paper, we assume that the increase in EV numbers will be endogenously influenced by the available charging capacity of CSs in addition to the overall growth trend. Therefore, we modeled the yearly growth of EV traffic in constraint (6.5b) where the total EV flow from origin r at year y ($\mathcal{Q}_r^y$) is calculated as the base growth from the previous year $(1 + \omega_r^y)\mathcal{Q}_r^{y-1}$ plus the additional EV growth based on the availability of the total charging capacity $k \sum_{i \in \mathcal{I}^{CS}} p_{i,y}^{CC}$. Other EV growth

mechanisms can also be modeled within the proposed modeling framework.

$$\min_{\substack{\boldsymbol{p}^{\text{CS}},\text{soc} \\ \boldsymbol{p}^{\text{CC},D}}} \quad \sum_{y\in\mathcal{Y}} \alpha^y \sum_{i\in\mathcal{I}^{\text{CS}}} \left[F_i^1(D_{i,y}) + F_i^2(p_{i,y}^{\text{CC}}) + \sum_{t\in\mathcal{T}} \left(\beta_{i,t,y}\, p_{i,t,y}^{\text{CS}} - \gamma_{i,t,y}\, p_{i,t,y}^{\text{CS}} \right) \right] \tag{6.5a}$$

$$\text{s.t.} \quad Q_r^y = (1 + \omega_r^y)\, Q_r^{y-1} + k \sum_{i\in\mathcal{I}^{\text{CS}}} p_{i,y}^{CC}, \ \forall r \in \mathcal{R}, y \in (0, Y] \tag{6.5b}$$

$$Q_r^0 = \bar{Q}_r^{\text{Init}}, \ \forall r \in \mathcal{R}, s \in \mathcal{S} \tag{6.5c}$$

$$Q_r^{e,y} = \delta_e\, Q_r^y, \ \forall r \in \mathcal{R}, e \in \mathcal{E}, y \in \mathcal{Y} \tag{6.5d}$$

$$q_{rs}^{e,y} = \text{pr}_{rs}^y\, Q_r^y, \ \forall r \in \mathcal{R}, s \in \mathcal{S}, y \in \mathcal{Y} \tag{6.5e}$$

$$\text{soc}_{i,r,t}^{e,y} = \text{soc}_{i,r,t-1}^{e,y} + p_{i,r,t}^{e,y}/\text{Cap}^e, \ \forall i \in \mathcal{I}^{\text{CS}}, r \in \mathcal{R}, e \in \mathcal{E}, t \in (T_{r,e}^{\text{arr}}, T_{r,e}^{\text{dep}}], y \in \mathcal{Y} \tag{6.5f}$$

$$q_{ri(s),t}^{e,y}\underline{\text{SOC}}^e \leq \text{soc}_{i,r,t}^{e,y} \leq q_{ri(s),t}^{e,y}\overline{\text{SOC}}^e, \ \forall i \in \mathcal{I}^{\text{CS}}, r \in \mathcal{R}, e \in \mathcal{E}, t \in [T_{r,e}^{\text{arr}}, T_{r,e}^{\text{dep}}], y \in \mathcal{Y}$$
$$\tag{6.5g}$$

$$\text{soc}_{i,r,T_{r,e}^{\text{arr}}}^{e,y} = q_{ri(s),t}^{e,y}\text{SOC}_{r,e}^{\text{arr}}, \ \forall i \in \mathcal{I}^{\text{CS}}, r \in \mathcal{R}, e \in \mathcal{E}, y \in \mathcal{Y} \tag{6.5h}$$

$$\text{soc}_{i,r,T_{r,e}^{\text{dep}}}^{e,y} \geq q_{ri(s),t}^{e,y}\text{SOC}_{r,e}^{\text{dep}}, \ \forall i \in \mathcal{I}^{\text{CS}}, r \in \mathcal{R}, e \in \mathcal{E}, y \in \mathcal{Y} \tag{6.5i}$$

$$0 \leq p_{i,r,t}^{e,y} \leq q_{ri(s),t}^{e,y}\bar{P}_{r,e}^{\text{ch}}, \forall i \in \mathcal{I}^{\text{CS}}, r \in \mathcal{R}, e \in \mathcal{E}, t \in [T_{r,e}^{\text{arr}}, T_{r,e}^{\text{dep}}], y \in \mathcal{Y} \tag{6.5j}$$

$$p_{i,t,y}^{\text{CS}} = \sum_{r\in\mathcal{R}} \sum_{e\in\mathcal{E}} \frac{p_{i,r,t}^{e,y}}{S^{\text{base}}}, \ \forall i \in \mathcal{I}^{\text{CS}}, t \in [T_{r,e}^{\text{arr}}, T_{r,e}^{\text{dep}}] \tag{6.5k}$$

$$0 \leq p_{i,t,y}^{\text{CS}} \leq p_{i,y}^{\text{CC}} \ \forall i \in \mathcal{I}^{\text{CS}}, t \in [T_{r,e}^{\text{arr}}, T_{r,e}^{\text{dep}}], y \in \mathcal{Y} \tag{6.5l}$$

$$p_{i,y}^{\text{CC}} = p_{i,y-1}^{\text{CC}} + D_{i,y}, \ \forall i \in \mathcal{I}^{\text{CS}}, y \in (0, Y] \tag{6.5m}$$

$$p_{i,0}^{\text{CC}} = \bar{P}_i^{\text{CC,Init}}, \ \forall i \in \mathcal{I}^{\text{CS}} \tag{6.5n}$$

$$\sum_{i\in\mathcal{I}^{\text{CS}}} F_i^1(D_{i,y}) \leq B_y^{\text{CS}}, \ \forall y \in \mathcal{Y} \tag{6.5o}$$

Objective (6.5a) minimizes the CSA's present value of costs, which is calculated as summing the discounted costs of (1) adding new charging capacity $\sum_{y\in\mathcal{Y}} \alpha^y \sum_{i\in\mathcal{I}} F_i^1(D_{i,y})$, (2) maintaining the existing CS based on its total charging capacity $\sum_{y\in\mathcal{Y}} \alpha^y \sum_{i\in\mathcal{I}} F_i^2(p_{i,y}^{CC})$, (3) purchasing en-

ergy from the system $\sum_{y \in \mathcal{Y}} \alpha^y \sum_{i \in \mathcal{I}} \sum_{t \in \mathcal{T}} \beta_{i,t,y}(p_{i,t,y}^{CS})$, and subtracting the revenue received from charging EVs $\sum_{y \in \mathcal{Y}} \alpha^y \sum_{i \in \mathcal{I}} \sum_{t \in \mathcal{T}} \gamma_{i,t,y}(p_{i,t,y}^{CS})$. Similar with electricity purchasing cost from DG ($\rho_{i,t,y}$), electricity cost for CSA ($\beta_{i,t,y}$) will be determined endogenously by the market electricity supply and demand, as discussed in Section 6.

In this paper, we assume that the increase in EV numbers will be endogenously influenced by the available charging capacity of CSs in addition to the overall growth trend. Therefore, we modeled the yearly growth of EV traffic in constraint (6.5b) where the total EV flow from origin r at year y ($\mathcal{Q}_r^y$) is calculated as the base growth from the previous year $(1 + \omega_r^y)\mathcal{Q}_r^{y-1}$ plus the additional EV growth based on the availability of the total charging capacity $k \sum_{i \in \mathcal{I}^{\mathrm{CS}}} p_{i,y}^{CC}$. Other EV growth mechanisms can also be modeled within the proposed modeling framework. Constraint (6.5c) sets the boundary conditions of initial EV traffic from each origin. We have grouped EVs with similar travel and charging characteristics in terms of arriving/departing time $T_{r,e}^{\mathrm{arr}}/T_{r,e}^{\mathrm{dep}}$, $\mathrm{SOC}_{r,e}^{\mathrm{arr}}$, and minimum $\mathrm{SOC}_{r,e}^{\mathrm{dep}}$ into different homogeneous groups, indexed by e. Constraint (6.5d) calculates the EV flow from origin r that fall into each group e, where δ_r^e is the percentage of group e EVs. The probability distribution of $\mathrm{SOC}_{r,e}^{\mathrm{arr}}$ and travel patterns from classic household travel survey, emerging large-scale vehicle GPS data, and charging session records [68, 106] can be used to estimate δ_r^e. The CS selection of EVs is specified in (6.5e) where EVs are distributed to candidate CSs based on the logit probability calculated in (6.4).

Constraints (6.5f)-(6.5i) specify EVs' SOC transition and charging needs that the CSA needs to fulfill. Constraint (6.5f) models the dynamics of the SOC of EV group e from r at CS i in the DS (i.e., location index s in the transportation network). Constraint (6.5g) limits the maximum and minimum SOC of each EV group based on drivers' desired SOC range and/or battery specification. Constraints (6.5h) and (6.5i) specify the initial arrival SOC and minimum departure SOC for each EV group at charging location i. Constraint (6.5j) restricts the charging/discharging power of EVs at each time step t to be within a certain range based on battery/charger characteristics. Constraint

(6.5k) determines the total power demand of CS $i \in \mathcal{I}^{\mathrm{CS}}$ at time t by summing the normalized discharging/charging of EVs at each station. Constraint (6.5l) ensures that the total hourly charging demand of each CS should be less than the total charging capacity of the CS. Constraint (6.5m) calculates the total charging capacity of each CS $p_{i,y}^{CC}$ by summing the charging capacity from the previous year $p_{i,y-1}^{CC}$ and the added charging capacity $D_{i,y}$. Constraint (6.5n) sets the existing charging capacity of CSs at each location i at year 0. Lastly, constraint (6.5o) specifies the yearly investment budget of CSA.

<div align="center">Market Clearing Conditions</div>

In a stable market, the locational power purchased by DSO needs to be balanced with the locational power generation. In addition, the locational CD fulfilled by the DSO should be balanced with the CD of CSs. These conditions are stated in the market clearing conditions (6.6). (6.6a) guarantees that the total energy purchased by DSO is equal to the total energy generated at each node with DGs, and (6.6b) ensures that the charging demand satisfied by DSO is equal to the charging demand required by the CSs. Locational prices of electricity $\rho_{i,t,y}$ and electricity cost for CSA and other users $\beta_{i,t,y}$ can be interpreted as dual variables for the market clearing conditions. The reason we multiply both sides of the clearing conditions with the discount factor α^y is to facilitate the convex reformation and interpretation of dual variables (ρ and β), as discussed in Section 6.

$$(\rho_{i,t,y}) \qquad \alpha^y p_{i,t,y}^s = \alpha^y p_{i,t,y}^{DG}, \; \forall i \in \mathcal{I}^{\mathrm{DG}}, \forall t \in \mathcal{T}, y \in \mathcal{Y} \qquad (6.6a)$$

$$(\beta_{i,t,y}) \qquad \alpha^y p_{i,t,y}^d = \alpha^y p_{i,t,y}^{\mathrm{CS}}, \; \forall i \in \mathcal{I}^{\mathrm{CS}}, t \in \mathcal{T}, y \in \mathcal{Y} \qquad (6.6b)$$

Remark 1: The modeling framework proposed in this manuscript does not require an explicit pricing model. Instead, the pricing of energy supplied by DGs and demanded by CSs are determined by market clearing conditions (6.6). In other words, each decision maker will try to make its own decisions to maximize their own benefits, as defined in (6.1), (6.2), and (6.5). Then the aggregated supply and demand at each node can be determined. If the energy supplied is less than the energy demanded at a particular node, the price will go up, and vice versa. The prices will be adjusted until the energy supply and demand at every node are balanced. This market clearing mechanism resembles the realistic dependency of locational prices on the balance of supply and demand. Such prices are refereed as equilibrium prices, which can be calculated as the dual variables of constraints (6.6b) and (6.6a) in the convex reformulation (6.7). This relates to the locational marginal price concept, where the dual variables indicate the marginal costs of one additional unit of demand to the objective function (6.7a). Therefore, although the objective function (6.7a) is manually constructed for computational purposes, it can be interpreted as the total system costs of the hypothetical market clearing operator.

Convex Reformulation

The multi-stage decision making of each stakeholder and market clearing conditions presented in Sections DG Owners Modeling~Market Clearing Conditions are closely coupled and need to be solved simultaneously to achieve the system equilibrium states. However, it is challenging to directly solve the NM-MOPEC due to the non-convex nature caused by the complementarity conditions. In this section, we present an exact convex reformulation that can recover the optimal primal and dual variables efficiently. We observe that models (6.1)~(6.5) individually are convex optimization problems with constraints completely separable. In addition, the objective functions of these models are almost separable except for the multiplication terms of primal and dual variables in market clearing conditions (6.6) (i.e., $\rho_{i,t}p_{i,t}^{s}$, $\rho_{i,t}p_{i,t}^{DG}$, $\rho_{i,t}P_{i,t}^{\mathrm{CS}}$, $\beta_{i,t,y}p_{i,t,y}^{d}$, $\beta_{i,t,y}p_{i,t,y}^{CS}$). This

type of problem can be reformulated by linearly combining all the (scaled) objective functions and intersecting all the constraint sets in (6.1)∼(6.5) following a reverse Lagrange relaxation procedure [67]. Accordingly, the NM-MOPEC (i.e., (6.1)∼(6.5) and (6.6)) can be equivalently reformulated as a single convex optimization problem (6.7), which can be efficiently solved by commercial nonlinear solvers (e.g., IPOPT). This reformulation can be easily seen if we apply Lagrangian relaxation on constraint (6.6) in model (6.7). For detailed proof, one can refer to [67]. After solving the problem defined in (6.7a), we can derive the locational energy prices ($\rho_{i,t}$) and charging prices ($\beta_{i,t,y}$) by retrieving the dual variables corresponding to constraints (6.6). Note that since the objective functions for all the stakeholders are scaled with the discount factor α^y for each year y, we have scaled the market clearing conditions (6.6) with the same discount factor α^y so that the prices derived from the dual variables are in the value of year y.

$$
\min_{\boldsymbol{p}^{\mathrm{CS}}, \boldsymbol{soc}} \quad \sum_{y \in \mathcal{Y}} \alpha^y \Bigg[\sum_{i \in \mathcal{I}^{DG}} \Big[C_i^1(U_{i,y}^{DG}) + C_i^2(\bar{S}_{i,y}^{DG}) + \sum_{t \in \mathcal{T}} C_i^3(p_{i,t,y}^{DG}) \Big] + \sum_{i \in \mathcal{I}} \Big[F_i^1(p_{i,y}^{\mathrm{CC}}) + F_i^2(D_{i,y}) \Big]
$$
$$
- \sum_{t \in \mathcal{T}} \gamma_{i,t,y} p_{i,t,y}^{\mathrm{CS}} \Bigg] \tag{6.7a}
$$

s.t. $\quad (6.1b), (6.1e), (6.2b) \sim (6.2f), (6.5b) \sim (6.5o), (6.6)$ \hfill (6.7b)

Remark 2: The original formulation, i.e., (DG Owners Modeling∼Market Clearing Conditions), is a multi-agent optimization problem with equilibrium constraints, which is non-convex if one solves it directly as a mixed complementarity problem (MCP), because MCP involves multiplication of two continuous variables (i.e., complementariy terms) from Karush–Kuhn–Tucker (KKT) conditions. Our reformulation is convex because the objective function is convex and all the constraints are linear. In addition, our reformulation is exact (i.e., our reformulation is not an approximation

and does not introduce any approximation error to the original equilibrium solutions). Because if one relaxes the market clearing condition (6.6) in model (6.7) using Lagrangian relaxation, model (6.7) can be separated into model (6.2), (6.1), and (6.5). For detail proof strategies, one can refer to [67].

Remark 3: The main motivation for developing our model, instead of using the existing multi-level modeling framework, is threefold. First, the distribution system is increasingly decentralized, which could involve a significant number of investors and aggregators. Each of these decision-makers may not have sufficient market power to influence the others' actions. For example, in the current charging network, we have several individual infrastructure investors, none of whom is dominating the market (see Figure 6.1). In such a decentralized setting, multilevel assumption is not justifiable because there is no "leading" decision maker that can assume the followers will simply react to his/her decisions. In contrast, multi-agent approaches are better fit for this setting, where multiple decision makers interact with each other in a competitive market to optimize their own objectives. Second, the focus of the multilevel modeling approach is typically on the decision support for the leader to optimize his/her objective, assuming the leader can expect the response of other decision makers. However, we are interested in understanding the market interaction outcome of all the market participants. Third, the classic multilevel optimization modeling approaches are extremely challenging to solve due to the non-convexity introduced by the inclusion of optimization problems as constraints. The traditional solution approaches, such as single-level reformulation of the multilevel optimization modeling or heuristic algorithms are not scalable and do not guarantee global optimal solutions. However, our proposed modeling framework can be solved by commercial non-linear solvers to exact solutions in an efficient manner.
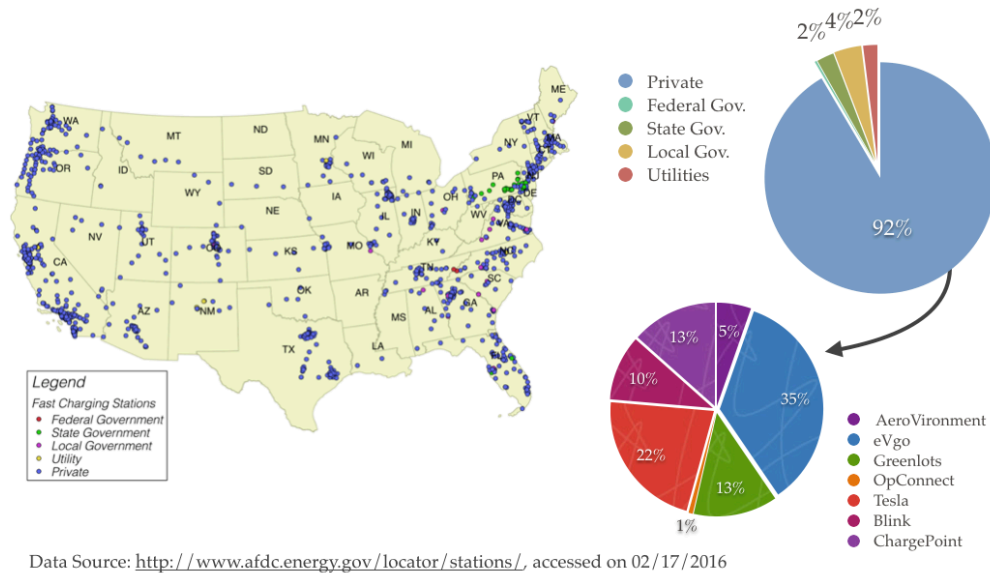
Figure 6.1: Current division of investors in charging station infrastructure

Results

We implemented our convex reformulation model (6.7) in Pyomo 5.6.7 and solved it using IPOPT 3.12.13. All the experiments were run on an AMD FX(tm)-8350 eight-core processor with 16 GB of RAM memory, under UBUNTU 20.04.2.

Test Systems and parameter settings

In this subsection, we present the test systems and a summary of key model parameters and data sources. The complete list of model inputs can be openly accessed [2].

We implemented the proposed model on the IEEE-33 feeder [98] coupled with Orlando Trans-

---

[2]Data set: https://github.com/SinaBaghali/InputData
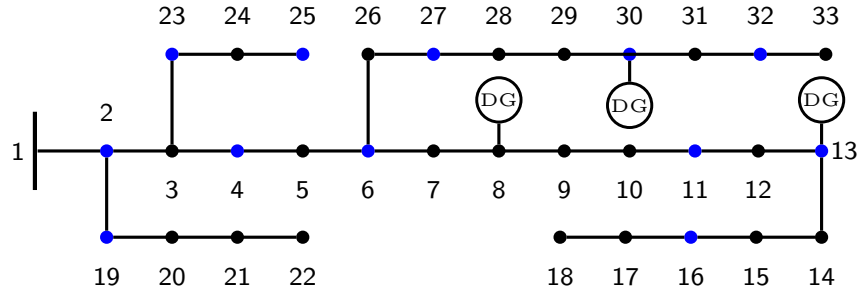
(a) IEEE 33-node
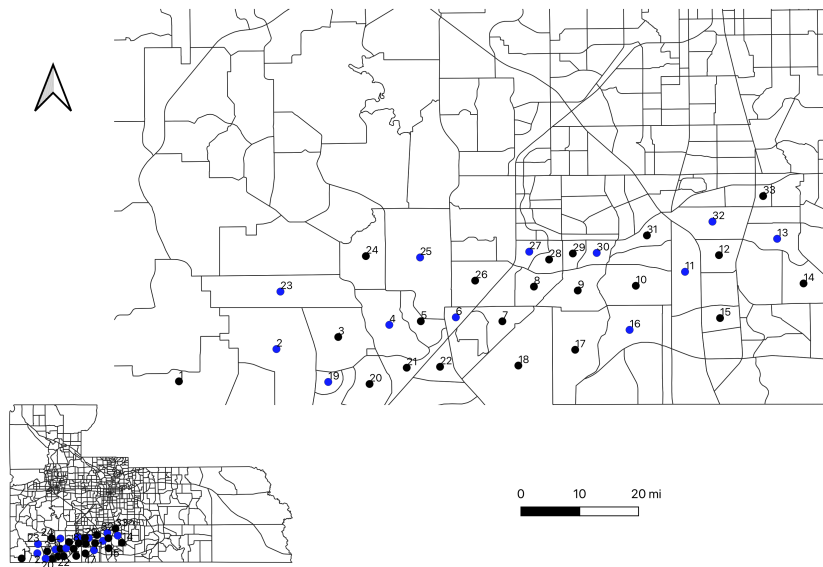
(b) Orlando transportation system

Figure 6.2: Coupled transportation and distribution test systems.

portation system (see Figure 6.2). In the distribution test system, nodes 8, 13, and 30 are the generation nodes, and the feeder is connected to the main grid at node 1. The cost functions defined in (6.1a) are assumed to be linear, and the upgrade costs of DGs are proportional to their average construction cost from [107]. The cost coefficients for different DG nodes, along with their minimum required generation, and cost coefficients [108, 109] of CSs/EVs are summarized in Table 6.1. The system pu is based on $S^{\text{base}} = 100$ MVA, and the discount factor is assumed to be $\alpha = 90\%$.

Table 6.1 Test system parameters

Generation nodes' cost coefficients and parameters						
Nodes	c_i^1 ($/pu)	c_i^2 ($/pu)	c_i^3 ($/pu.h)	$\underline{P}_i^{\mathrm{DG}}$ (pu)	$\bar{S}_i^{\mathrm{Init}}$ (pu)	B_i^{DG} ($)
1	–	–	200	–	–	–
8	934.5	9.34	36	0.02	1.6	400
13	934.5	9.34	36	0.01	1.5	400
30	934.5	9.34	36	0.01	1	400
Yearly growth rate of the number of EVs						
Year	0	1	2	3	4	
ω_r^y	0	1	0.5	0.33	0.25	
Year	5	6	7	8	9	
ω_r^y	0.8	1	0.556	0.571	0.432	
Parameter settings for CSs and EVs						
Parameter	f^1 ($/pu)	f^2 ($/pu)	γ ($/pu.h)	k (#/pu)	Cap^e (pu)	B^{CS} ($)
value	1,781.4	17.184	150	0.2	0.001	100

To model the base power demand (i.e., loads excluding the EV charging demand), we use the demand data from PJM Interconnection [95]. Hourly historical load forecast data was collected for a representative date (March 31) from 2012 (initial year $y = 0$) to 2021 (final year $y = 9$), specifically for the American Electric Power (AEP) area. The considered hourly load over the years in system pu is shown in Figure 6.3. This load demand is used in addition to the CS energy requirements to model the total power demand in the DS.

To model the traffic distribution in Orlando metropolitan area, origin-destination (OD) travel demand from the 2020 Central Florida Regional Planning Model (CFRPM) was used. This data includes daily traffic counts between origin and destination (OD) TAZs in Orange County, Florida in April 2015. In order to match the IEEE 33-node DS, 33 TAZs with the most trips were used for modeling the transportation system, with 35 % of these vehicles are assumed to be EVs. The travel demand from CFRPM generated from the origin nodes is treated as the initial EV travel demand ($\bar{\mathcal{Q}}^{\mathrm{Init}}$). For the years after, a base growth factor (ω^y), which is estimated from global outlooks on EV growth from the International Energy Agency [110] (see Table 6.1), was applied to simulate
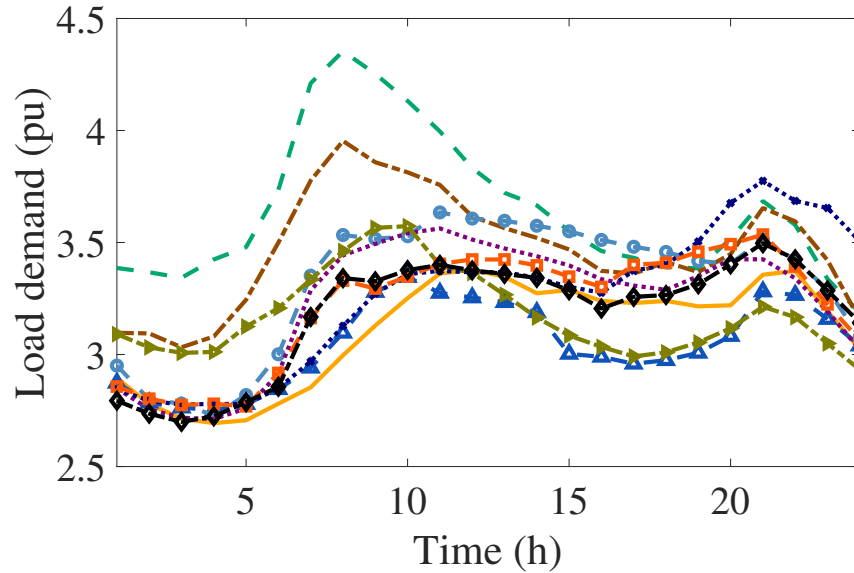
Figure 6.3: Hourly load demand over the planning horizon with y: — 0, – –△ 1, – – – 2, – · – 3, –
—○ 4, · · · 5, – ·▷ 6, · · ∗ 7, – –□ 8, – -◇ 9.

EV growth. The coefficients of EVs' utility functions are $b_0 = 0$, $b_1 = 0.06$, and $b_2 = 0.05$.

Trips are equally divided into three groups ($e \in \mathcal{E}$), representing low, medium, and high initial SOC, with initial SOC sampled from uniform distributions [0, 0.3], [0.3, 0.6], and [0.6, 0.9], respectively. We focus on destination charging in this study, which is the dominant charging type now [106]. We leveraged the 2017 National Household Travel Survey [111] to estimate the distribution of arrival times as shown in Figure 6.4. After the arrival time was determined, the departure time was calculated with dwelling time uniformly sampled between four to six hours[3].

---

[3]All the randomized values were generated with random seed 1.
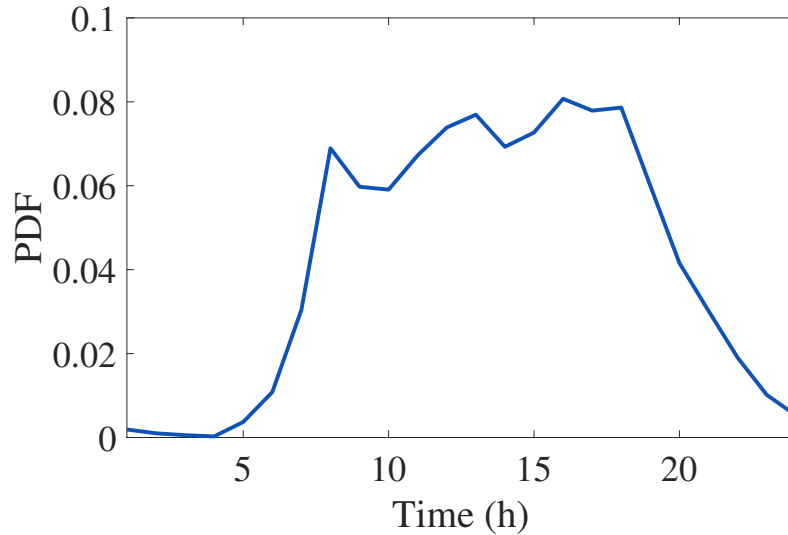
Figure 6.4: Probability Distribution of Arrival Times

Results Analyses

In this section, we will present and analyze the resultant multi-year allocations of CS charging/DG capacities and hourly operational variables, such as hourly DG generation and energy prices, based on the proposed modeling.

The optimal yearly capacity expansion for different CSs is presented in Fig. 6.5, which shows that the CSA gradually increases the capacities on different nodes to the response of CD growth in the system. The charging capacity increases significantly after the 5th year following a drastic increase in EV growth rate (see Table 6.1) and it reaches its maximum value in the last year ($y =$ 9) for all the CSs. CSs at nodes 16 and 27 are the two nodes with the highest invested capacities (0.2948 pu and 0.2885 pu respectively) over the studied time horizon, while node 2 attracts the lowest investment (0.1178 pu). Higher investment of charging capacity shows the favorability of these locations by investors, which is based on multiple factors, including the travel time (which influences charging demand) and power distribution feasibility (which influences energy price).

As nodes 16 and 27 are in close proximity to multiple origin nodes of EV drivers (see Fig. 6.2), they have become favorable for the travelers considering the travel time. Additionally, they are close to the nodes with DGs in DS (see Fig. 6.2), which makes power distribution to these nodes easier without violating distribution system constraints including voltage constraints and distribution line capacity. Different nodes may invest differently in different years. For example, node 16 significantly increases the capacity in year 7 while nodes 25 and 32 receive minimum investment in the same year so that the marginal investment profits at each node are the same. However, the overall increasing trend of CS capacity is similar for all the nodes.
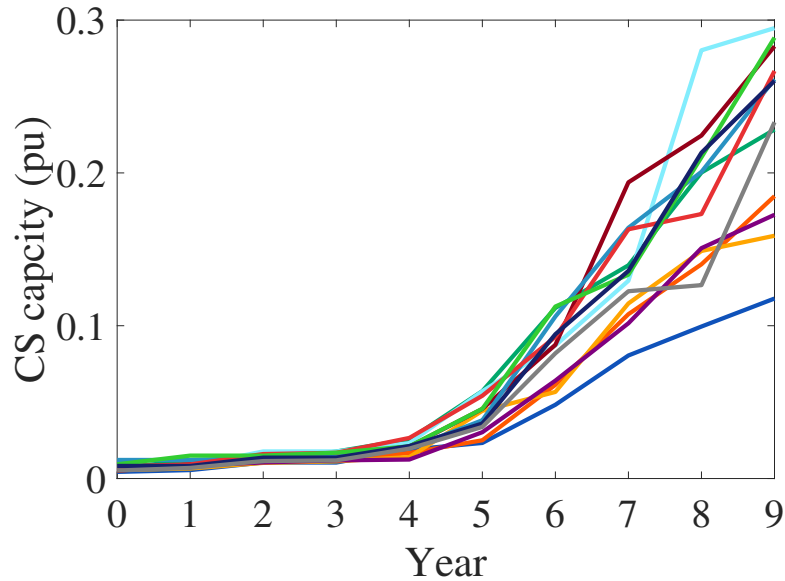
Figure 6.5: CS capacities in the planning horizon for CSs at nodes: — 2, — 4, — 6, — 11, — 13, — 16, — 19, — 23, — 25, — 27, — 30, — 32.

The optimal generation capacity of DGs for each year is presented in Fig. 6.6, which shows that DG owners have increased their capacity in the first and last two years in response to the load demand and CD increase of the corresponding years. As shown in Fig. 6.3, the load demand is higher in the first two years of the planning horizon, with the peak load demand of 4.354 (pu) in

$y = 2$. Therefore, the DGs have invested early in the first two years and increased their generation capacity. The generation capacity of DGs remains constant during $y = 2 \sim 7$ (see 6.6) since there is no more load demand increase during this period (see Fig. 6.3) and the generation capacity is able to cover the increasing charging demand for this period. After the 7th year, DGs at nodes 8 and 13 have increased their capacity in response to the higher CD during the last two years of the planning horizon, which is also leading to the increased charging capacity of CSs as shown in Fig. 6.5.
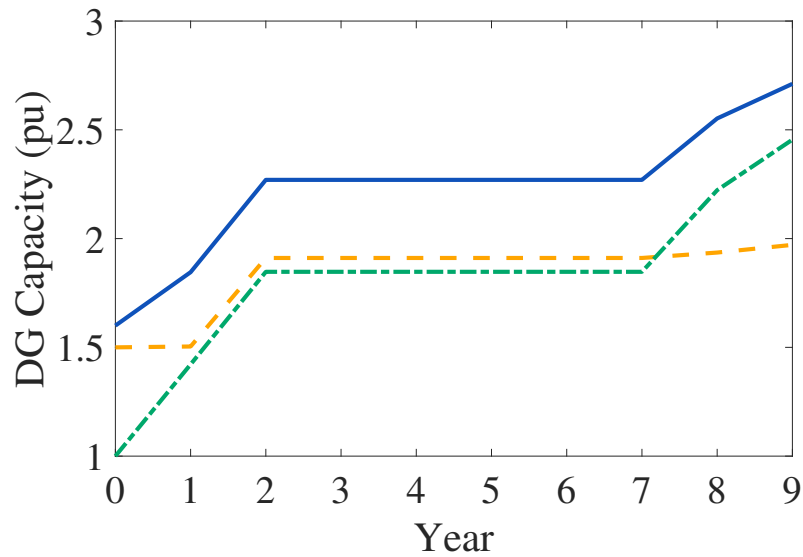
Figure 6.6: Generation capacity of DGs in the planning horizon for DGs at nodes: —— 8, – – – 13, – · – 30.

Another observation from Fig. 6.6 is that the generation capacity of DG at node 8 has remained the highest capacity among other DGs during the planning horizon. This stems from the fact that compared with the other DGs, DG 8 is located in a part of the network that has more CS nodes and load nodes in its vicinity without other competing generation units (see Fig. 6.2). Additionally, the generation capacity of DG at node 30 has remained close to the generation capacity of DG 13 during $y = 1 \sim 7$, however, its capacity surpasses DG 13 after $y = 7$. This increase stems from

the structure of the network where node 30 is the only DG providing the energy of a branch while nodes 13 and 8 share the same branch, and node 8 already has a high generation capacity which reduces energy demand from node 13.

Next, we evaluate the operational variables of the system including the power generation of DGs (p^{DG}), CD of CSs (p^{CS}), energy prices of DG nodes (ρ), and electricity prices for CSA (β). For the purpose of illustration, we will present the results for the mentioned variables on the representative day of the last year (year 9) of the planning horizon (see Fig. 6.7). This year has the maximum number of EVs throughout the planning horizon and consequently imposes the maximum CD on the system.

The hourly generation output shows that the DG at node 8 serves the highest percentage of the power demand (both charging demand and the electricity demand for other usages) and reaches its maximum capacity at $t = 8$ (see Figure 6.7a). Even though all DGs at nodes 8 and 13 have the same generation costs (see Table 6.1), DG 8 generates more energy because it is closer to the region where there is no DG unit (see Fig.6.2). The power generation of other DGs has a similar pattern with maximum generation during $t = 8 \sim 21$, because of higher CD during that period (see Fig. 6.7c) based on the EVs' arrival time distribution presented in Fig. 6.4. Moreover, the optimal generation capacities have evolved in a way that there is no need to purchase energy from the upper grid (node 1), and the energy from the upper grid is only been used for reactive power support.

Fig. 6.7b shows that the electricity prices ρ are low for all the DG nodes during $t = 1 \sim 9$ and $22 \sim 23$ when the generation of the DGs has not reached their maximum capacity (see Fig. 6.7a). As the DGs reach their maximum capacity during $t = 10 \sim 22$, prices on all nodes increase drastically because ρ represents the marginal cost of an additional unit of electricity generation, which is equal to either the cost of purchasing energy from the main grid or the marginal cost

113

(a) Generation output

(b) Energy prices

(c) Charging demand of CSs

(d) Charging prices for CSA
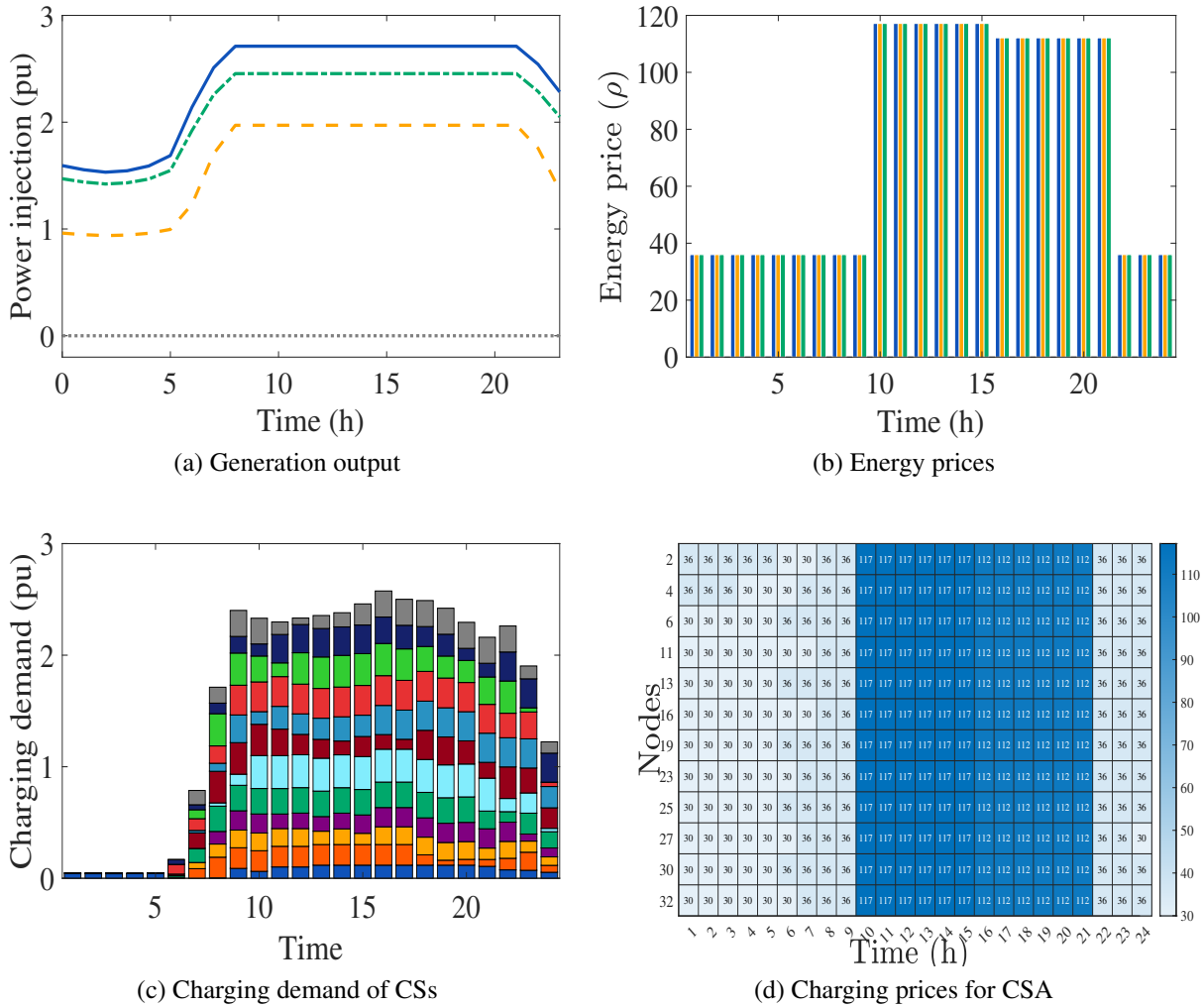
Figure 6.7: Operational parameters in year 9; (a) Nodes: $\cdots$ 1, — 8, – – – 13, and – $\cdot$ – 30; (b) DG nodes: ■ 8, ■ 13, and ■ 30; (c) CS nodes: ■ 2, ■ 4, ■ 6, ■ 11, ■ 13, ■ 16, ■ 19, ■ 23, ■ 25, ■ 27, ■ 30, ■ 32.

of both capacity expansion and generation. The temporal pattern of the daily CD presented in Fig. 6.7c, follows the arrival time distribution as considered in Fig. 6.4 which is higher during $t = 10 \sim 23$. This is also reflected in the DG generation outputs in Fig. 6.7a where DGs were producing energy at their capacity during that period. Fig. 6.7d shows the charging prices for CSA at CS nodes. The temporal pattern of β follows the electricity prices presented in Fig. 6.7b. The

charging price is high and equal to the energy price during $t = 10 \sim 22$ as the DGs are operating with their maximum capacities, and it is low at other times of the day when the CD is lower and DGs are operating at a level lower than their capacity.

Computation performance comparison

Another solution algorithm for the proposed multi-agent problem is to consider an iterative process where each stakeholder solves his/her own problem based on the received price signals until market equilibrium conditions are satisfied. In other words, problems defined in (6.1), 6.2, and (6.5) can be solved independently given energy and charging prices ρ and β. The prices gets updated in each iteration based on aggregated locational supply and demand. This solution method is highly volatile and needs careful parameter selection to converge. Additionally, even if it converges, the computation time and solution accuracy may be compromised.

For the sake of comparison, we applied an iterative process to solve our model and to show how our reformulation technique outruns iterative algorithms in terms of computational efficiency and accuracy. Fig. 6.8 shows the pattern of energy price on node 8 at time step 3 in year 9 as an example. It shows that after 200 iterations (more than 5 hours of running) the algorithm hasn't converged to the equilibrium price and keeps oscillating with an threshold of 0.1%. The investigation on the other variables e.g., the generated power by DGs (p^{DG}) also shows oscillating patterns (see Fig. 6.9). This indicates that iterative algorithms may not be salable for the proposed multi-stage multi-agent problem and our proposed exact convex reformulation provides a more reliable solution method to determine the equilibrium outcome of the system.

To the best of the authors' knowledge, limited scalable global-convergence algorithms in the area of a decentralized decision environment for multi-stage charging stations and distributed generator capacity expansion are available. For example, studies like [27,28,31,32,112] design CS planning
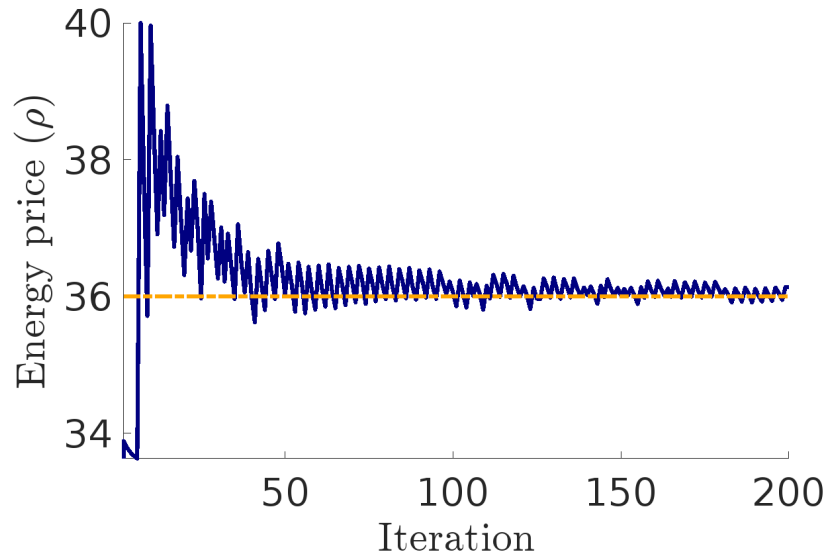
Figure 6.8: Electricity price convergence: - - - Equilibrium price; — Iterative algorithm.

problems with the focus on satisfying the charging demand of the vehicles in their charging sessions with limited system modeling, so that their main study focuses are distinct from our study and the solution methods are not applicable. Other studies that have more extensive modeling at a system level proposed tailored solution approaches for their problems. For example [44–46] proposed reformulation techniques to solve the CS planning problems that are suitable for mixed integer linear programming problems but not for our problem, which is nonlinear non-convex.

Sensitivity analysis

The investment decision making of DG owners and CSA depends on a number of important factors including yearly budget ($B^{\mathrm{DG}}/B^{\mathrm{CS}}$), discount factor ($\alpha$), and the EV adoption coefficient (k). Here, we will analyze how changes in these factors will influence the decision making of the stakeholders. For the sake of clarity, our analyses focus on 3 representative CSs in the test system since other CSs have similar resulting patterns. The baseline case is defined in Section Test Systems and

116
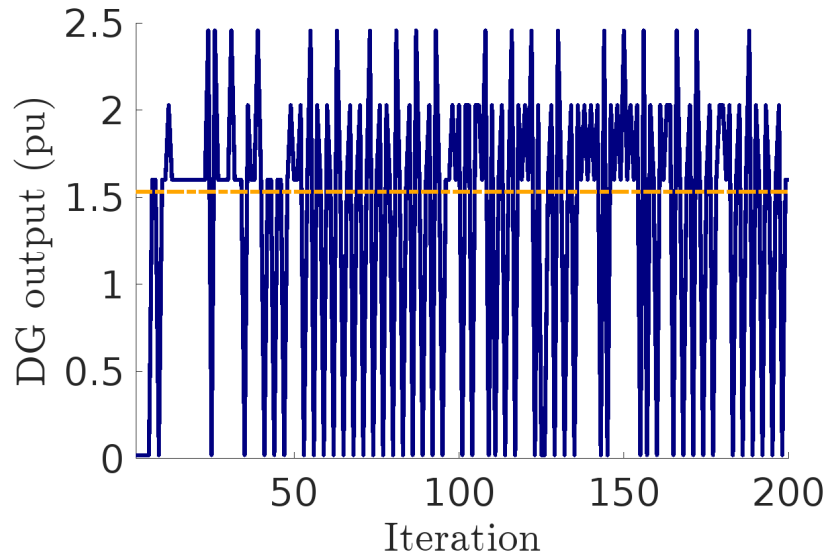
Figure 6.9: Generation output of DG 8: - - - Equilibrium result; — Iterative algorithm.

parameter settings.

Yearly budget

We considered three budget levels: 1) 50% of the base case budget, 2) the base case budget, and 3) twice the base case budget. The results of the considered cases are illustrated in Fig. 6.10, which shows that with less yearly budget (case 1), DGs are not able to invest more in the first years of the planning horizon as they would in the base case (case 2). Consequently, they have increased their capacity later in the last 3 years of the planning, which is one year earlier compared to the capacity increase pattern of the base case. For example, in case 1 at $y = 2 \sim 6$, DG at node 8 has a capacity 0.2419 (pu) less than that of the base case, and it has started increasing its capacity in the 6th year to reach its desired capacity in the last year of the planning horizon. Whereas the same DG has invested more in the first years, and its capacity has remained constant during $y = 2 \sim 7$, which is then increased in the last two years of the planning horizon.
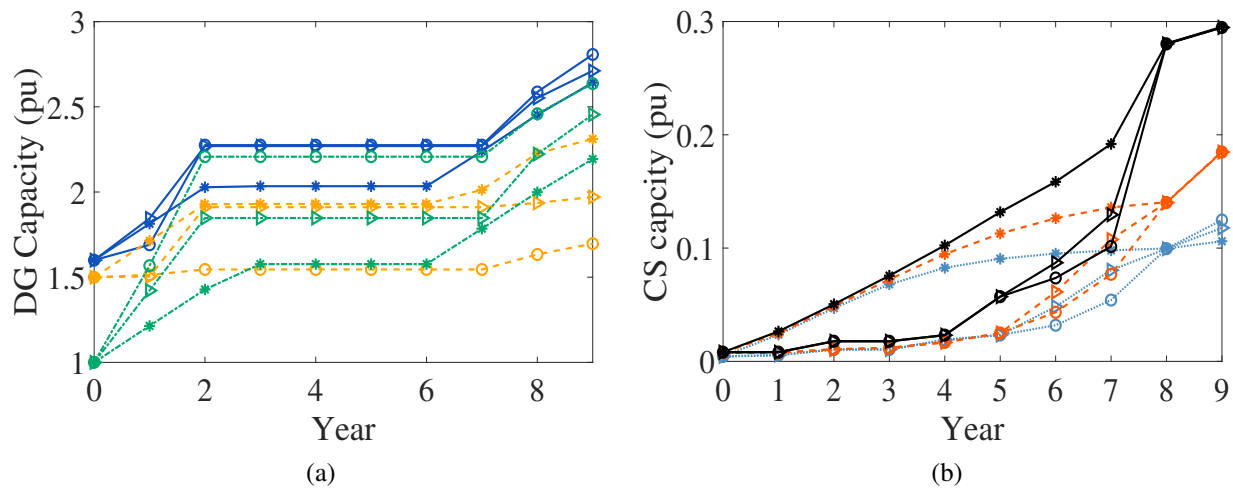
Figure 6.10: Optimal capacities for (a) DGs (b) CSs. DG nodes: — 8, – – – 13, – · – 30; CS nodes: · · · 2, – – – 4, — 16; Cases: ∗ 1, ▷ 2 (base), and ○ 3.

On the other hand, a higher budget allows DGs to have more flexibility for increasing their capacity each year and DGs have responded differently to this flexibility in case 3 (see Fig. 6.10a). The capacity of DG 8 has remained close to the base case, reaching higher capacities in the last two years of the planning horizon compared to the base case (case 2). DG 30 was able to invest more and we observe that its capacity has increased drastically compared to the base case (case 2) and it is close to the capacity of DG 8. The reason may stem from the fact that DG 30 is located in a part of the network that is critical and its higher capacity with the available budget is useful for the system and will increase the DG owners' profits. With a higher capacity for DG 30, it has been more beneficial for DG 13 to invest less because much of the load demand and CD would be already fulfilled by DG 30.

The lower budget limits the yearly investments for the CSA, hindering high investments for the last years of the planning horizon and promoting earlier investments. Therefore, in case 1, we observe a higher installed capacity for CSs in the first years of the planning horizon compared to the base case

(see Fig. 6.10b). For example, the CS at node 2 has gradually increased its capacity throughout the 9 years to reach its required high capacity at the final year. As the budget of CSA has increased from case 1 to case 3, we observe that CSs have a less installed capacity in the first years of the planning since the high budget allows them to increase their capacity drastically in the final years of the planning when needed. This behavior is more evident in the charging capacity of CS 16, where we observe a drastic increase in capacity from years 7 to 8. Therefore, we can say that investing as late as possible is more beneficial for the CSA in this setting as long as the budget allows and the CD each year can be served. In other words, the CSA may not have economic motivations to invest in charging capacity early in a decentralized system and government incentives may be needed to encourage the charging infrastructure investment in the early stage of EV adoption.

Discount factor

We considered three levels of α, 0.7, 0.9 (base case), and 1, to observe the stakeholders' response (see Fig. 6.11). With $\alpha = 1$, the costs of future years will not be discounted, which resulted in earlier investments for both CSA and DG owners. For example, as α increases from 0.7 to 1, DG 8 has invested more in the first two years (see Fig. 6.11a). The impact of the discount factor is more evident in the capacity of CSs (see Fig. 6.11b). The timing of CSA capacity investment depends on two main factors. On one hand, investing early can attract more EV adoption early on and increase the charging revenue. On the other hand, investing late can reduce the present value of the investment costs due to the discounted factor. When $\alpha = 1$, the capacity of CSs in the first years is significantly higher compared to the cases when $\alpha = 0.7$ or 0.9. This major difference is because the benefits of attracting more EV adoption in the early years outweigh the disadvantage of a higher present value of investment costs when the discount factor is closer to one.
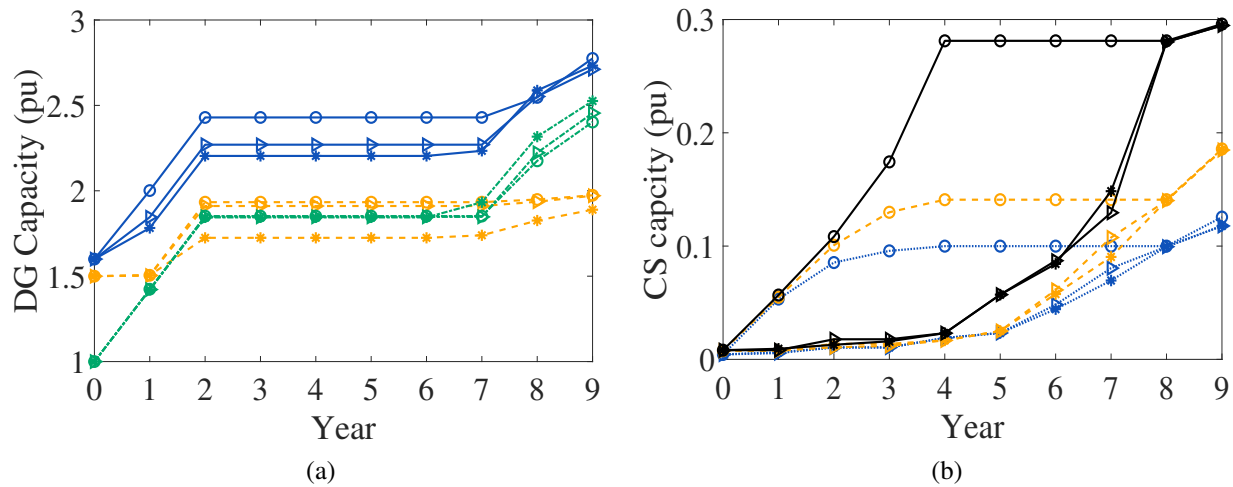
Figure 6.11: Optimal capacities for (a) DGs (b) CSs. DG nodes: —— 8, – – – 13, – · – 30; CS nodes: · · · 2, – – – 4, —— 16; α: $*$ 0.7, $\triangleright$ 0.9 (base), and $\circ$ 1.

EV adoption coefficient

The investigated factors so far did not have a major impact on the additional number of EVs each year.To demonstrate the sensitivity of the EV adoption coefficient k on the system equilibrium patterns, we consider three levels for k (#/pu): 0.2 (as in base case), 2, and 5. As we can see from Fig. 6.12, the total number of EVs increases more from the expected number of EVs as k increases. The optimal capacities of DGs and CSs are shown in Fig. 6.13. The resulting pattern for the capacities of DGs did not change significantly from the base case (see Fig. 6.13a). We observe higher DG capacities only for the last two years of the planning horizon because of the additional number of EVs as the k has become larger. The yearly pattern of CS capacities has changed notably as k has increased (see Fig. 6.13b). With a higher k, the CSA has a higher incentive to invest more charging capacity early in the planning horizon to increase EV adoption. As a positive feedback effect, in order to fulfill the additional CD resulting from more EVs, the CSA will need to invest in more charging capacity over the years. For example, the capacity of CS 16 increases drastically

during $y = 1 \sim 5$ with $k = 5$, reaching a higher capacity compared to the cases with smaller values of k.
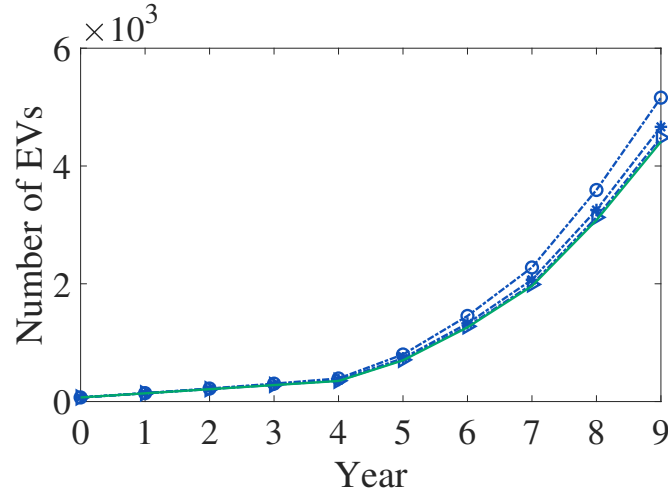
Figure 6.12: Resulted and expected yearly number of EVs departing from origin node 3; – – – resulted and — expected; k: ▷ 0.2 (base), ∗ 2, and ○ 5.

Conclusion

In this study, we proposed a multi-agent multi-stage optimization approach to study the interaction of decentralized decision makings of the DSO, DG owners, and charging station aggregator (CSA) in the CS and DG capacity expansion problem. We explicitly modeled the endogenous market electricity prices as well as the feedback effects of charging availability on the growth of EVs. Moreover, we applied a convex reformulation technique to simultaneously solve the decentralized multi-agent problems efficiently. The proposed model provides a computationally tractable framework to understand how the system evolves over time to fulfill a growing level of EV adoption. The simulation results on a synthetic test system, coupling IEEE 33-node DS and Orlando transportation network, show that our modeling strategy is able to effectively identify the equilibrium
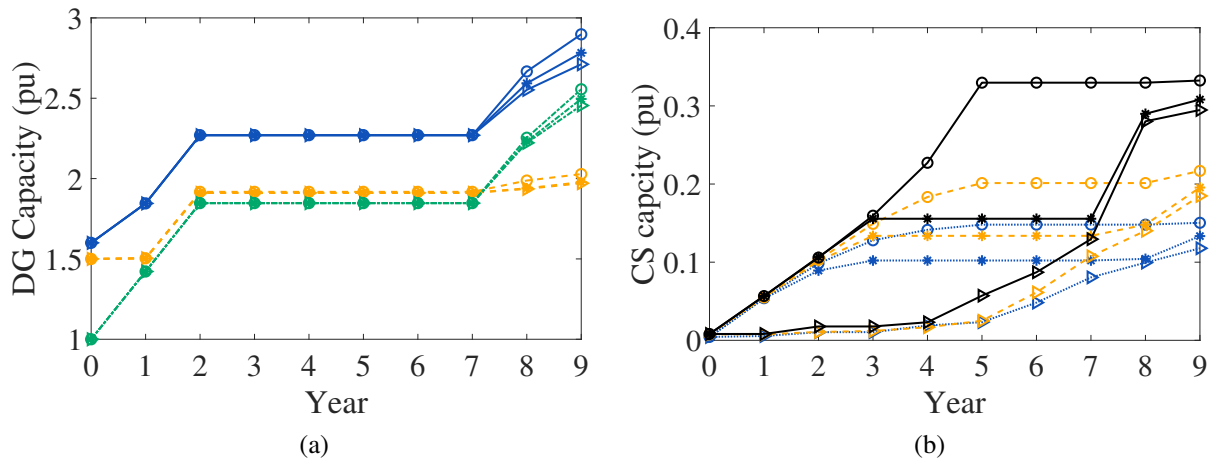
Figure 6.13: Optimal capacities for (a) DGs (b) CSs. DG nodes: — 8, – – – 13, – · – 30; CS nodes: · · · 2, – – – 4, — 16; k: ▷ 0.2, * 2, and ∘ 5.

investment patterns over space and time for both DG and CS to satisfy the growing number of EVs in a decentralized environment.

This work can be extended in several directions. First, a more detailed transportation network modeling reflecting routing and traffic congestion can be coupled with the existing model to provide a more accurate spatial distribution of EVs. Second, decomposition and dynamic programming algorithms can be designed to further enhance the computational efficiency for large-scale problems. Third, government intervention can be investigated to influence the interaction of stakeholders for social benefits while ensuring system-level targets of EV adoption. Fourth, the modeling framework can be extended to a stochastic model in order to incorporate the impacts of key uncertainties, e.g., load demand, generation, and EVs' charging requirements, on the system equilibrium patterns.

CHAPTER 7: CHARGING INFRASTRUCTURE PLANNING CONSIDERING MOBILITY NEEDS AND POWER GRID SERVICES: A BI-LEVEL OPTIMIZATION FRAMEWORK

Introduction

This chapter proposes a novel charging infrastructure planning framework for electric vehicles (EVs) that considers both the mobility needs and power grid services opportunities of EVs. The framework aims to address the increasing trend of EV adoption worldwide following net zero emission policies, and the need for efficient charging infrastructure network planning. Existing literature on charging infrastructure planning has mostly focused on either power system-centric or transportation system-centric approaches, but these systems are increasingly coupled with large-scale EV adoption. The proposed framework utilizes a bi-level optimization approach, where a government planning agency (charging infrastructure planner) makes decisions on charging station allocation at the upper level, while the lower level models the interaction of stakeholders from both power distribution and transportation systems in a market-based equilibrium model.

The resulting bi-level optimization problem is highly non-convex due to the presence of integer variables and the bi-level model structure, which presents computational challenges. To address this, we propose a novel value-decomposition-based solution algorithm that solves a series of mixed integer linear problems (MILPs) and convex optimization problems iteratively. The key strategy of the proposed algorithm is to relax the non-linear constraints in the original bi-level problem to a solvable MILP and then add linear cuts to tighten the feasible region based on strong duality theory. The algorithm starts with formulating the upper-level problem as a MILP, including all the constraints from both upper and lower problems, and solving it as the master problem (MP).

Then, the lower-level equilibrium problem is solved independently with the charging station allocation results from the MP. The objective value of the MP provides a lower bound for the solution, and further iterations are performed to tighten the bounds and converge to the optimal solution.

Lastly, we analyzed our model with simulation results on test systems based on the Sioux Falls transportation network and IEEE distribution networks. The results showed the effectiveness of our model and the convergence pattern of the proposed solution algorithm. The interdependent nature of power and transportation systems in the planning problem is investigated with case analysis and detailed discussions on results. With the proposed bi-level model, we can model the realistic feedback effect of planning decision variables on the operation of systems and how, in return, operational requirements and drivers' choices would impact the planning decisions. The system operators can use this model to investigate planning strategies for the ever-increasing charging demand and grid services opportunity for EVs in the future.

Methodology

The proposed framework will be explained in detail in this section. Figure 7.1 represents the summary of the proposed model. At the upper level, a government planning agency, i.e., the charging infrastructure planner, decides charging station allocation among candidate locations, minimizing investment costs, total travel time of drivers in the transportation system, and the value of EV grid services. At the lower level, we have modeled the interaction of stakeholders from both power distribution and transportation systems, including distribution system operator (DSO), charging station aggregator (CSA), distributed generators (DGs), and EV drivers, in a market-based equilibrium model.

The interaction between stakeholders in the lower-level equilibrium is modeled as follows. DSO

124
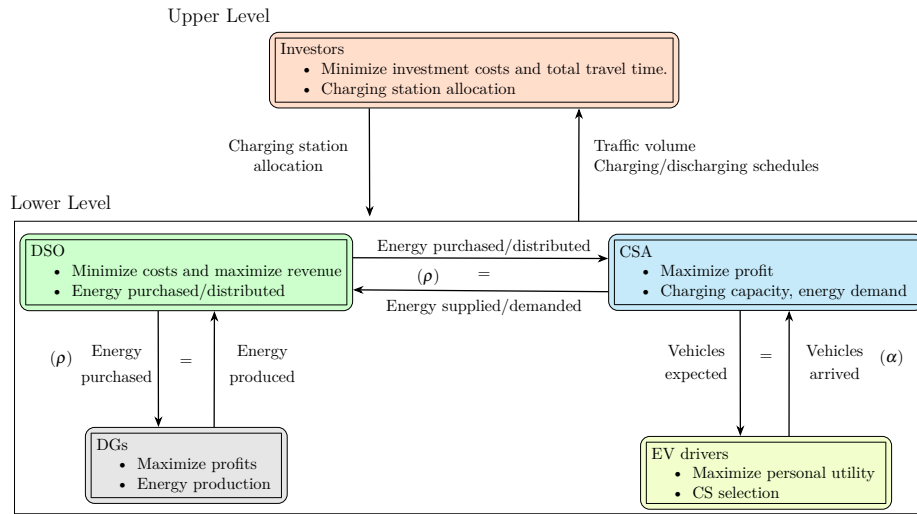
Figure 7.1: Methodology overview

optimizes its energy purchases from DGs and CSA to minimize its costs considering system requirements; DGs aim to maximize their profits by selling the generated energy to the DS. On the other hand, the CSA maximizes its profit by managing EV charging and energy exchange with the DSO. Note that CSA can either purchase energy from the system (if it is required to charge the EVs) or provide energy to DSO whenever EVs want to participate in system support by discharging their stored energy. A market clearing is enforced on the energy exchange in the system which requires the supplied energy by CSA and DGs to be equal to the energy demanded by DSs. Energy prices (ρ) are associated with this market clearing condition. The other main interaction is between the EV owners and CSA. EVs travel through transportation networks and select a CS to maximize their individual utilities. A market clearing condition is considered on this interaction which balances the number of EVs selecting a CS with the number of EVs expected by CSA. This clearing condition is associated with the locational incentives (α) offered by CSs to EV drivers. Therefore, the EVs' charging flexibility and the urgency of the DS energy needs will determine the incentives they receive.

The mathematical modeling of each stakeholder and the proposed bi-level problem will be discussed in the remaining part of this section.

Investor's Modeling

The charging infrastructure planner has a system-level objective of minimizing the total travel time of vehicles and the investment costs of installing new CSs which is modeled as an optimization problem in (7.1).

$$\min_{\delta} \quad \frac{\beta_1}{\beta_2} \sum_{n,m \in A} \sum_{\tau \in \mathcal{T}^{\text{arr}}} \text{tff}_{n,m}\, v_{n,m,t} \left(1 + b_{n,m}\left(\frac{v_{n,m,t}}{\text{Cap}_{n,m}}\right)^{\alpha}\right) + \sum_{i \in \mathcal{I}^{\text{CS}}} \delta_i C_i P_i^{\text{CS,cap}} \tag{7.1a}$$

$$\text{s.t} \quad \sum_{i \in \mathcal{I}^{\text{CS}}} \delta_i C_i P_i^{\text{CS,Cap}} \leq B \tag{7.1b}$$

The Bureau of Public Roads (BPR) function is used for the total travel time in the objective function (7.1a) and $(\sum \delta_i C_i P_i^{\text{CS,cap}})$ is for modeling the total investment cost of CSs. The cost coefficient C_i represents the cost of installing each unit of charging capacity ($P^{\text{CS,cap}}$) at candidate locations $i \in \mathcal{I}^{\text{CS}}$, and δ is a set of binary variables used to determine the optimal investment decision. Constraint (7.1b) ensures that the investment does not exceed the budget limit.

DG Modeling

For each DG i ($\in \mathcal{I}^{DG}$), the optimization of its profit involves determining the generation quantity $p_{i,t}^{DG}$ for each time step t ($\in \mathcal{T}$). Since the generation capacity of individual DGs is limited and falls

below the threshold of DSO dispatch, we assume that DG owners are perfectly competitive and do not possess market power to influence locational electricity prices $\rho_{i,t}$. As a result, the decision-making of all DG owners can be consolidated into a single optimization problem, as formulated in model (7.2).

$$\max_{\boldsymbol{p}^{DG} \geq \boldsymbol{0}} \quad \sum_{i \in \mathcal{I}^{DG}} \sum_{t \in \mathcal{T}} \left(\rho_{i,t} p_{i,t}^{DG} - C_i(p_{i,t}^{DG}) \right) \tag{7.2a}$$

$$\text{s.t.} \quad \underline{P}_{i,t}^{DG} \leq p_{i,t}^{DG} \leq \bar{P}_{i,t}^{DG}, \ \forall i \in \mathcal{I}^{DG}, t \in \mathcal{T}. \tag{7.2b}$$

The objective (7.2a) aims to maximize the profits of DG owners, which are calculated as the total revenue $\sum_{i \in \mathcal{I}^{DG}} \sum_{t \in \mathcal{T}} \rho_{i,t} p_{i,t}^{DG}$ minus the total production costs $\sum_{i \in \mathcal{I}^{DG}} \sum_{t \in \mathcal{T}} C_i(p_{i,t}^{DG})$. The production costs are assumed to be a convex function with respect to $p_{i,t}^{DG}$ [77], with different cost parameters for different DGs, implying a non-decreasing marginal cost.

Constraint (7.2b) establishes the upper and lower bounds on power generation at DG node i for time t. In cases where DGs can be disconnected from the system, $\underline{P}_{i,t}^{DG} = 0$.

DSO Modeling

The DSO has a key responsibility to maintain services in accordance with system requirements. In our model (7.3), we assume that the DSO aims to minimize the cost of energy purchased while adhering to system constraints.

$$\min_{\substack{\boldsymbol{v}\geq\boldsymbol{0},\\ \boldsymbol{p^s},\boldsymbol{pf},\boldsymbol{qf}}} \quad \sum_{i\in\mathcal{I}^{\mathrm{DG}}\cup\mathcal{I}^{\mathrm{CS}}}\sum_{t\in\mathcal{T}}\rho_{i,t}p^s_{i,t} \tag{7.3a}$$

s.t.
$$\sum_{l\in\mathcal{L}} pf_{l,t}\cdot\mathrm{LT}_{l,i} - \sum_{l\in\mathcal{L}} pf_{l,t}\cdot\mathrm{LF}_{l,i} = p^d_{i,t} - p^s_{i,t},\ \forall i\in\mathcal{I}, t\in\mathcal{T} \tag{7.3b}$$

$$\sum_{l\in\mathcal{L}} qf_{l,t}\cdot\mathrm{LT}_{l,i} - \sum_{l\in\mathcal{L}} qf_{l,t}\cdot\mathrm{LF}_{l,i} = q^d_{i,t} - q^s_{i,t},\forall i\in\mathcal{I}, t\in\mathcal{T} \tag{7.3c}$$

$$0 \leq p^d_{i,t} \leq \bar{P}^d_{i,t},\ \forall i\in\mathcal{I}^l, t\in\mathcal{T} \tag{7.3d}$$

$$q^d_{i,t} = (\bar{Q}^d_{i,t}/\bar{P}^d_{i,t})\cdot p^d_{i,t},\ \forall i\in\mathcal{I}^l, t\in\mathcal{T} \tag{7.3e}$$

$$pf^2_{l,t} + qf^2_{l,t} \leq \lambda_{l,t}\cdot(S^{\max}_l)^2, \forall l\in\mathcal{L}, t\in\mathcal{T} \tag{7.3f}$$

$$v_{\mathrm{FN}_l,t} - v_{\mathrm{TN}_l,t} = 2\cdot(r_l\cdot pf_{l,t} + x_l\cdot qf_{l,t}), \forall l\in\mathcal{L}, t\in\mathcal{T} \tag{7.3g}$$

$$(V^{\min}_i)^2 \leq v_{i,t} \leq (V^{\max}_i)^2,\ \forall i\in\mathcal{I}, t\in\mathcal{T}. \tag{7.3h}$$

In the objective (7.3a), the term $\sum_{i\in\mathcal{I}^{\mathrm{DG}}\cup\mathcal{I}^{\mathrm{CS}}}\sum_{t\in\mathcal{T}}\rho_{i,t}p^s_{i,t}$ represents the cost of energy purchased from DG/CSA. The operational constraints are formulated in (7.3b)-(7.3h), which are based on the Dist-Flow equations proposed in [78] and later adopted in [50, 79]. These constraints include the balance of active and reactive power flows in (7.3b) and (7.3c), respectively. Constraint (7.3f) limits power flow to not exceed line capacity. Constraints (7.3g) calculate the voltage at each node, while constraint (7.3h) defines the acceptable voltage range at each node.

CSA Modeling

A CSA is typically required to manage the communication and control challenges of EVs and CSs individually for the DSO. The CSA's objective is to maximize profits while maintaining the required charging demand of EVs, as formulated in model (7.4). The CSA's profits are calculated as the revenue made by selling electricity to the DSO, minus incentives and battery degradation

compensation paid to EV drivers. Note that $p_{i,t}^{\text{CS}}$ can have negative values, indicating that EVs are charging instead of discharging, in which case $\sum_{i \in \mathcal{I}^{\text{CS}}} \sum_{t \in \mathcal{T}} \rho_{i,t} p_{i,t}^{\text{CS}}$ would be the cost for the CSA to charge EVs. Electricity prices $\rho_{i,t}$ and EV incentives α_{rs}^e are determined endogenously by the market, as discussed in Section 7. If the market setting of interest is oligopolistic, where private-owned CSs strategically adjust prices to compete for clients, prices need to be explicitly considered as decisions of CS providers, and a Stackelberg game-theoretical modeling framework may be more appropriate. However, if the focus is on the optimal pricing strategies of individual private-owned CSs, they can be studied individually without considering the entire transportation and DSs, as shown in studies such as [83] and [84].

$$\max_{\boldsymbol{p}^{\text{CS}}, \boldsymbol{q'}, \boldsymbol{soc}} \quad \sum_{i \in \mathcal{I}^{\text{CS}}} \sum_{t \in \mathcal{T}} \rho_{i,t} p_{i,t}^{\text{CS}} - \sum_{r \in \mathcal{R}} \sum_{i \in \mathcal{I}^{\text{CS}}} \sum_{e \in \mathcal{E}} \alpha_{rs}^e q_{ri(s)}^{\prime e} - \sum_{i \in \mathcal{I}^{\text{CS}}} \sum_{r \in \mathcal{R}} \sum_{t \in \mathcal{T}} \sum_{e \in \mathcal{E}} C_{i,r,t}^{\text{deg},e} \tag{7.4a}$$

$$\text{s.t.} \quad \text{soc}_{i,r,t}^e = \text{soc}_{i,r,t-1}^e - p_{i,r,t}^e / \text{Cap}^e, \ \forall i \in \mathcal{I}^{\text{CS}}, r \in \mathcal{R}, e \in \mathcal{E}, t \in (T_{r,e}^{\text{arr}}, T_{r,e}^{\text{dep}}] \tag{7.4b}$$

$$q_{ri(s)}^{\prime e} \underline{\text{SOC}}^e \leq \text{soc}_{i,r,t}^e \leq q_{ri(s)}^{\prime e} \overline{\text{SOC}}^e, \ \forall i \in \mathcal{I}^{\text{CS}}, r \in \mathcal{R}, e \in \mathcal{E}, t \in [T_{r,e}^{\text{arr}}, T_{r,e}^{\text{dep}}] \tag{7.4c}$$

$$\text{soc}_{i,r,T_{r,e}^{\text{arr}}}^e = q_{ri(s)}^{\prime e} \text{SOC}_{r,e}^{\text{arr}}, \ \forall i \in \mathcal{I}^{\text{CS}}, r \in \mathcal{R}, e \in \mathcal{E} \tag{7.4d}$$

$$\text{soc}_{i,r,T_{r,e}^{\text{dep}}}^e \geq q_{ri(s)}^{\prime e} \text{SOC}_{r,e}^{\text{dep}}, \ \forall i \in \mathcal{I}^{\text{CS}} r \in \mathcal{R}, e \in \mathcal{E} \tag{7.4e}$$

$$- q_{ri(s)}^{\prime e} \bar{P}_{r,e}^{\text{ch}} \leq p_{i,r,t}^e \leq q_{ri(s)}^{\prime e} \bar{P}_{r,e}^{\text{dch}} \ \forall i \in \mathcal{I}^{\text{CS}}, r \in \mathcal{R}, e \in \mathcal{E}, t \in [T_{r,e}^{\text{arr}}, T_{r,e}^{\text{dep}}] \tag{7.4f}$$

$$p_{i,t}^{\text{CS}} = \sum_{r \in \mathcal{R}} \sum_{e \in \mathcal{E}} \frac{p_{i,r,t}^e}{S^{\text{base}}}, \ \forall i \in \mathcal{I}^{\text{CS}}, t \in [T_{r,e}^{\text{arr}}, T_{r,e}^{\text{dep}}], \tag{7.4g}$$

$$- \delta_i M \leq p_{i,r,t}^e \leq \delta_i M, \ \forall i \in \mathcal{I}^{\text{CS}}, r \in \mathcal{R}, t \in \mathcal{T} \tag{7.4h}$$

$$(\underline{\phi}_{i,t}^{\text{CS}}, \overline{\phi}_{i,t}^{\text{CS}}) \quad - \delta_i P_i^{\text{CS,Cap}} \leq P_{i,t}^{\text{CS}} \leq \delta_i P_i^{\text{CS,Cap}}, \ \forall i \in \mathcal{I}^{\text{CS}}, t \in \mathcal{T}. \tag{7.4i}$$

Constraints (7.4b)-(7.4i) specify the SOC transition and requirements of EVs that the CSA needs to fulfill. EVs are discretized into different homogeneous groups based on their travel and charging

characteristics, such as arriving/departing time and state of charge (SOC), meaning that EVs with similar battery SOC, charging demand, and travel schedules are grouped together. Incentives α_{rs}^e depend on EV groups and are determined endogenously by the market, considering factors such as initial SOC, charging needs, and dwelling time. Constraint (7.4b) models the dynamics of the SOC of EVs from r at CS i. Constraint (7.4c) limits the maximum and minimum SOC of each EV group based on the drivers' desired SOC range. Constraints (7.4d) and (7.4e) specify the initial arrival SOC and minimum departure SOC for each EV group at charging location i. Constraint (7.4f) restricts the charging/discharging power of EVs at each time step t based on battery/charger characteristics. The number of EVs demanded by the CSA at each CS is modeled as variable $q_{ri(s)}'^e$, which plays an important role in coupling transportation and DS, as further discussed in Section 7. Constraint (7.4g) determines the total power supply/demand of CS $i \in \mathcal{I}^{\mathrm{CS}}$ at time t by summing the normalized discharging/charging of EVs at each station. Constraint (7.4h) avoids charging instances for all EV groups where δ_i is equal to zero in candidate location i, where M is a big number to ensure that $p_{i,r,t}^e$ and δ_i are independent when $\delta_i=1$. Lastly, constraint (7.4i) limits the total charging/discharging of CSs with the system based on their capacities ($P_i^{\mathrm{CS,Cap}}$).

One of the primary concerns that dissuade drivers from participating in Vehicle-to-Grid (V2G) services is the degradation of batteries caused by continuous charging and discharging. This degradation can occur in two forms: shelf degradation and cycle degradation, as described in the study by Smith et al. [85]. In this paper, the Ah-throughput counting model proposed by Peterson et al. [86] is utilized to model these types of degradation. The formulation of the degradation cost for Electric Vehicles (EVs), denoted as $C_{i,r,t}^{\mathrm{deg},e}$, is presented in model (7.5), which is adapted from [50] to account for EV groups and the time index.

$$z_{i,r,t}^e \geq p_{i,r,t}^e \ \forall i \in \mathcal{I}^{\text{CS}}, r \in \mathcal{R}, e \in \mathcal{E}, t \in \mathcal{T} \tag{7.5a}$$

$$z_{i,r,t}^e \geq -p_{i,r,t}^e \ \forall i \in \mathcal{I}^{\text{CS}}, r \in \mathcal{R}, e \in \mathcal{E}, t \in \mathcal{T} \tag{7.5b}$$

$$\text{cap}_{i,r,t}^{\text{loss},e} = \zeta^e \cdot z_{i,r,t}^e \cdot \Delta T, \ \forall i \in \mathcal{I}^{CS}, r \in \mathcal{R}, t \in [T_r^{\text{arr}}, T_{r,e}^{\text{dep}}] \tag{7.5c}$$

$$d_{i,r,t}^{\text{cycle},e} = \frac{\text{cap}_{i,r,t}^{\text{loss},e}}{1 - \text{Cap}^{\text{end},e}}, \ \forall i \in \mathcal{I}^{CS}, r \in \mathcal{R}, e \in \mathcal{E}, t \in [T_{r,e}^{\text{arr}}, T_{r,e}^{\text{dep}}] \tag{7.5d}$$

$$d_{i,r,t}^e = \max\{d_{i,r,t}^{\text{cycle},e}, d^{\text{shelf},e}\},$$
$$\forall i \in \mathcal{I}^{CS}, r \in \mathcal{R}, e \in \mathcal{E}, t \in [T_r^{\text{arr}}, T_{r,e}^{\text{dep}}] \tag{7.5e}$$

$$C_{i,r,t}^{\text{deg},e} = d_{i,r,t}^e (C^{\text{rep},e} - C^{\text{res},e}) \text{Cap}^e,$$
$$\forall i \in \mathcal{I}^{CS}, r \in \mathcal{R}, e \in \mathcal{E}, t \in [T_r^{\text{arr}}, T_{r,e}^{\text{dep}}]. \tag{7.5f}$$

EV Drivers Modeling

In this section, we will further extend our model to include the routing and charging location choices made by decentralized EVs in transportation systems. The utility function denoted as U_{rs}^e for a driver in group e selecting charging station s from route r is formulated in equation (7.6), as proposed in [50, 67].

To model the charging location choices, we assume that EV drivers consider four factors: locational attractiveness denoted as $\beta_{0,s}$, travel time represented as $-\beta_1 tt_{rs}$, charging cost/revenue from charging/discharging denoted as $\beta_2 \alpha_{rs}^e$, and a random term ϵ. Without loss of generality, other exogenous factors can also be incorporated into equation (7.6) without affecting the proposed modeling and computational strategies in this paper. For example, different strategies implemented by Charging Stations (CSs) to attract EVs can be included as part of the locational attractiveness ($\beta_{0,s}$), reflecting varying levels of convenience and corresponding incentives offered by each CS.

$$U_{rs}^e = \beta_{0,s} - \beta_1 tt_{rs} + \beta_2 \alpha_{rs}^e + \epsilon. \tag{7.6}$$

The choice of destination (q_{rs}^e) for Electric Vehicles (EVs) and the corresponding path travel time (tt_{rs}) are interconnected. On one hand, the selection of Charging Stations (CSs) by EV drivers impacts the distribution of travel demand, which in turn affects the travel time for all drivers. On the other hand, the CS selection process is partially influenced by the travel time tt_{rs}, as indicated in equation (7.6). To capture these interdependencies, we adopt the combined distribution and assignment (CDA) model proposed by Sheffi (1985) [87], which allows us to simultaneously model the destination choices and route choices of EVs. The CDA model is formulated in equation (7.7). It's important to note that for each time period τ in the set of arrival times $\mathcal{T}^{\text{arr}}$, we will solve the CDA model denoted as CDA_τ to obtain the traffic pattern at that specific time τ.

$$\min_{\boldsymbol{x},\bar{\boldsymbol{x}},\boldsymbol{q} \geq 0} \quad \sum_{a \in \mathcal{A}} \int_0^{v_a^\tau} tt_a(u)\mathrm{d}u$$

$$+ \frac{1}{\beta_1} \sum_{r \in \mathcal{R}, s \in \mathcal{S}} \sum_{e \in \mathcal{E}^\tau} q_{rs}^e \left(\ln q_{rs}^e - 1 - \beta_2 \alpha_{rs}^e - \beta_{0,s} \right) \tag{7.7a}$$

$$\text{s.t.} \quad \boldsymbol{v}^\tau = \sum_{r \in \mathcal{R}, s \in \mathcal{S}} \boldsymbol{x}_{rs}^\tau + \sum_{r \in \bar{\mathcal{R}}, s \in \bar{\mathcal{S}}} \bar{\boldsymbol{x}}_{rs}^\tau, \; \forall \tau \in \mathcal{T}^{\text{arr}} \tag{7.7b}$$

$$(\boldsymbol{\eta}_{rs}^\tau) \quad A\boldsymbol{x}_{rs}^\tau = \sum_{e \in \mathcal{E}^\tau} q_{rs}^e E_{rs}, \; \forall r \in \mathcal{R}, s \in \mathcal{S}, \tau \in \mathcal{T}^{\text{arr}} \tag{7.7c}$$

$$A\bar{\boldsymbol{x}}_{rs}^\tau = \bar{q}_{rs}^\tau E_{rs}, \; \forall r \in \bar{\mathcal{R}}, s \in \bar{\mathcal{S}}, \tau \in \mathcal{T}^{\text{arr}} \tag{7.7d}$$

$$\sum_{s \in \mathcal{S}} q_{rs}^e = Q_r^e, \forall r \in \mathcal{R}, e \in \mathcal{E}^\tau. \tag{7.7e}$$

The objective function in equation (7.7a) is composed of two parts. The first part is the summation of the area under all the link travel cost functions $tt_a(\cdot)$, such as the BPR function, which can also

accommodate scenarios where transportation links have reduced capacity or significantly large free-flow travel time [88]. The second part includes the entropy of traffic distribution $q_{rs}^e(\ln q_{rs}^e - 1)$ and utility terms (excluding time) from equation (7.6) [88]. The construction of objective function (7.7a) ensures that the optimal solutions of the CDA model (equation (7.7)) are consistent with the first Wardrop principle [89] and the multinomial logit destination choice assumption. Technical details to prove this claim can be found in [87].

Constraint (7.7b) calculates the link flows by summing the link flows of EVs (x_{rs}^τ) and conventional vehicles ($\bar{x}rs^\tau$) traveling at the same time period τ for all origin and destination pairs. Constraints (7.7c) to (7.7d) represent the vehicle flow conservation at each node for EV travel demand qrs^e and conventional vehicle travel demand $\bar{q}rs^\tau$, respectively. Constraint (7.7e) ensures that the summation of EV traffic flow distribution to each s (qrs^e) equals the total EV travel demand from r, denoted as Q_r^e. The equilibrium travel time for each origin-destination (OD) pair rs can be calculated as $tt_{rs} \doteq \eta^\tau rs, r - \eta^\tau rs, s$, where $\eta_{rs,i}^\tau$ is the dual variable associated with constraint (7.7c).

Market Clearing

In a stable market, the power purchased by the DSO must be balanced with the power generated at each location. Additionally, the EV demand at each CS needs to be balanced with the EVs traveling to that station. The hourly market clearing conditions can be expressed as equation (7.8). Equation (7.8a) ensures that the total energy purchased by the DSO is equal to the total energy generated at each node, including Distributed Generators (DGs) and CSs. Equation (7.8b) enforces the balance between the EV flow of group e demanded and supplied at each location s from r. This equation establishes a coupling between the traffic flow (q_{rs}^e) determined from the CDA problem (7.7) and the number of EVs ($q_{rs}'^e$) demanded in the CSA modeling (7.4).

133

$$(\rho_{i,t}) \qquad\qquad p_{i,t}^{s} = p_{i,t}^{DG} + P_{i,t}^{\mathrm{CS}}, \ \forall i \in \mathcal{I}^{\mathrm{DG}} \cup \mathcal{I}^{\mathrm{CS}}, \ \forall t \in \mathcal{T} \qquad\qquad (7.8a)$$

$$(\alpha_{rs}^{e}) \qquad\qquad q_{rs}^{'e} = q_{rs}^{e}, \ \forall r \in \mathcal{R}, s \in \mathcal{S}, e \in \mathcal{E}. \qquad\qquad (7.8b)$$

The locational prices of electricity ($\rho_{i,t}$) and EV incentives (α_{rs}^{e}) can be understood as dual variables associated with the market clearing conditions. These clearing conditions allow us to model the interdependencies between transportation and D) operations, as well as the models defined in (7.2) to (7.7). It's important to note that the CSA sells/purchases electricity to/from the DSO based on the electricity price ($\rho_{i,t}$), while EVs receive incentives (α_{rs}^{e}) from the CSA based on their participation in DS support and their charging requirements. It's worth mentioning that both incentives and energy prices are endogenously determined within the network equilibrium framework. The incentives may be negative if EVs require a significant amount of energy while providing minimum services. In other words, the incentives can be interpreted as the net value of the system support service payments subtracting charging costs.

Equilibrium Problem

We consider the investor as the leading decision maker as its CS location decision will influence the operation of the other stakeholders, i.e., DG owners, DSO, CSA, and EV drivers. We can construct an equivalent problem that incorporates the problem of these stakeholders. We observe that if ρ and α were known, models (7.2) to (7.4) and (7.7) are convex optimization problems with completely separable constraints. This type of problem can be reformulated by linearly combining all the (scaled) objective functions and intersecting all the constraint sets in (7.2) to (7.4) and (7.7).

Subsequently, we can apply the reverse procedures of Lagrangian relaxation to the market clearing conditions (7.8) [103]. As a result, the models in (7.2) to (7.4) and (7.7) can be equivalently reformulated as a single convex optimization problem (7.9), which can be efficiently solved using commercial nonlinear optimization techniques. For extensive proof and deriving of the equivalent equilibrium problem, one can refer to our previous publication at [75].

$$
\min_{\substack{(\boldsymbol{p}^{DG},\boldsymbol{v},\boldsymbol{x},\bar{\boldsymbol{x}},\boldsymbol{q},\boldsymbol{q}')\geq 0, \\ \boldsymbol{p^s},\boldsymbol{pf},\boldsymbol{qf},\boldsymbol{p},\boldsymbol{p^{CS}},\textbf{soc}}} \sum_{t\in\mathcal{T}} \left[\sum_{i\in\mathcal{I}^{\mathrm{DG}}} C(p_{i,t}^{DG}) + \sum_{i\in\mathcal{I}^{\mathrm{CS}},r\in\mathcal{R},e\in\mathcal{E}} C_{i,r,t}^{deg,e} \right]
$$

$$
+ \sum_{\tau\in\mathcal{T}^{\mathrm{arr}}} \sum_{e\in\mathcal{E}^\tau} \sum_{r\in R,s\in S} \frac{q_{rs}^e}{\beta_2} \left(\ln q_{rs}^e - 1 - \beta_0^s\right) + \frac{\beta_1}{\beta_2} \sum_{\tau\in\mathcal{T}^{\mathrm{arr}}_{,a\in\mathcal{A}}} \int_0^{v_a^\tau} tt_a(u)du
$$

$$
\tag{7.9a}
$$

s.t $\qquad\qquad (7.2b), (7.3b) \sim (7.3h), (7.4b) \sim (7.4i), (7.5), (7.7b) \sim (7.7e), (7.8).$ (7.9b)

Bi-level Modeling and solution approach

As previously stated, our bi-level problem involves two main parts: the investors' problem as the upper-level problem and the defined equilibrium problem as the lower-level problem. We can express this problem as the optimization problem (7.10), with the equilibrium problem (7.8) incorporated as a constraint on the investors' problems (7.1).

$$\min_{\boldsymbol{\delta}} \quad \frac{\beta_1}{\beta_2} \sum_{n,m \in A} \sum_{\tau \in \mathcal{T}^{\mathrm{arr}}} \mathrm{tff}_{n,m}\, v_{n,m,t} \left(1 + b_{n,m}\left(\frac{v_{n,m,t}}{\mathrm{Cap}_{n,m}}\right)^\alpha\right) + \sum_{i \in \mathcal{I}^{\mathrm{CS}}} \delta_i C_i P_i^{\mathrm{CS,cap}} \qquad (7.10\mathrm{a})$$

$$\mathrm{s.t} \quad \sum_{i \in \mathcal{I}^{\mathrm{CS}}} \delta_i P_i^{\mathrm{CS,Cap}} \le B \qquad (7.10\mathrm{b})$$

$$\min \quad (7.9a) \qquad (7.10\mathrm{c})$$

$$\mathrm{s.t} \quad (7.9b). \qquad (7.10\mathrm{d})$$

Solution Algorithm

To simplify the notation, we will consider the general structure of a bi-level program, as shown in 7.11a. Specifically, for our particular problem, the functions $f(.)$ and $g(.)$, along with their decision variables x and y, correspond to the models defined in (7.10) and (7.9), respectively. It should be noted that the lower-level problem is a convex problem when the upper-level decisions $\boldsymbol{y}$ are given. However, it is important to highlight that $h_3(\boldsymbol{x}, \boldsymbol{y})$ contains bilinear terms of both $\boldsymbol{x}$ and $\boldsymbol{y}$.

$$\min_{x,y} \quad f(x,y) \tag{7.11a}$$

$$\text{s.t.} \quad h_1(y) \leq 0 \tag{7.11b}$$

$$x \in \operatorname{argmin} g(x,y) \tag{7.11c}$$

$$\text{s.t.} \quad h_2(x) \leq 0 \tag{7.11d}$$

$$h_3(x,y) \leq 0 \tag{7.11e}$$

Given that model 7.11a is a mixed-integer nonlinear and bilevel mathematical problem, traditional methods such as generalized Benders decomposition and KKT reformulation are not scalable. Therefore, we propose a value decomposition algorithm[1].

To begin, we relax the optimality condition for the lower-level problem, resulting in the relaxed problem shown in 7.12. Solving model 7.12 directly using commercial solvers poses challenges for two reasons. First, the objective function $f(\boldsymbol{x}, \boldsymbol{y})$ is nonlinear and includes the polynomial function of $\boldsymbol{x}$ (the BPR function in (7.10a)) and the integer variable $\boldsymbol{y}$ (the investment term in (7.10a)). To address these challenges, we utilize second-order conic reformulation techniques for the polynomial function (See Appendix for the details of the conic reformulation for the BPR function). Second, constraint (7.12d) contains bi-linear terms, which we reformulate using the big-M reformulation.

---

[1]The value decomposition algorithm results from discussion with Dr. Weijun Xie from Georgia Institute of Technology.

$$\min_{\boldsymbol{x}\in\mathbb{R}^n_+,\boldsymbol{y}\in\{0,1\}^m} \quad f(\boldsymbol{x},\boldsymbol{y}) \tag{7.12a}$$

$$\text{s.t.} \quad h_1(\boldsymbol{y}) = 0 \tag{7.12b}$$

$$h_2(\boldsymbol{x}) = 0 \tag{7.12c}$$

$$h_3(\boldsymbol{x},\boldsymbol{y}) = 0 \tag{7.12d}$$

The two bilinear terms in our formulation, which are part of $h_3(\boldsymbol{x},\boldsymbol{y})$, correspond to the complementarity terms defined in (7.13) for the CS capacity constraints.

$$0 \leq \delta_i \perp \overline{\phi}^{\mathrm{CS}}_{i,t} P^{\mathrm{CS},Cap}_i \geq 0 \tag{7.13a}$$

$$0 \leq \delta_i \perp \underline{\phi}^{\mathrm{CS}}_{i,t} P^{\mathrm{CS},Cap}_i \geq 0 \tag{7.13b}$$

We can reformulate the complementarity terms by defining helper variables $\overline{z}$ and $\underline{z}$ and applying the big-M method, as shown below:

$$(\delta_i - 1)M \leq \overline{z}_{i,t} - \overline{\phi}^{\mathrm{CS}}_{i,t} P^{\mathrm{CS},Cap}_i \leq (1-\delta_i)M \tag{7.14a}$$

$$-\delta_i M \leq \overline{z}_{i,t} \leq \delta_i M \tag{7.14b}$$

$$(\delta_i - 1)M \leq \underline{z}_{i,t} - \underline{\phi}^{\mathrm{CS}}_{i,t} P^{\mathrm{CS},Cap}_i \leq (1-\delta_i)M \tag{7.14c}$$

$$-\delta_i M \leq \underline{z}_{i,t} \leq \delta_i M \tag{7.14d}$$

In order to guarantee that the optimal solution $\boldsymbol{x}, \boldsymbol{y}$ satisfies the optimality condition of the lower-level problem (i.e., 7.15a), it is necessary to add sufficient and necessary conditions. There are two approaches to ensuring these conditions: branch-and-bound algorithms and branch-and-cut algorithms. It is worth noting that both algorithms take advantage of the fact that the lower-level problem, as shown in (7.15), is convex given upper-level decisions $\boldsymbol{y}^U$.

$$\min_{\boldsymbol{x}\in\mathbb{R}^n_+} \qquad g(\boldsymbol{x}) \qquad\qquad (7.15a)$$

$$\text{s.t.} \qquad h_2(\boldsymbol{x}) = 0 \qquad\qquad (7.15b)$$

$$h_3(\boldsymbol{x}|\boldsymbol{y}^U) = 0 \quad (\boldsymbol{\mu}) \qquad\qquad (7.15c)$$

We explain the basic ideas of the branch-and-bound algorithms in the remainder of this section.

Branch-and-bound algorithm

Achieving the upper bound of the original problem (7.11a) is a straightforward process. Starting with an upper-level integer decision $\boldsymbol{y}^U$ of the relaxed problem (7.12), one can solve the lower-level problem (7.15) and obtain the lower-level optimal solutions $\boldsymbol{x}^L$. The upper bound of the original problem (7.11a) can be obtained by computing $f(\boldsymbol{y}^U, \boldsymbol{x}^L)$. The lower bound of the original problem (7.11a) is simply the objective value of the relaxed problem (7.12). To enhance the tightness of the lower bound, cuts are added iteratively.

It is worth noting that for the upper-level optimal solutions $\boldsymbol{x}^U$ and $\boldsymbol{y}^U$ to satisfy the optimality

conditions of the lower-level problem (7.15), it is equivalent to have condition (7.16) due to strong duality.

$$g(\boldsymbol{x}^U) \leq \max_{\boldsymbol{\mu}} \min_{\boldsymbol{x}} \mathcal{L}(\boldsymbol{x}, \boldsymbol{\mu}|\boldsymbol{y}^U) \tag{7.16}$$

where $\mathcal{L}(\boldsymbol{x}, \boldsymbol{\mu}|\boldsymbol{y}^U)$ is the Lagrangian function if one relaxes constraint (7.15c) in model (7.15), see (7.17).

$$\mathcal{L}(\boldsymbol{x}, \boldsymbol{\mu}|\boldsymbol{y}^U) = g(\boldsymbol{x}) - \langle \boldsymbol{u}, h_3(\boldsymbol{x}|\boldsymbol{y}^U)\rangle \tag{7.17}$$

Condition (7.16) is equivalent to the following condition (condition (7.18)).

$$\exists \boldsymbol{\mu}, \quad \text{s.t.} \quad g(\boldsymbol{x}^U) \leq \min_{\boldsymbol{x}} \mathcal{L}(\boldsymbol{x}, \boldsymbol{\mu}|\boldsymbol{y}^U) \tag{7.18}$$

The lower-level constraints, specifically constraints (7.15b) and (7.15c), are satisfied by any optimal solutions of the upper-level relaxed problem (7.12) and lower-level problem (7.15) denoted as $\boldsymbol{x}^L$ and $\boldsymbol{x}^U$. By iteratively adding cuts (7.19) to model (7.12), we can improve the lower bound.

$$g(\boldsymbol{x}) \leq \mathcal{L}(\boldsymbol{x}^L, \boldsymbol{\mu}, \boldsymbol{y}) \tag{7.19}$$

There are two reasons why directly adding cut (7.19) to model (7.12) results in nonlinearity. First, $g(\boldsymbol{x})$ is a nonlinear but convex function. Second, $\mathcal{L}(\boldsymbol{x}^L, \boldsymbol{\mu}, \boldsymbol{y})$ contains bilinear terms of $\boldsymbol{\mu}$ and $\boldsymbol{y}$. To overcome the first issue, we use Taylor series to linearize $g(\boldsymbol{x})$ around $\boldsymbol{x}^L$ and $\boldsymbol{x}^U$. As a result, we add two cuts, namely (7.20) and (7.21), at each iteration.

$$g'(\boldsymbol{x}, \boldsymbol{x}^L) \leq \mathcal{L}(\boldsymbol{x}^L, \boldsymbol{\mu}, \boldsymbol{y}) \tag{7.20}$$

$$g'(\boldsymbol{x}, \boldsymbol{x}^U) \leq \mathcal{L}(\boldsymbol{x}^L, \boldsymbol{\mu}, \boldsymbol{y}) \tag{7.21}$$

where $g'(\boldsymbol{x}, \boldsymbol{x}^{L/U})$ is the Taylor linear approximation of $g(\boldsymbol{x})$ at points $\boldsymbol{x}^{L/U}$.

Second, to address the second issue, we use big-M reformulation, similar to the strategies discussed in (7.14).

In order to improve the efficiency of the algorithm's runtime, we suggest incorporating an extra cut that eliminates binary solutions that were previously examined in earlier iterations. The cut is expressed through equation (7.22), and is applicable only to binary variables ($\boldsymbol{y}^B$) which are a subset of the upper-level variables ($\boldsymbol{y}$). This step helps to avoid redundant computations when the optimal integer solution has already been obtained. The effectiveness of this cut will be assessed in the numerical results section to determine its impact on efficiency.

$$\sum_{i \in Y_1^B} 1 - y_i^B + \sum_{i \in Y_0^B} y_i^B \geq 1, \tag{7.22}$$

where,

$$Y_1^B = \{i | y_i^{B,iter} > 0.5\}$$

$$Y_0^B = \{i | y_i^{B,iter} < 0.5\}$$

The complete form of the bi-level model for our problem along with the detailed formulation of the cuts is explained in the Appendix section.

We summarize our algorithm in Algorithm 1.

Algorithm 1 Branch-and-Bound Algorithm

1: Solve the relaxed problem (7.12). Store the optimal solution as $\{\boldsymbol{x}^{U,0}, \boldsymbol{\mu}^{U,0}, \boldsymbol{y}^{U,0}\}$ and objective value as $Obj^{U,0}$.
2: Given $\boldsymbol{y}^{U,0}$, solve the lower-level problem (7.15) and store the optimal solutions and objective value as $\boldsymbol{x}^{L,0}$ and $Obj^{L,0}$ respectively.
3: Initialize LB = $Obj^{U,0}$, UB = $f(\boldsymbol{x}^{L,0}, \boldsymbol{y}^{U,0})$, $iter = 0$
4: **while** (UB-LB)/UB $> \epsilon$ **do**
5:     Add cuts (7.20), (7.21), and (7.22).
6:     $iter = iter + 1$
7:     Solve relaxed problem (7.12). Store the optimal solution as $\{\boldsymbol{x}^{U,iter}, \boldsymbol{\mu}^{U,iter}, \boldsymbol{y}^{U,iter}\}$ and objective value $Obj^{U,iter}$
8:     Given $\boldsymbol{y}^{U,iter}$, solve lower-level problem (7.15) and store the optimal solutions as $\{\boldsymbol{x}^{L,iter}, \boldsymbol{\mu}^{L,iter}\}$.
9:     Update LB = $Obj^{U,iter}$, UB = $f(\boldsymbol{x}^{L,iter}, \boldsymbol{y}^{U,iter})$
10: **end while**

Numerical results

Our goal is to evaluate the decision-making of investors when determining the location of CSs and investigate the operation of entities that are impacted by these decisions. To achieve this, we implemented the defined bi-level model and the solution algorithms on two test systems. It is important to note that in this section, the term "node" refers specifically to the nodes of DS unless otherwise specified. We utilized Pyomo 5.6.7 [92, 93] and IPOPT 3.12.13 [94] to implement and solve our model. All experiments were conducted on a system running UBUNTU 18.04.2, with a 3.6 GHz 9-Core Intel Core i9 and 64 GB of RAM.

Four-node test system

The test system being evaluated is a small four-node system, which is illustrated in Fig. 7.2. Nodes 2 and 3 are the candidate CSs and serve as the links between the distribution and transportation
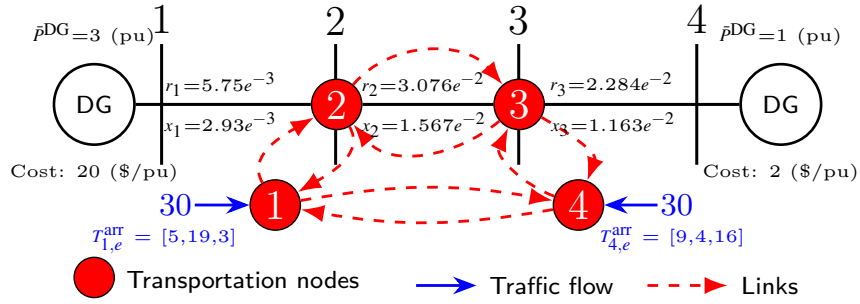
Figure 7.2: Four-node test system

systems, while nodes 2 through 4 represent the load nodes. The load demand pattern is based on data from the PJM dataset, with September 2, 2022, from the AEP zone selected for this study. In contrast to previous chapters, it is assumed that the load demand is equal among the nodes, with a factor of 0.2 retrieved from the PJM dataset. The results are presented in per unit (pu) values, with a base capacity of $S^{\text{base}} = 1000$ kVA. All the distribution lines have the same maximum capacity of $S_l^{\max} = 2$ (pu), and the transportation links have a capacity of 10 (vehicles/hour). It is assumed that each candidate CS will have a total capacity of 0.3 (pu).

The development of EVs with higher battery capacities that provide a longer driving range is a recent advancement in EV manufacturing. Tesla's Model S, for example, currently offers the highest battery capacity of 100 kW, with a charging rate of 17.2 kWh. We assume that future EVs will have similar or higher capacities, and in our test system, we assume that the EVs have the same characteristics as Tesla's Model S. The EVs are divided into three groups based on their initial state of charge (SOC^{arr}), where group $e = 1$ requires the most charging, group $e = 2$ is intermediate, and group $e = 3$ requires the least charging. Each group's initial state of charge is randomly selected within the defined ranges mentioned above.

EVs leave from transportation nodes 1 and 4, and there is incoming traffic of 20 EVs. The arrival times of EVs are randomly distributed during the hours $\tau \ (\in \mathcal{T}_{r,e}^{\text{arr}})$ and can go to either of the CSs.

The randomly generated arrival times for EV groups are shown in Fig. 7.2.

Based on the above-mentioned system characteristics, the algorithm converges quickly, even at the first iteration since it is a small test system with only two candidate locations. The optimal location for the CS investment was found to be node 3. It should be noted that the transportation system is symmetrical, so choosing either node 2 or 3 as the CS location would not affect the total travel time of the system, which is part of the upper-level objective function. In fact, we solved the problem by assuming that only node 2 was the candidate CS location, and the resulting objective function was the same as when node 3 was chosen. We conducted sensitivity analysis by changing system parameters in the transportation system to introduce asymmetry and further investigate investors' decision-making.

We began by increasing the number of incoming EVs from node 1 to 80 vehicles while setting the incoming EVs from node 2 to 20 (as shown in Fig. 7.3). As the number of incoming EVs from node 1 surpassed 20 vehicles, node 2 became the optimal location for the CS since it was closer to the origin nodes with more EVs, thereby reducing the total travel time of the system. This trend continued until the number of EVs from node 1 reached 45 vehicles. At this point, the increased congestion on link 1–2 caused the total travel time to become higher than when the CS was located at node 3, making node 3 the optimal location. When the number of EVs from node 1 reached 70 vehicles, having only one CS was not sufficient to meet the charging and DS requirements, so both candidate locations were selected for CS installations. The CS output for 65 and 70 vehicles from node 1, as shown in Fig. 7.4, demonstrates how the charging demand was distributed between the CSs.

The previous analysis demonstrated the influence of transportation network congestion and increased CD on CS investment decisions. In the next step, we will perform a similar analysis from the perspective of the DS to determine how limitations in power distribution affect investment de-

144
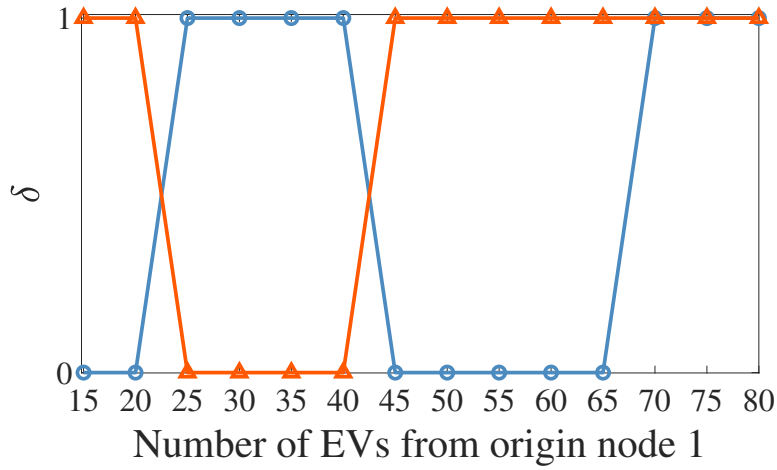
Figure 7.3: CS investment decision with EV increase from node 1; —o node 2 and —△ node 3
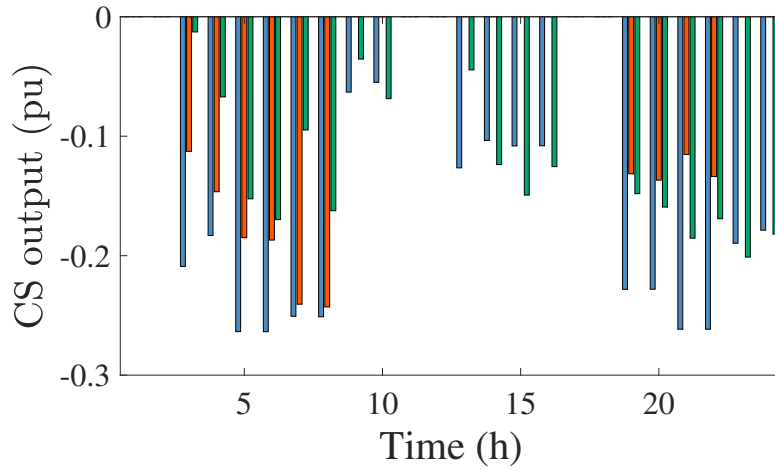
Figure 7.4: CS out put with EV increase from node 1; ▬ node 3 with 65 EVs, ▬ node 3 with 70 EVs, and ▬ node 2 with 70 EVs.

cisions. We will model this impact by increasing the load demand at node 3, as shown in Fig. 7.5. Following a 15% increase in load demand, the optimal CS location shifts from node 3 to both nodes 2 and 3. This is because the additional demand at node 3 limits the power transferability to that node, making node 2 a more favorable option for meeting the charging requirements of EVs.
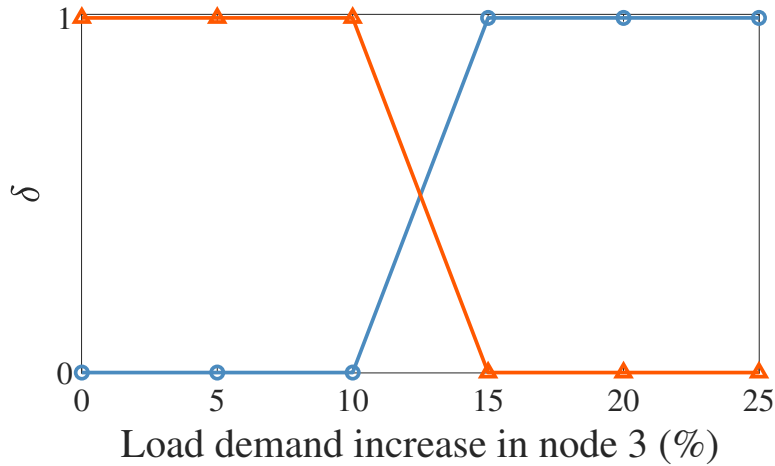
Figure 7.5: CS investment decision with load demand increase in node 3; —○ node 2 and —△ node 3

In the next step, we explored an extreme scenario in which we double the load demand at node 3 and assume that all EVs belong to group 3 to investigate a case where EVs can provide more energy to the system. We then compare the system's operational performance to the base case where the optimal location for the CS was at node 3. The CS output during the day is shown with blue bars in the graph in Fig. 7.6. When we double the load demand at node 3, the CS location changes to node 2 due to the voltage constraint (7.3g) limiting power transferability to node 3. Additionally, the CS output becomes limited, as illustrated with orange bars in Fig. 7.6. This demonstrates how the DS requirement, specifically the voltage constraint, affects the selection of the CS location for charging. However, if we relax this constraint, the optimal CS location reverts to node 3, as depicted by the green bars in Fig. 7.6), and the CS output is no longer limited, resulting in a similar operational performance to the base case.
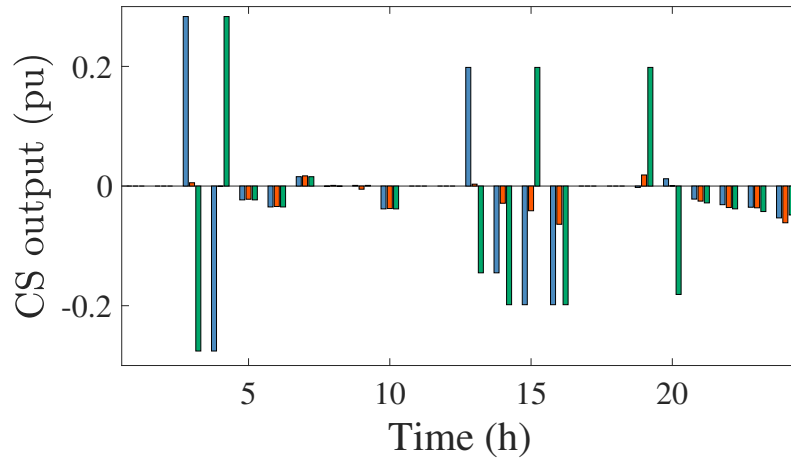
Figure 7.6: CS output; ▭ node 3 with base-case load, ▭ node 2 with load increase, and ▭ node 3 with load increase and relaxing the voltage constraint.

IEEE-33 node and Sioux Falls test systems

In the previous subsection, we demonstrated that our model and solution algorithm can effectively capture the interdependence of power and transportation systems in CS investment problems, using small test systems. Now, we will assess the performance of our model on larger, interconnected test systems, and evaluate the convergence and run time of our solution algorithm.

Fig. 7.7 shows the coupled test systems that we have considered here. The blue nodes in both systems show the total candidate CS locations and the numbers with arrows on the transportation network show the incoming number of EVs from the origin nodes.

Base case analysis

We begin with a base case consisting of 5 origin nods and 5 candidate CS locations (destination nodes) represented by green circled nodes in Figure 7.7. The proposed algorithm reaches con-

(a) IEEE 33-node   (b) Sioux Falls transportation network
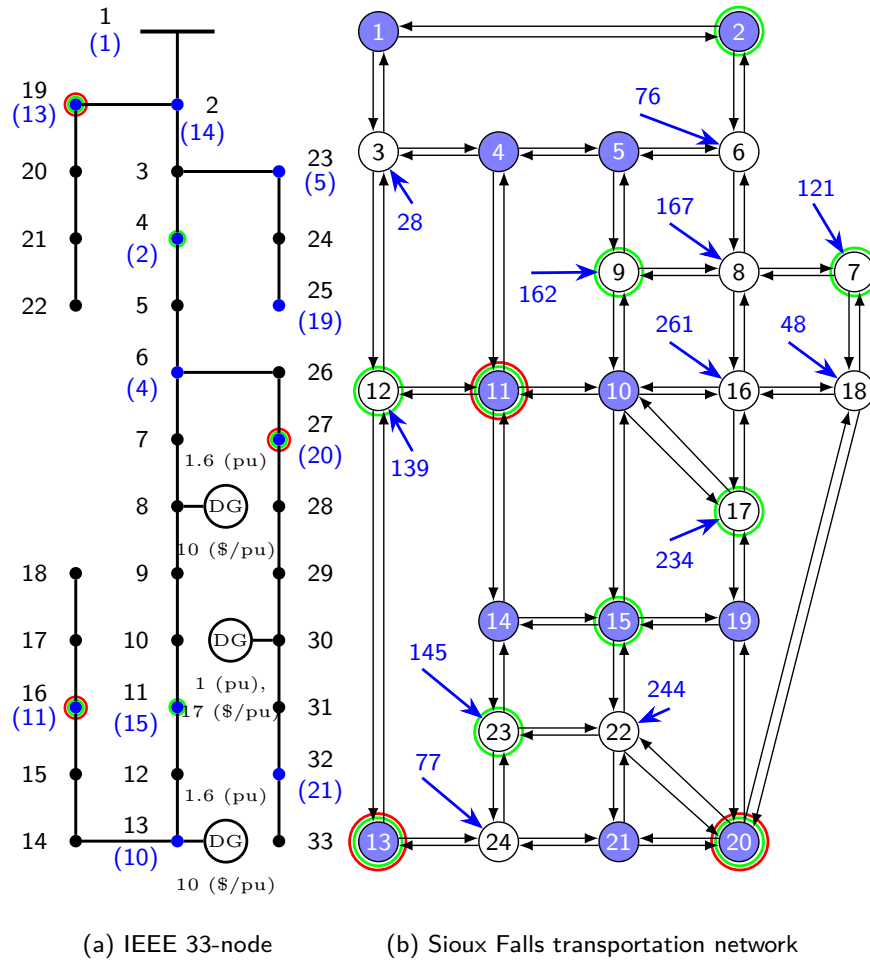
Figure 7.7: Test systems (a) 33-node DS (b) Transportation system. ●: nodes; ●: corresponding nodes in transportation system (CSs). ○: origin nodes; ●: destination (CS) nodes; and →: EV incoming traffic flow. ○: selected ODs for base case and ○: resulting optimal CS locations for base case.

vergence after 6 iterations, which takes approximately 8.05 minutes to run. The fast convergence is attributed to the inclusion of cuts that eliminate binary solutions from the previous iterations. Without this cut, the algorithm would run for many iterations, gradually increasing the LB until it meets the termination criterion. Figure 7.8 illustrates the upper and lower bounds with and without the cuts. Without the mentioned cuts, even though the optimal solution has been found, the algorithm continues to make slight improvements to the LB for 100 iterations (2.41 hours of run
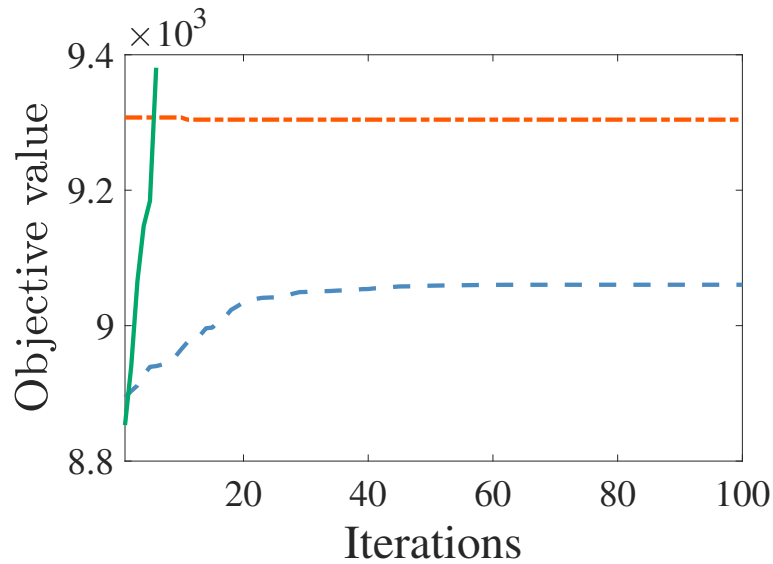
Figure 7.8: Investor's objective value; **- . -** UB, **—** LB with the additional cuts, and **- - -** LB without the additional cuts.

time) without reaching the desired distance to the UB. With the addition of the cuts, the algorithm stops more quickly because the LB exceeds the UB (see the green line in Fig. 7.8), indicating that the optimal integer solution has already been found through the omitted binary solutions, and the previous optimal points are not explored any further.

The red circles highlighted in Figure 7.7 demonstrate that the CS investments were made in closer proximity to origin nodes that receive a greater number of incoming vehicles. In Figure 7.9, the output of CSs at nodes 16 and 27 indicate that they attracted EVs with more significant charging requirements in comparison to the CS at node 19. This is because nodes 16 and 27 are located in closer proximity to the DG nodes, which supply more dependable energy and meet the system's requirements. On the other hand, node 19 is farther from the DG nodes and contributes more to the system by discharging more energy, resulting in more instances of discharging and fewer charging instances observed at this node.
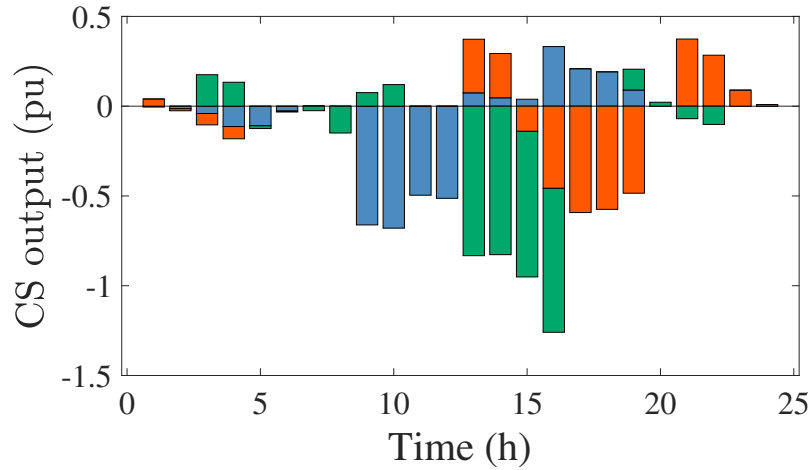
Figure 7.9: CS output; ▬ node 16, ▬ node 19, and ▬ node 27.

Computational analysis

Initially, we conducted the base case and then proceeded to expand our test system by adding more candidate CS locations and origin nodes, resulting in a total of 12 candidate CS and origin nodes. Table 7.1 summarizes the run time and the number of iterations required for the algorithm to converge in each case.

We observed a linear increase in run time as the number of ODs increased until we reached 10 OD pairs. At this point, the run time and iteration count increased significantly because there were multiple possible and feasible solutions with similar objective values, causing the algorithm to run for more iterations. However, once we exceeded 10 OD pairs, the number of iterations required to achieve optimal results decreased, resulting in a reduction in run time. This can be attributed to the fact that a larger number of CSs are necessary to meet the changing requirements of EVs, resulting in fewer feasible optimal solutions with similar objective values and faster convergence of the algorithm.

Table 7.1 Algorithm performance analysis

Number of OD pairs	Selected ODs	Run time (minutes)	No. of Iterations	Optimal CS locations in TN	Optimal CS nodes in DS
5	O: 7,9,12,17,23 D: 2,11,13,15,20	8.05	6	11,13,20	16,19,27
6	O: 7,9,12,17,23,6 D: 2,11,13,15,20,14	14.22	6	13,15,20	19,11,27
7	O: 7,9,12,17,23,6,18 D: 2,11,13,15,20,14,4	38.80	10	2,13,15,20,14	4,19,11,27,2
8	O: 7,9,12,17,23,6,18,3 D: 2,11,13,15,20,14,4,10	34.93	6	2,13,20,14,4,10	4,19,27,2,6,13
9	O: 7,9,12,17,23,6,18,3,24 D: 2,11,13,15,20,14,4,10,5	53.34	7	13,20,14,4,10	19,27,2,6,13
10	O: 7,9,12,17,23,6,18,3,24,16 D: 2,11,13,15,20,14,4,10,5,21	225.13	20	13,15,20,10,5	19,11,27,13,23
11	O: 7,9,12,17,23,6,18,3,24,16,22 D: 2,11,13,15,20,14,4,10,5,21,19	48.45	4	2,13,20,10,21,19	4,19,27,13,32,25
12	O: 7,9,12,17,23,6,18,3,24,16,22,8 D: 2,11,13,15,20,14,4,10,5,21,19,1	38.69	2	2,13,20,10,5,21,19,1	4,19,27,13,23,32,25,1

Conclusion

In conclusion, this chapter has presented a detailed overview of a proposed bi-level framework for managing the allocation of charging stations for electric vehicles. The framework involves two levels, with a government planning agency making decisions on charging station allocation at the upper level and the interaction of stakeholders from power distribution and transportation systems modeled at the lower level. The framework employs a market-based equilibrium model that models the interaction of stakeholders from both power distribution and transportation systems, and a novel value-decomposition-based solution algorithm that solves a series of mixed integer linear problems and convex optimization problems iteratively. Simulation results on small test systems and bigger test systems based on the Sioux Falls transportation network and IEEE distribution networks demonstrate the effectiveness of the proposed model and the convergence pattern of the solution algorithm. The model provides a realistic representation of the feedback effect of planning decisions on system operations and can help system operators investigate planning strategies for the increasing charging demand and grid services opportunities for EVs in the future.

151

APPENDIX: PROPOSED BI-LEVEL MODEL FORMULATION

The complete mathematical problem for the proposed bi-level model is presented in (8.23)

$$
\min_{\boldsymbol{\delta}} \quad \frac{\beta_1}{\beta_2} \sum_{n,m \in A} \sum_{\tau \in \mathcal{T}^{\mathrm{arr}}} \mathrm{tff}_{n,m}\, v_{n,m,t} \left(1 + b_{n,m} (\frac{v_{n,m,t}}{\mathrm{Cap}_{n,m}})^\alpha \right) + \sum_{i \in \mathcal{I}^{\mathrm{CS}}} \delta_i C_i P_i^{\mathrm{CS,cap}} \tag{8.23a}
$$

$$
\text{s.t} \quad \sum_{i \in \mathcal{I}^{\mathrm{CS}}} \delta_i\, C_i\, P_i^{\mathrm{CS,Cap}} \leq B \tag{8.23b}
$$

Lower level problem constraints :

$$
(7.2\mathrm{b}), (7.3\mathrm{b}) \sim (7.3\mathrm{h}), (7.4\mathrm{b}) \sim (7.4\mathrm{i}), (7.5), (7.7\mathrm{b}) \sim (7.7\mathrm{e}), (7.8) \tag{8.23c}
$$

Reformulated complementarity terms : (7.14) $\tag{8.23d}$

Cuts :

$$
f(\boldsymbol{v}^{(\mathrm{eq})}, \boldsymbol{q}^{(\mathrm{eq})}) \leq \eta \tag{8.23e}
$$

$$
f(\boldsymbol{v}^{(\mathrm{up})}, \boldsymbol{q}^{(\mathrm{up})}) \leq \eta \tag{8.23f}
$$

$$
\mathcal{L}(\boldsymbol{v}^{\mathrm{eq}}, \boldsymbol{q}^{(\mathrm{eq})}), \boldsymbol{C}^{\mathrm{deg}}, \boldsymbol{p}^{\mathrm{DG}}, \boldsymbol{p}^{\mathrm{CS}}) \leq \eta \tag{8.23g}
$$

$$
\sum_{i \in \Delta_1} 1 - \delta_i + \sum_{i \in \Delta_0} \delta_i \geq 1, \tag{8.23h}
$$

where $f(.)$ is the first-order Fourier approximation of the equilibrium objective function (7.9a) around the given points. And $\mathcal{L}(.)$ is the simplified Lagrangian function of the equilibrium problem:

$$f(\boldsymbol{V}, \boldsymbol{Q}) = \frac{\beta_1}{\beta_2} \left(\sum_{(n,m)\in A} \sum_{\tau\in\mathcal{T}^{\mathrm{arr}}} \mathrm{tff}_{n,m} \left(V_{n,m,\tau} + \frac{b}{\alpha+1} \frac{V_{n,m,\tau}^{\alpha+1}}{\mathrm{Cap}^{\alpha}} \right) \right)$$

$$+ \frac{\beta_1}{\beta_2} \left[\sum_{(n,m)\in A} \sum_{\tau\in\mathcal{T}^{\mathrm{arr}}} \left(\mathrm{tff}_{n,m} \left(1 + b(\frac{V_{n,m,\tau}}{\mathrm{Cap}})^{\alpha} \right) (v_{n,m,\tau} - V_{n,m,\tau}) \right) \right]$$

$$+ \frac{1}{\beta_2} \sum_{r\in\mathcal{R}s\in\mathcal{S}e\in\mathcal{E}} \left(Q_{r,s}^e \left(\ln(Q_{r,s}^e) - 1 - \beta_0^s \right) + \left(\ln Q_{r,s}^e - \beta_0^s \right)(q_{r,s}^e - Q_{r,s}^e) \right)$$

$$\sum_{t\in\mathcal{T}} \left[\sum_{i\in\mathcal{I}^{\mathrm{DG}}} C(p_{i,t}^{DG}) + \sum_{i\in\mathcal{I}^{\mathrm{CS}},r\in\mathcal{R},e\in\mathcal{E}} C_{i,r,t}^{deg,e} \right] \tag{8.24}$$

$$\mathcal{L}(\boldsymbol{V}, \boldsymbol{Q}, \boldsymbol{C}^d, \boldsymbol{P}^{\mathrm{DG}}, \boldsymbol{P}^{\mathrm{CS}}) = \frac{\beta_1}{\beta_2} \left(\sum_{(n,m)\in A} \sum_{\tau\in\mathcal{T}^{\mathrm{arr}}} \mathrm{tff}_{n,m} \left(V_{n,m,\tau} + \frac{b}{\alpha+1} \frac{V_{n,m,\tau}^{\alpha+1}}{\mathrm{Cap}^{\alpha}} \right) \right)$$

$$+ \frac{1}{\beta_2} \sum_{r\in\mathcal{R}s\in\mathcal{S}e\in\mathcal{E}} Q_{r,s}^e \left(\ln(Q_{r,s}^e) - 1 - \beta_0^s \right) + \sum_{t\in\mathcal{T}} \left(\sum_{i\in\mathcal{I}^{\mathrm{CS}},r\in\mathcal{R}} C_{i,r,t}^{d,e} + C(P_{i,t}^{\mathrm{DG}}) \right)$$

$$+ \sum_{i\in\mathcal{I}^{\mathrm{CS}}} \overline{\phi}_{i,t} P_{i,t}^{\mathrm{CS}} - \overline{z}_{i,t} + \underline{\phi}_{i,t} P_{i,t}^{\mathrm{CS}} + \underline{z}_{i,t} \right) \tag{8.25}$$

Additionally, Δ_1 denotes a collection of potential CS indexes where the binary solution from the previous iteration is equal to 1, while Δ_0 denotes a collection of potential CS indexes where the binary solution from the previous iteration is equal to 0. We can represent these sets similar to (7.22) as:

$$\Delta_1 = \{i | \delta_i^{iter} > 0.5\} \tag{8.26}$$

$$\Delta_0 = \{i | \delta_i^{iter} < 0.5\} \tag{8.27}$$

LIST OF REFERENCES

[1] IEA, *World Energy Outlook 2021*. IEA, Paris, 2021. [Online]. Available: https://www.iea.org/topics/world-energy-outlook

[2] ——, *Global EV Outlook 2022, Securing supplies for an electric future*. IEA: Paris, 2022. [Online]. Available: https://www.iea.org/reports/global-ev-outlook-2022

[3] U. S. D. of Energy. (2022) Alternative fuels data center. [Online]. Available: https://afdc.energy.gov/data/10964

[4] Michael Wayland, "Biden wants to build a national EV charging system under $2 trillion infrastructure plan, but it won't be easy," https://www.cnbc.com/2021/03/31/us-ev-charging-system-a-priority-under-bidens-2-trillion-infrastructure-plan.html, 2021.

[5] M. Yilmaz and P. T. Krein, "Review of the impact of vehicle-to-grid technologies on distribution systems and utility interfaces," *IEEE Trans. on Power Electron*, vol. 28, no. 12, pp. 5673–5689, 2012.

[6] J. Hu, A. Saleem, S. You *et al.*, "A multi-agent system for distribution grid congestion management with electric vehicles," *Eng. Appl. Artif. Intell.*, vol. 38, pp. 45–58, 2015.

[7] S. Azad, K. Sanjani, and M. T. Ameli, "Optimal co-generation of electric and heat energy systems considering heat energy storage systems and chp units," in *Whole Energy Systems: Bridging the Gap via Vector-Coupling Technologies*. Springer, 2021, pp. 199–214.

[8] H. Jahangir, H. Tayarani *et al.*, "Charging demand of plug-in electric vehicles: Forecasting travel behavior based on a novel rough artificial neural network approach," *J. Clean. Prod*, vol. 229, pp. 1029–1044, Aug. 2019.

[9] M. Li, M. Lenzen, F. Keck *et al.*, "GIS-based probabilistic modeling of BEV charging load for australia," *IEEE Trans. Smart Grid*, vol. 10, no. 4, pp. 3525–3534, Apr. 2018.

[10] S. Baghali, S. Hasan, and Z. Guo, "Analyzing the travel and charging behavior of electric vehicles-a data-driven approach," in *2021 IEEE Kansas Power and Energy Conference (KPEC)*. IEEE, 2021, pp. 1–5.

[11] B. D. Emami, Y. Song, and A. Khani, "Prioritizing bus routes for electrification: Gis-based multi-criteria analysis considering operational, environmental, and social benefits and costs," *Transportation Research Record*, vol. 2676, no. 8, pp. 10–23, 2022.

[12] Z. Tian, Y. Wang, C. Tian *et al.*, "Understanding operational and charging patterns of electric vehicle taxis using gps records," in *17th International IEEE Conference on Intelligent Transportation Systems (ITSC)*. IEEE, Oct. 2014, pp. 2472–2479.

[13] M. De Gennaro, E. Paffumi, H. Scholz, and G. Martini, "GIS-driven analysis of e-mobility in urban areas: An evaluation of the impact on the electric energy grid," *Appl. Energy*, vol. 124, pp. 94–116, Jul. 2014.

[14] T. Yang, X. Xu, Q. Guo *et al.*, "EV charging behaviour analysis and modelling based on mobile crowdsensing data," *IET Gener. Transm.*, vol. 11, no. 7, pp. 1683–1691, Jan. 2017.

[15] J. Fraile-Ardanuy, S. Castano-Solis, R. Álvaro-Hermana *et al.*, "Using mobility information to perform a feasibility study and the evaluation of spatio-temporal energy demanded by an electric taxi fleet," *Energy Convers. Manag.*, vol. 157, pp. 59–70, Feb. 2018.

[16] A. Ashtari, E. Bibeau, S. Shahidinejad, and T. Molinski, "Pev charging profile prediction and analysis based on vehicle usage data," *IEEE Transactions on Smart Grid*, vol. 3, no. 1, pp. 341–350, Sep. 2011.

[17] K. Qian, C. Zhou, M. Allan, and Y. Yuan, "Modeling of load demand due to ev battery charging in distribution systems," *IEEE Trans. Power Syst.*, vol. 26, no. 2, pp. 802–810, Aug. 2010.

[18] M. B. Arias and S. Bae, "Electric vehicle charging demand forecasting model based on big data technologies," *Appl. Energy*, vol. 183, pp. 327–339, Dec. 2016.

[19] R.-C. Leou, C.-L. Su, and C.-N. Lu, "Stochastic analyses of electric vehicle charging impacts on distribution network," *IEEE Trans. Smart Grid*, vol. 29, no. 3, pp. 1055–1063, Dec. 2013.

[20] D. Tang and P. Wang, "Probabilistic modeling of nodal charging demand based on spatial-temporal dynamics of moving electric vehicles," *IEEE Trans. Smart Grid*, vol. 7, no. 2, pp. 627–636, Jun 2015.

[21] S. Sun, Q. Yang, and W. Yan, "A novel markov-based temporal-soc analysis for characterizing pev charging demand," *IEEE Trans. Ind. Informat.*, vol. 14, no. 1, pp. 156–166, Jun 2017.

[22] D. Wang, X. Guan, J. Wu, and J. Gao, "Analysis of multi-location pev charging behaviors based on trip chain generation," in *2014 IEEE International Conference on Automation Science and Engineering (CASE)*. IEEE, Aug. 2014, pp. 151–156.

[23] T. Shun, L. Kunyu, X. Xiangning, W. Jianfeng, Y. Yang, and Z. Jian, "Charging demand for electric vehicle based on stochastic analysis of trip chain," *IET Gener., Transm. Distrib.*, vol. 10, no. 11, pp. 2689–2698, Aug. 2016.

[24] D. Panahi, S. Deilami, M. A. Masoum, and S. M. Islam, "Forecasting plug-in electric vehicles load profile using artificial neural networks," in *2015 Australasian Universities Power Engineering Conference (AUPEC)*. IEEE, Sep. 2015, pp. 1–6.

[25] A. Mansour-Saatloo, A. Moradzadeh, B. Mohammadi-Ivatloo, A. Ahmadian, and A. Elka-mel, "Machine learning based pevs load extraction and analysis," *Electronics*, vol. 9, no. 7, p. 1150, July 2020.

[26] H. Zhang, Z. Hu, Z. Xu, and Y. Song, "Optimal planning of PEV charging station with single output multiple cables charging spots," *IEEE Transactions on Smart Grid*, vol. 8, no. 5, pp. 2119–2128, 2017.

[27] G. Graber, V. Calderaro, P. Mancarella, and V. Galdi, "Two-stage stochastic sizing and packetized energy scheduling of BEV charging stations with quality of service constraints," *Applied Energy*, vol. 260, p. 114262, 2020. [Online]. Available: https://www.sciencedirect.com/science/article/pii/S030626191931949X

[28] W. Khan, F. Ahmad, and M. S. Alam, "Fast ev charging station integration with grid ensuring optimal and quality power exchange," *Engineering Science and Technology, an International Journal*, vol. 22, no. 1, pp. 143–152, 2019. [Online]. Available: https://www.sciencedirect.com/science/article/pii/S2215098617315057

[29] J. C. Mukherjee and A. Gupta, "A review of charge scheduling of electric vehicles in smart grid," *IEEE Systems Journal*, vol. 9, no. 4, pp. 1541–1553, Oct. 2014.

[30] M. Goodarzi and Q. Li, "Evaluate the capacity of electricity-driven water facilities in small communities as virtual energy storage," *Applied Energy*, vol. 309, p. 118349, 2022.

[31] D. Xiao, S. An, H. Cai, J. Wang, and H. Cai, "An optimization model for electric vehicle charging infrastructure planning considering queuing behavior with finite queue length," *Journal of Energy Storage*, vol. 29, p. 101317, 2020. [Online]. Available: https://www.sciencedirect.com/science/article/pii/S2352152X19309053

[32] Z. Zhao, M. Xu, and C. K. Lee, "Capacity planning for an electric vehicle charging station considering fuzzy quality of service and multiple charging options," *IEEE Transactions on Vehicular Technology*, vol. 70, no. 12, pp. 12 529–12 541, 2021.

[33] M. Abapour, K. Zare *et al.*, "Stackelberg based optimal planning of dgs and electric vehicle parking lot by implementing demand response program," *Sustainable Cities and Society*, vol. 51, p. 101743, Nov. 2019.

[34] M. F. Shaaban, S. Mohamed, M. Ismail, K. A. Qaraqe, and E. Serpedin, "Joint planning of smart ev charging stations and dgs in eco-friendly remote hybrid microgrids," *IEEE Transactions on Smart Grid*, vol. 10, no. 5, pp. 5819–5830, Jan. 2019.

[35] F. Guo, J. Yang, and J. Lu, "The battery charging station location problem: Impact of users' range anxiety and distance convenience," *Transportation Research Part E: Logistics and Transportation Review*, vol. 114, pp. 1–18, 2018.

[36] Y. Zhang, Y. Wang, F. Li, B. Wu, Y.-Y. Chiang, and X. Zhang, "Efficient deployment of electric vehicle charging infrastructure: Simultaneous optimization of charging station placement and charging pile assignment," *IEEE Transactions on Intelligent Transportation Systems*, vol. 22, no. 10, pp. 6654–6659, 2021.

[37] G. Dong, J. Ma, R. Wei, and J. Haycox, "Electric vehicle charging point placement optimisation by exploiting spatial statistics and maximal coverage location models," *Transportation Research Part D: Transport and Environment*, vol. 67, pp. 77–88, 2019.

[38] C. Li, Z. Dong, G. Chen, B. Zhou, J. Zhang, and X. Yu, "Data-driven planning of electric vehicle charging infrastructure: A case study of sydney, australia," *IEEE Transactions on Smart Grid*, vol. 12, no. 4, pp. 3289–3304, Jan. 2021.

159

[39] Z. Guo, J. Deride, and Y. Fan, "Infrastructure planning for fast charging stations in a competitive market," *Transportation Research Part C: Emerging Technologies*, vol. 68, pp. 215–227, Jul. 2016.

[40] Y. Fang, W. Wei, S. Mei, L. Chen, X. Zhang, and S. Huang, "Promoting electric vehicle charging infrastructure considering policy incentives and user preferences: An evolutionary game model in a small-world network," *Journal of cleaner production*, vol. 258, p. 120753, Jun. 2020.

[41] Y. Zhao, Y. Guo, Q. Guo, H. Zhang, and H. Sun, "Deployment of the electric vehicle charging station considering existing competitors," *IEEE Transactions on Smart Grid*, vol. 11, no. 5, pp. 4236–4248, Apr. 2020.

[42] B. D. Emami and A. Khani, "Charging infrastructure planning for networks including electric and diesel trucks," Tech. Rep., 2023.

[43] F. He, D. Wu, Y. Yin, and Y. Guan, "Optimal deployment of public charging stations for plug-in hybrid electric vehicles," *Transportation Research Part B: Methodological*, vol. 47, pp. 87–101, 2013.

[44] W. Wei, L. Wu, J. Wang, and S. Mei, "Expansion planning of urban electrified transportation networks: A mixed-integer convex programming approach," *IEEE Transactions on Transportation Electrification*, vol. 3, no. 1, pp. 210–224, 2017.

[45] Y. Lin, K. Zhang, Z.-J. M. Shen, B. Ye, and L. Miao, "Multistage large-scale charging station planning for electric buses considering transportation network and power grid," *Transportation Research Part C: Emerging Technologies*, vol. 107, pp. 423–443, Oct. 2019.

[46] F. Xia, H. Chen, M. Shahidehpour, W. Gan, M. Yan, and L. Chen, "Distributed expansion planning of electric vehicle dynamic wireless charging system in coupled power-traffic networks," *IEEE Transactions on Smart Grid*, 2021.

[47] S. Li, Y. Huang, and S. J. Mason, "A multi-period optimization model for the deployment of public electric vehicle charging stations on network," *Transportation Research Part C: Emerging Technologies*, vol. 65, pp. 128–143, Apr. 2016.

[48] F. Xie, C. Liu, S. Li, Z. Lin, and Y. Huang, "Long-term strategic planning of inter-city fast charging infrastructure for battery electric vehicles," *Transportation Research Part E: Logistics and Transportation Review*, vol. 109, pp. 261–276, Jan 2018.

[49] S. Huang and Q. Wu, "Dynamic tariff-subsidy method for PV and V2G congestion management in distribution networks," *IEEE Trans. Smart Grid*, vol. 10, no. 5, pp. 5851–5860, Jan. 2019.

[50] Z. Guo, Z. Zhou, and Y. Zhou, "Impacts of integrating topology reconfiguration and vehicle-to-grid technologies on distribution system operation," *IEEE Trans. Sustain. Energy*, vol. 11, no. 2, pp. 1023–1032, May 2019.

[51] J. Zhao, Y. Wang, G. Song *et al.*, "Congestion management method of low-voltage active distribution networks based on distribution locational marginal price," *IEEE Access*, vol. 7, pp. 32 240–32 255, Mar. 2019.

[52] Q. Wu, M. Shahidehpour *et al.*, "Transactive real-time electric vehicle charging management for commercial buildings with pv on-site generation," *IEEE Trans. Smart Grid*, vol. 10, no. 5, pp. 4939–4950, Sep. 2018.

[53] T. Ding, Z. Zeng, J. Bai *et al.*, "Optimal electric vehicle charging strategy with markov decision process and reinforcement learning technique," *IEEE Trans. Ind. Appl.*, vol. 56, no. 5, pp. 5811–5823, Apr. 2020.

[54] S. Deb, A. K. Goswami, P. Harsh *et al.*, "Charging coordination of plug-in electric vehicle for congestion management in distribution system integrated with renewable energy sources," *IEEE Trans. Ind. Appl.*, vol. 56, no. 5, pp. 5452–5462, 2020.

[55] K. Knezović, S. Martinenas, P. B. Andersen, A. Zecchino, and M. Marinelli, "Enhancing the role of electric vehicles in the power grid: field validation of multiple ancillary services," *IEEE Trans. Transp. Electrific.*, vol. 3, no. 1, pp. 201–209, Oct. 2016.

[56] M. R. Sarker, M. A. Ortega-Vazquez, and D. S. Kirschen, "Optimal coordination and scheduling of demand response via monetary incentives," *IEEE Trans. Smart Grid*, vol. 6, no. 3, pp. 1341–1352, 2014.

[57] S. Huang and Q. Wu, "Dynamic subsidy method for congestion management in distribution networks," *IEEE Trans. Smart Grid*, vol. 9, no. 3, pp. 2140–2151, 2016.

[58] B. Moradzadeh and K. Tomsovic, "Two-stage residential energy management considering network operational constraints," *IEEE Trans. Smart Grid*, vol. 4, no. 4, pp. 2339–2346, 2013.

[59] S. Weckx, R. D'Hulst, B. Claessens, and J. Driesensam, "Multiagent charging of electric vehicles respecting distribution transformer loading and voltage limits," *IEEE Trans. Smart Grid*, vol. 5, no. 6, pp. 2857–2867, 2014.

[60] J. Hu, C. Si, M. Lind, and R. Yu, "Preventing distribution grid congestion by integrating indirect control in a hierarchical electric vehicles' management system," *IEEE Trans. Transport. Electrific.*, vol. 2, no. 3, pp. 290–299, Apr. 2016.

[61] A. Asrari, M. Ansari, J. Khazaei, and P. Fajri, "A market framework for decentralized congestion management in smart distribution grids considering collaboration among electric vehicle aggregators," *IEEE Trans. Smart Grid*, vol. 11, no. 2, pp. 1147–1158, 2019.

[62] M. Goodarzi and Q. Li, "Hybrid physics and data-driven contingency filtering for security operation of micro energy-water nexus," *CSEE Journal of Power and Energy Systems*, 2023.

[63] F. Ahmad, M. S. Alam, S. M. Shariff, and M. Krishnamurthy, "A cost-efficient approach to EV charging station integrated community microgrid: A case study of indian power market," *IEEE Trans. Transport. Electrific.*, vol. 5, no. 1, pp. 200–214, 2019.

[64] W. Wei, W. Danman, W. Qiuwei, M. Shafie-Khah, and J. P. Catalao, "Interdependence between transportation system and power distribution system: A comprehensive review on models and applications," *Journal of Modern Power Systems and Clean Energy*, vol. 7, no. 3, pp. 433–448, 2019.

[65] Y. Wang, Y. Xu, J. Li *et al.*, "Dynamic load restoration considering the interdependencies between power distribution systems and urban transportation systems," *CSEE J. Power Energy Syst.*, vol. 6, no. 4, pp. 772–781, Aug. 2020.

[66] W. Wei, L. Wu, J. Wang, and S. Mei, "Network equilibrium of coupled transportation and power distribution systems," *IEEE Trans. on Smart Grid*, vol. 9, no. 6, pp. 6764–6779, 2017.

[67] Z. Guo, F. Afifah, J. Qi, and S. Baghali, "A stochastic multi-agent optimization framework for interdependent transportation and power system analyses," *IEEE Transactions on Transportation Electrification*, 2021.

[68] S. Baghali, Z. Guo, and S. Hasan, "Investigating the spatiotemporal charging demand and travel behavior of electric vehicles using gps data: A machine learning approach," in *2022 IEEE Power & Energy Society General Meeting (PESGM)*. IEEE, 2022.

[69] G. Oh, D. J. Leblanc, and H. Peng, "Vehicle energy dataset (VED), a large-scale dataset for vehicle energy consumption research," *IEEE trans Intell Transp Syst*, 2020.

[70] S. R. Khazeiynasab and J. Qi, "Resilience analysis and cascading failure modeling of power systems under extreme temperatures," *J. Mod. Power Syst. Clean Energy*, Oct. 2020.

[71] S. D. Jadhav and H. Channe, "Comparative study of K-NN, naive bayes and decision tree classification techniques," *International Journal of Science and Research (IJSR)*, vol. 5, no. 1, pp. 1842–1845, 2016.

[72] C. Prehofer and S. Mehmood, "Big data architectures for vehicle data analysis," in *2020 IEEE International Conference on Big Data (Big Data)*. IEEE, Dec. 2020, pp. 3404–3412.

[73] U. S. D. of Energy. (2020) Alternative fuels data center. [Online]. Available: https://afdc.energy.gov/

[74] H. Jahangir, H. Tayarani *et al.*, "A novel electricity price forecasting approach based on dimension reduction strategy and rough artificial neural networks," *IEEE Trans. Ind. Informat.*, vol. 16, no. 4, pp. 2369–2381, 2019.

[75] S. Baghali, Z. Guo, W. Wei, and M. Shahidehpour, "Electric vehicles for distribution system load pickup under stressed conditions: A network equilibrium approach," *IEEE Transactions on Power Systems*, 2022.

[76] A. Dargahi, K. Sanjani, M. Nazari-Heris, B. Mohammadi-Ivatloo, S. Tohidi, and M. Marzband, "Scheduling of air conditioning and thermal energy storage systems considering demand response programs," *Sustainability*, vol. 12, no. 18, p. 7311, 2020.

[77] M. Yan, N. Zhang, X. Ai, M. Shahidehpour, C. Kang, and J. Wen, "Robust two-stage regional-district scheduling of multi-carrier energy systems with a large penetration of wind power," *IEEE Trans Sustain Energy*, vol. 10, no. 3, pp. 1227–1239, 2018.

[78] M. E. Baran and F. F. Wu, "Network reconfiguration in distribution systems for loss reduction and load balancing," *IEEE Power Engineering Review*, vol. 9, no. 4, pp. 101–102, 1989.

[79] S. Lei, C. Chen, H. Zhou, and Y. Hou, "Routing and scheduling of mobile power sources for distribution system resilience enhancement," *IEEE Trans. Smart Grid*, vol. 10, no. 5, pp. 5650–5662, Dec. 2018.

[80] R. Li, Q. Wu, and S. S. Oren, "Distribution locational marginal pricing for optimal electric vehicle charging management," *IEEE Transactions on Power Systems*, vol. 29, no. 1, pp. 203–211, Sept. 2013.

[81] A. Schroeder and T. Traber, "The economics of fast charging infrastructure for electric vehicles," *Energy Policy*, vol. 43, pp. 136–144, 2012.

[82] X. Duan, Z. Hu, and Y. Song, "Bidding strategies in energy and reserve markets for an aggregator of multiple ev fast charging stations with battery storage," *IEEE trans Intell Transp Syst*, 2020.

[83] M. Seyedyazdi, M. Mohammadi, and E. Farjah, "A combined driver-station interactive algorithm for a maximum mutual interest in charging market," *IEEE Transactions on Intelligent Transportation Systems*, vol. 21, no. 6, pp. 2534–2544, Jun. 2019.

[84] E. Erdin, M. Cebe, K. Akkaya, S. Solak, E. Bulut, and S. Uluagac, "Building a private bitcoin-based payment network among electric vehicles and charging stations," in *2018 IEEE International Conference on Internet of Things (iThings) and IEEE Green Computing and Communications (GreenCom) and IEEE Cyber, Physical and Social Computing (CPSCom) and IEEE Smart Data (SmartData)*. IEEE, Jul. 2018, pp. 1609–1615.

[85] K. Smith, E. Wood, S. Santhanagopalan, G.-h. Kim, Y. Shi, and A. Pesaran, "Predictive models of li-ion battery lifetime," NREL (National Renewable Energy Laboratory (NREL), Tech. Rep., June 2015.

[86] S. B. Peterson, J. Apt, and J. Whitacre, "Lithium-ion battery cell degradation resulting from realistic vehicle and vehicle-to-grid utilization," *J. Power Sources*, vol. 195, no. 8, pp. 2385–2392, Apr. 2010.

[87] Y. Sheffi, *Urban transportation networks.* Prentice-Hall, Englewood Cliffs, NJ, 1985, vol. 6.

[88] F. Afifah and Z. Guo, "Spatial pricing of ride-sourcing services in a congestedtransportation network," *arXiv preprint arXiv:2006.00164*, 2020.

[89] J. Wardrop, "Some theoretical aspects of road traffic research," *Proc. Inst. Civ. Eng.*, no. Part II, pp. 325–378, 1952.

[90] L. Walras, *Elements of pure economics.* Routledge, Oct. 2013.

[91] A. J. Kleywegt, A. Shapiro, and T. Homem-de Mello, "The sample average approximation method for stochastic discrete optimization," *SIAM Journal on Optimization*, vol. 12, no. 2, pp. 479–502, 2002.

[92] W. E. Hart, J.-P. Watson, and D. L. Woodruff, "Pyomo: modeling and solving mathematical programs in python," *Math. Program. Comput.*, vol. 3, no. 3, pp. 219–260, 2011.

[93] M. L. Bynum, G. A. Hackebeil, W. E. Hart *et al.*, *Pyomo–optimization modeling in python*, 3rd ed. Springer Science & Business Media, 2021, vol. 67.

[94] A. Wächter and L. T. Biegler, "On the implementation of a primal-dual interior point filter line search algorithm for large-scale nonlinear programming," *Math. Program.*, vol. 106, pp. 25–57, 2006.

[95] "PJM Market Data," https://dataminer2.pjm.com/list, 2021.

[96] S. Davis and R. G. Boundy, "Transportation energy data book: Edition 39," Oak Ridge National Lab.(ORNL), Oak Ridge, TN (United States), Tech. Rep., 2021.

[97] M. Frank and P. Wolfe, "An algorithm for quadratic programming," *Naval research logistics quarterly*, vol. 3, no. 1-2, pp. 95–110, 1956.

[98] H. Haggi and W. Sun, "Multi-round double auction-enabled peer-to-peer energy exchange in active distribution networks," *IEEE Transactions on Smart Grid*, 2021.

[99] B. Taheri, A. Safdarian, M. Moeini-Aghtaie, and M. Lehtonen, "Distribution system resilience enhancement via mobile emergency generators," *IEEE Trans. Power Del.*, Jul. 2020.

[100] M. Panteli, C. Pickering, S. Wilkinson, R. Dawson, and P. Mancarella, "Power system resilience to extreme weather: fragility modeling, probabilistic impact assessment, and adaptation measures," *IEEE Trans. Power Syst*, vol. 32, no. 5, pp. 3747–3757, Dec. 2016.

[101] M. Goodarzi and Q. Li, "Security-constrained optimal operation of energy-water nexus based on a fast contingency filtering method," in *2022 IEEE Power & Energy Society General Meeting (PESGM)*.   IEEE, 2022, pp. 1–5.

[102] H. Heitsch and W. Römisch, "Scenario reduction algorithms in stochastic programming," *Computational optimization and applications*, vol. 24, no. 2, pp. 187–206, Feb. 2003.

[103] Z. Guo, F. Afifah, J. Qi, and S. Baghali, "A stochastic multi-agent optimization framework for interdependent transportation and power system analyses," *IEEE Trans. Transp*, 2021.

[104] J. R. Birge and F. Louveaux, *Introduction to stochastic programming*.   Springer Science & Business Media, 2011.

[105] B. Davazdah Emami and A. Khani, "Nonlinear complementarity model for mixed-user equilibrium traffic assignment and mode choice of electric and gasoline vehicles," *Transportation Research Record*, p. 03611981221149433, 2023.

[106] C. Siddique, F. Afifah, Z. Guo, and Y. Zhou, "Data mining of plug-in electric vehicles charging behavior using supply-side data," *Energy Policy*, vol. 161, p. 112710, Feb. 2022.

[107] EIA, "2019 annual electric generator report," U.S. Energy Information Administration, Tech. Rep., 2019. [Online]. Available: https://www.eia.gov/electricity/generatorcosts/

[108] C. Nelder and E. Rogers, "Reducing ev charging infrastructure costs," *Rocky Mountain Institute*, Dec. 2019.

[109] B. Borlaug, S. Salisbury, M. Gerdes, and M. Muratori, "Levelized cost of charging electric vehicles in the united states," *Joule*, vol. 4, no. 7, pp. 1470–1485, Jul. 2020.

[110] IEA, "Global EV outlook 2020, entering the decade of electric drive," IEA: Paris, Tech. Rep., 2020. [Online]. Available: https://www.iea.org/reports/global-ev-outlook-2020

[111] United States Department of Transportation, "National Household Travel Survey 2017," https://nhts.ornl.gov/, 2019.

[112] P. salyani, M. Abapour, and K. Zare, "Stackelberg based optimal planning of dgs and electric vehicle parking lot by implementing demand response program," *Sustainable Cities and Society*, vol. 51, p. 101743, 2019. [Online]. Available: https://www.sciencedirect.com/science/article/pii/S2210670719305062